LEVEL II

12

NW

NADC-77153-30

TITANIUM ALLOY IGNITION AND COMBUSTION

V. G. Anderson
B. A. Manty
United Technologies Corporation
Pratt & Whitney Aircraft Group
Box 2691, West Palm Beach, Fla 33402

30 October 1978

Final Report

for Period 30 September 1977 through 30 September 1978

Approved for Public Release; Distribution Unlimited

Prepared for
Department of the Navy
Naval Air Development Center
Warminster, Pa 18974

UNCLASSIFIED

SECURITY CLASSIFICATION OF THIS PAGE (When Data Entered)

REPORT DOCUMENTATION PAGE

READ INSTRUCTIONS BEFORE COMPLETING FORM

1. REPORT NUMBER: NADC-77153-30	2. GOVT ACCESSION NO.
3. RECIPIENT'S CATALOG NUMBER: (9) rept.	
4. TITLE (and Subtitle): TITANIUM ALLOY IGNITION AND COMBUSTION	5. TYPE OF REPORT & PERIOD COVERED: Final 30 Sep 1977 through 30 Sep 1978
6. PERFORMING ORG. REPORT NUMBER: (14) PWA-FR-10520	
7. AUTHOR(s): (10) V. G. Anderson, B. A. Manty	8. CONTRACT OR GRANT NUMBER(s): (15) N62269-77-C-0481 new
9. PERFORMING ORGANIZATION NAME AND ADDRESS: United Technologies Corporation, Pratt & Whitney Aircraft Group, Government Products Division, West Palm Beach, Florida 33402	10. PROGRAM ELEMENT, PROJECT, TASK AREA & WORK UNIT NUMBERS
11. CONTROLLING OFFICE NAME AND ADDRESS: Department of the Navy, Naval Air Development Center, Warminster, Pa. 18974	12. REPORT DATE: (11) 30 October 1978
	13. NUMBER OF PAGES: 96
14. MONITORING AGENCY NAME & ADDRESS (if different from Controlling Office): (12) 99p.	15. SECURITY CLASS. (of this report): Unclassified
	15a. DECLASSIFICATION/DOWNGRADING SCHEDULE

16. DISTRIBUTION STATEMENT (of this Report)

Approved for Public Release; Distribution Unlimited

17. DISTRIBUTION STATEMENT (of the abstract entered in Block 20, if different from Report)

18. SUPPLEMENTARY NOTES

19. KEY WORDS (Continue on reverse side if necessary and identify by block number)

Laser Ignition	Compressor Environment
Combustibility	Vanguard Motion Analyzer
Titanium Alloy	Chordwise Velocity
Sustained Combustion	Burn Severity

20. ABSTRACT (Continue on reverse side if necessary and identify by block number)

The objective of this program was to determine the relative ignition and combustibility characteristics of titanium alloys. Nine titanium alloys were subjected to a laser ignition source at each of two conditions of temperature, pressure, and airsteam velocity typical of gas turbine engine compressor environments. In addition a concurrent study was conducted on the effect of Ti 8-1-1 specimen thickness on combustion parameters.

DD FORM 1 JAN 73 1473 EDITION OF 1 NOV 65 IS OBSOLETE

(13) UNCLASSIFIED 392 887

SECURITY CLASSIFICATION OF THIS PAGE (When Data Entered)

All alloys ignited but two (Ti 20Ni and Ti 13Cu) failed to sustain combustion. Burn severity and chordwise and spanwise burn velocities were determined for those alloys which burned. Thickness was found to influence these burn parameters. The extent of this influence was shown to have a high degree of correlation.

SUMMARY

The primary objective of this program was to determine the relative ignition and combustion characteristics of the following titanium alloys:

Ti 8Al-1Mo-1V
Ti 6Al-2Sn-4Zr-6Mo
Ti 13V-11Cr-3Al
Ti 13.5Al-21.5Nb
Ti 13Cu
Beta III (Ti 11.5Mo-6Zr-4.5Sn)
Ti 5Ni
Ti 10Ni
Ti 20Ni

A secondary objective was to evaluate the effect of specimen thickness on combustion parameters.

Using a laser energy source for specimen ignition, tests were conducted at two conditions of temperature, pressure and airstream velocity typical of gas turbine engine compressor environments.

Testing of Ti 8-1-1 specimens established that thickness variation produces several well-defined effects on combustion parameters which, for example, can be expressed mathematically in the case of chordwise burn velocity.

Alloys Ti 20Ni and Ti 13Cu ignited but failed to sustain combustion at four environmental test conditions. Alloys Ti 13-11-3, Ti 13.5Al-21.5Nb and Beta III experienced sustained combustion but the severity of burn was low to moderate (less than 20%). All other test alloys burned moderately to severely with alloy Ti 6-2-4-6 experiencing total destruction (100% severity) in all tests.

Variations in test run environmental conditions showed that pressure has a greater influence on burn velocity and severity than previous studies had indicated. In addition, airstream velocity was shown to either increase or decrease burn severity depending upon the alloy being tested.

TABLE OF CONTENTS

LIST OF ILLUSTRATIONS

LIST OF ILLUSTRATIONS (Continued)

LIST OF TABLES

SECTION I

INTRODUCTION

The rapid development of high performance aircraft gas turbine engines has necessitated corresponding advances in materials technology. Included in these advances are titanium alloys for fan and compressor components. These have contributed to gains in performance and efficiency because of their high strength and low density, resulting in favorable strength-to-weight ratios. Titanium alloys have gained wide acceptance and are currently being used at operating temperatures up to 482°C (900°F). Typical components made of titanium include static structures such as fan and compressor vanes and cases, and rotating components such as fan and compressor disks and blades.

Titanium, like several other metals, can be made to ignite and react in a rapid oxidation (exothermic) process. In the specific case of titanium, the reactivity is enhanced by a unique combination of thermophysical properties including a high heat of combustion, a low thermal conductivity and a spontaneous ignition temperature below its melting point. This latter property favors ignition rather than melting, thus producing additional rapid local temperature increases and rapid propagation of the resultant combustion once ignition occurs.

Several instances of titanium blade and vane ignition and combustion have occurred in gas turbine compressors over a wide range of ambient pressures and temperatures. Initiating conditions may include tip rubbing on the adjacent casing or blade/structure rubbing as a result of compressor stalls (blades deflect into the casing), rotor imbalance, entrapment of broken airfoil elements, and aircraft maneuvers. Aerodynamic heating of compressor components during a stall also has been established as the cause of ignition of titanium gas turbine components. Improved compressor seals have helped to reduce the blade tip-rubbing problem. However, the high-velocity airstream in axial-flow compressors enhances the continued combustion of any titanium blade or vane that does ignite and causes burning particles and molten metal to be sloughed off. These particles can be entrained in the airstream and impinge on downstream components, thereby spreading combustion. The results and extent of this spreading depends largely on the environmental conditions prevalent at the time of ignition and can vary from burning the tips of a few compressor blades, as illustrated in Figure 1, to the catastrophic destruction of an entire engine.

When the frequency of titanium fires showed a marked increase in 1970, an analytical study was initiated to define the gas turbine conditions conducive to sustained combustion. The results of the initial analytical study was a titanium combustion model which defined a sustained combustion limit above which fires were sustained and below which they were not. The model was based on an understanding of fires at that time and established combustion limits in terms of air temperature and compressor blade leading edge Reynolds Number. When the environmental conditions of the compressor vane stages of a typical gas turbine engine were compared with this initial model, the limit (stage) of utilization of a given alloy could be predicted. Figure 2 illustrates the manner in which this model could be used to predict the use of three alloys in a hypothetical compressor. Based upon figure 2, Ti 8-1-1 could be used in only the first stage, alloy Ti 13-11-3 in the first and second and Ti 13Cu could be used in stages 1 through 5.

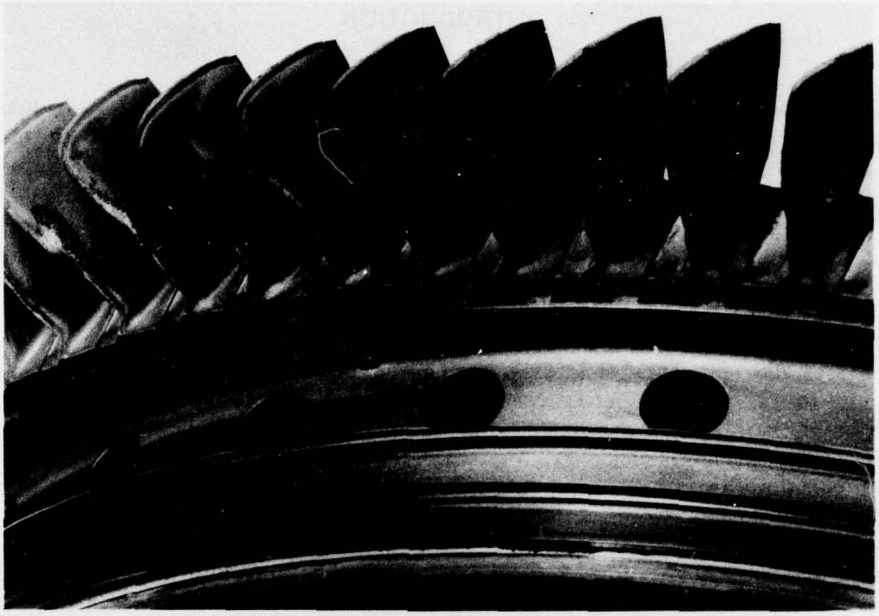

FE 134595

Figure 1. Compressor Blades in Gas Turbine After Minor Titanium Fire

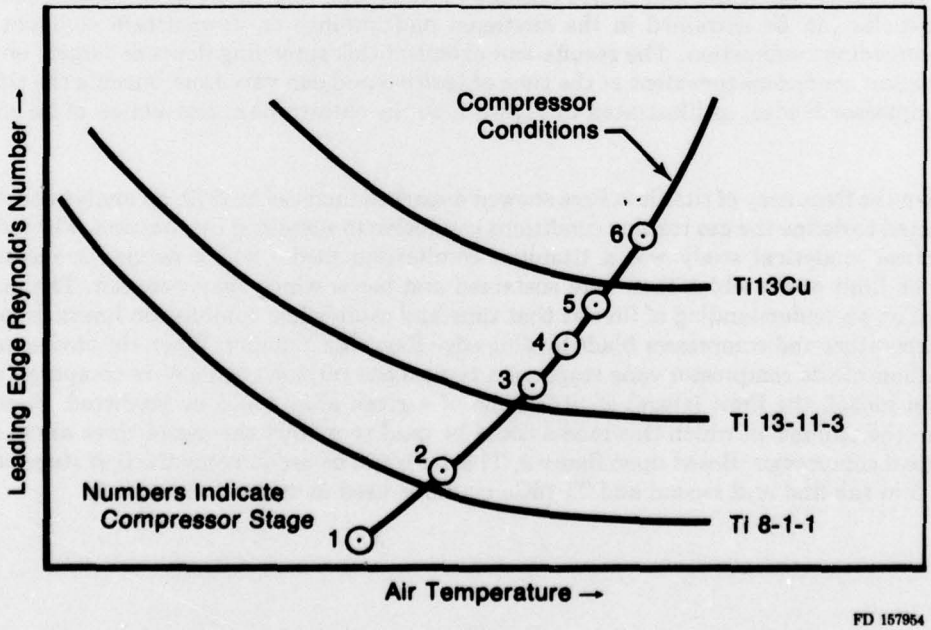

FD 157954

Figure 2. Predicted Combustion Limits for Titanium

More recently, under Air Force contract, the initial P&WA/Florida computer model for predicting the occurrence of fires is being modified to account for those things learned over the last several years such as the extent of molten metal flow across the titanium surface. In addition, improvements are being added to account for known coating and alloy effects which can, in effect, move the sustained combustion limit curve up, resulting in a wider safe environmental region of use for titanium alloys. Other factors are being added to allow analysis of rotating components and analysis of components ignited at any location on the airfoil rather than just the leading edge of an airfoil. These improvements make possible wider use of the model in predicting occurrence of fires.

The objective of the program described in this report was to delineate the relative ignition and combustion of several titanium alloys. In addition, a secondary objective was to explore the effect of specimen thickness on various combustion parameters.

SECTION II

TITANIUM IGNITION AND COMBUSTION TESTS

A. TEST MATERIALS AND CONDITIONS

1. Materials

The ignition and combustion characteristics of the following titanium alloys were tested during this program:

Ti 8Al-1Mo-1V
Ti 6Al-2Sn-4Zr-6Mo
Ti 13V-11Cr-3A1
Ti 13.5Al-21.5Nb
Ti 13Cu
Beta III (Ti 11.5Mo-6Zr-4.5Sn)
Ti 5Ni
Ti 10Ni
Ti 20Ni

The selection of these particular alloys was based upon several considerations. First, because of their extensive use in gas turbine engine applications, alloys Ti 8-1-1 and Ti 6-2-4-6 were chosen to provide a baseline performance upon which to compare the other test alloys.

During previous ignition and combustion studies, the alloys Ti 13-11-3 and Ti 13Cu failed to sustain combustion at the environmental test conditions employed. These alloys were included in this program, therefore, to extend their characterization to more severe environmental conditions.

The Ti_3Al alloy, modified to a composition of Ti 13.5Al-21.5Nb, was selected because it has potential for gas turbine engine component applications at temperatures above those currently possible for titanium alloys.

One of the objectives of this program was to investigate the ignition and combustion characteristics of a series of alloys formed by incremental additions of an alloying element in titanium. The element chosen was nickel since previous work had shown promise that a 20% nickel alloy of titanium would not sustain combustion. Nickel percentages of 1, 5, 10 and 20 were selected as the series of alloys to be investigated. The first test of this series, using the Ti 5Ni alloy, produced such an extensive burn that the Ti 1Ni alloy was eliminated from the test program since it held no apparent potential for providing useful data.

Two specimens of each of these special nickel alloys were produced by triple melting weighed amounts of commercially pure titanium and nickel. The resulting "buttons", approximately 50 grams in weight, were then forged into "pancakes" at 843 to 871°C (1550 to 1600°F). Each "pancake" was approximately 1.8 mm thick by 90 mm diameter (0.070 in. thick by 3.5 in. diameter) and served for the subsequent machining into one test specimen.

2. Test Conditions

The above alloys were tested at the following environmental conditions:

Temperature °C(°F)	*Pressure MPa (psia)*	*Airstream Velocity m/sec (ft/sec)*
454(850)	0.7(100)	244(800)
454(850)	0.7(100)	137(450)

These conditions were selected to provide needed data points to support alloy effect validation of the analytical combustion model and to supplement test data on the same or similar alloys previously obtained at other environmental conditions.

To facilitate and increase the significance of data analysis, temperature and pressure were maintained the same for both test conditions during the initially planned test series.

The higher velocity condition chosen was considered to be sufficiently severe to effect the combustion of all test alloys. This proved not to be the case. Therefore, late in the combustion test phase, temperature and pressure conditions of increased severity were selectively imposed during additional test runs of specific alloys in an attempt to define limits of combustibility for these alloys. The extent of these changes and the rationale governing their selection are discussed in paragraph III.C.

The lower velocity condition was selected to attempt the identification of the lower limits of combustibility for the alloys under evaluation.

B. TEST SPECIMEN CONFIGURATION

The configuration of the test specimens employed for the ignition and combustion tests is shown in Figure 3. This constant cross-section specimen was chosen to facilitate fabrication to close tolerances and improve the quality and interpretation of combustion rate data.

Except for the Ti Ni alloys, five to ten specimens were machined from each test alloy. Two specimens were prepared from each Ti Ni alloy being tested. Two test specimens from each alloy were then selected on the basis of thickness, width and knife-edge width. The primary selection criteria was to minimize specimen thickness variation.

Specimen thickness was determined by averaging micrometer readings taken at the seven locations shown in Figure 4. An initial, more comprehensive set of measurements taken on several samples established that these seven readings yielded a representative value for average thickness.

Knife-edge width was recorded as the average of the two sides taken at midspan.

Table 1 lists the weight, thickness, width and knife-edge width of the specimens selected for test. Length was also determined to aid in the reconstruction of burned specimens.

Prior to testing, the specimen was given a black nickel electroplated coating in the triangular area shown shaded in Figure 4. This dull black coating, centered on the knife-edge, serves to maximize and equalize the coupling of laser energy to the specimen by eliminating variations caused by reflectivity differences among the various alloys.

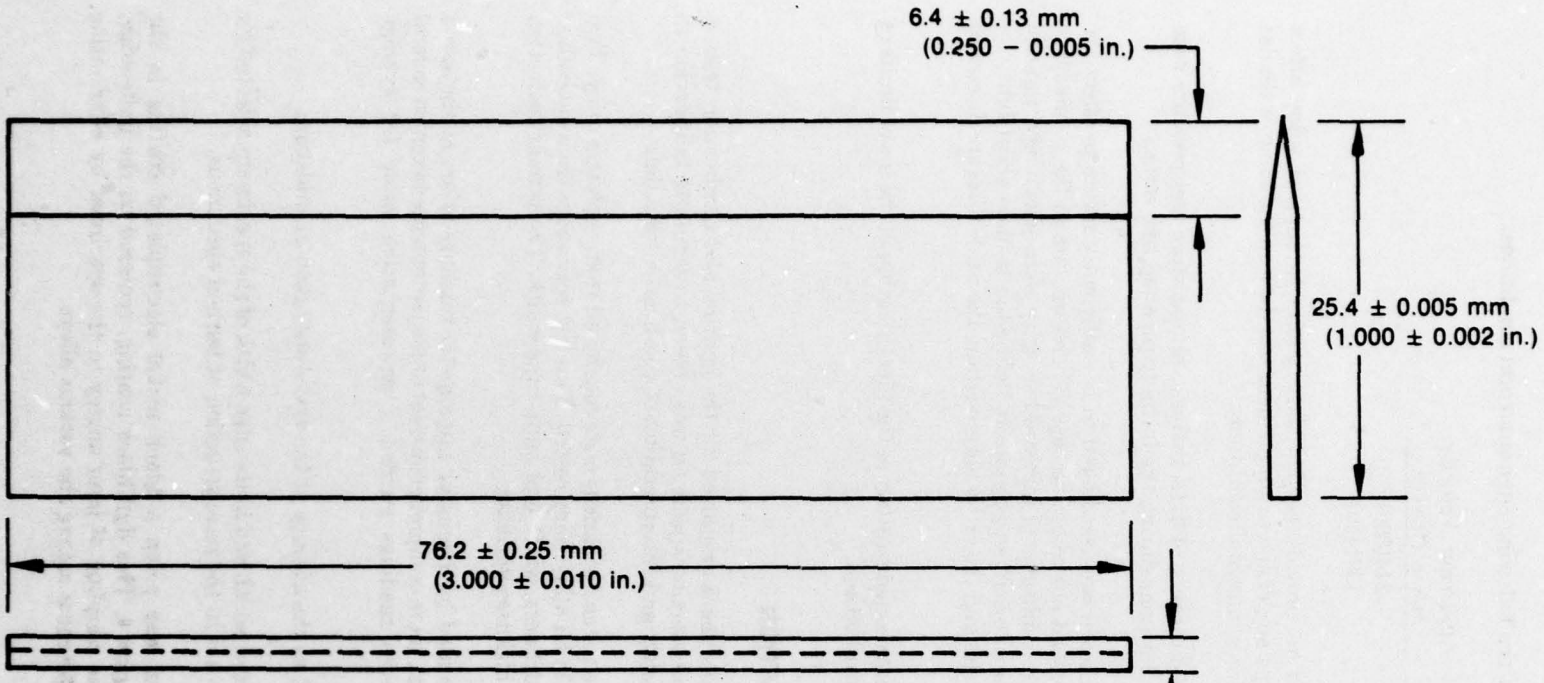

Nominal (mils)	Specimen Thicknesses	
	mm	in.
20	0.51 ± 0.03	0.020 ± 0.001
30	0.76 ± 0.03	0.030 ± 0.001
40	1.04 ± 0.03	0.041 ± 0.001
55	1.40 ± 0.03	0.055 ± 0.001
70	1.78 ± 0.05	0.070 ± 0.002

FD 145912

Figure 3. Test Specimen Configuration

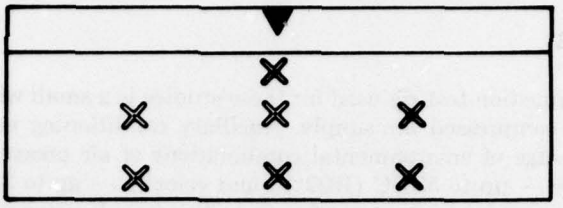

FD 139563

Figure 4. Specimen Thickness Measurement Points

TABLE 1. TEST SPECIMEN WEIGHT AND DIMENSIONS

Specimen Number	Alloy (mils)	Weight g	Dimensions							
			Thickness		Width		Knife-Edge Width		Length	
			mm	(inch)	mm	(inch)	mm	(inch)	mm	(inch)
N2-1	13-11-3	8.5424	1.034	(0.0407)	25.78	(1.015)	5.94	(0.234)	77.27	(3.042)
N2-2	13-11-3	8.0490	1.021	(0.0402)	24.64	(0.970)	7.11	(0.280)	77.57	(3.054)
N2-3	6-2-4-6	8.0282	1.059	(0.0417)	25.76	(1.014)	8.51	(0.335)	76.48	(3.011)
N2-4	6-2-4-6	7.7567	1.029	(0.0405)	25.76	(1.014)	7.85	(0.309)	76.35	(3.006)
N2-5	13 Cu	8.4429	1.011	(0.0398)	25.45	(1.002)	6.76	(0.266)	76.33	(3.005)
N2-6	13 Cu	8.3421	1.011	(0.0398)	25.45	(1.002)	6.81	(0.268)	76.33	(3.005)
N2-7	Beta III	8.7194	1.072	(0.0422)	25.43	(1.001)	7.11	(0.280)	77.06	(3.034)
N2-8	Beta III	8.5955	1.067	(0.0420)	25.40	(1.000)	7.32	(0.288)	76.78	(3.023)
N2-9	Ti_3Al	8.3310	1.069	(0.0421)	25.37	(0.999)	6.35	(0.250)	76.56	(3.014)
N2-10	Ti_3Al	8.4120	1.059	(0.0417)	25.32	(0.997)	6.32	(0.249)	76.50	(3.012)
N2-11	8-1-1(40)	8.2954	1.072	(0.0422)	25.45	(1.002)	6.50	(0.256)	76.23	(3.001)
N2-12	8-1-1(40)	8.3132	1.080	(0.0425)	25.45	(1.002)	6.07	(0.239)	76.35	(3.006)
N2-13	8-1-1(20)	3.8824	0.508	(0.0200)	25.45	(1.002)	6.50	(0.256)	76.50	(3.012)
N2-14	8-1-1(70)	14.0320	1.887	(0.0743)	25.40	(1.000)	6.86	(0.270)	76.28	(3.003)
N2-17	5 Ni	8.3171	1.062	(0.0418)	25.27	(0.995)	6.71	(0.264)	75.97	(2.991)
N2-18	5 Ni	8.2281	1.044	(0.0411)	25.25	(0.994)	6.60	(0.260)	75.95	(2.990)
N2-19	10 Ni	8.2365	1.034	(0.0407)	25.22	(0.993)	6.68	(0.263)	75.97	(2.991)
N2-20	10 Ni	8.1224	1.024	(0.0403)	25.20	(0.992)	6.91	(0.272)	75.95	(2.990)
N2-21	20 Ni	8.5157	1.021	(0.0402)	24.61	(0.969)	6.45	(0.254)	76.00	(2.992)
N2-21-1	20 Ni	8.5146	1.021	(0.0402)	24.61	(0.969)	6.45	(0.254)	76.00	(2.992)
N2-22	20 Ni	8.6686	1.024	(0.0403)	25.25	(0.994)	6.60	(0.260)	75.97	(2.991)
N2-22-1	20 Ni	8.6650	1.024	(0.0403)	25.25	(0.994)	6.60	(0.260)	75.97	(2.991)
N2-23	8-1-1(70)	14.0374	1.900	(0.0748)	25.37	(0.999)	7.16	(0.282)	76.56	(3.014)
N2-24	8-1-1(20)	4.0298	0.513	(0.0202)	25.45	(1.002)	6.48	(0.255)	76.40	(3.008)
N2-25	8-1-1(40)	7.6588	1.087	(0.0428)	24.21	(0.953)	6.53	(0.257)	76.45	(3.010)
N2-26	8-1-1(70)	14.0908	1.892	(0.0745)	25.35	(0.998)	7.52	(0.296)	76.48	(3.011)
N2-27	8-1-1(20)	3.9871	0.505	(0.0199)	25.43	(1.001)	6.50	(0.256)	76.23	(3.001)
N2-28	8-1-1(55)	10.6185	1.427	(0.0562)	25.40	(1.000)	7.01	(0.276)	76.05	(2.994)
N2-29	8-1-1(55)	10.3577	1.435	(0.0565)	25.50	(1.004)	8.05	(0.317)	76.71	(3.020)
N2-30	8-1-1(30)	6.3625	0.823	(0.0324)	25.40	(1.000)	6.40	(0.252)	77.67	(3.058)
N2-31	8-1-1(30)	6.0406	0.828	(0.0326)	25.40	(1.000)	7.19	(0.283)	77.70	(3.059)
N2-32	Ti_3Al	8.1586	1.026	(0.0404)	25.40	(1.000)	6.15	(0.242)	76.53	(3.013)
N2-33	Ti_3Al	8.0455	1.069	(0.0421)	25.40	(1.000)	6.81	(0.268)	76.43	(3.009)
N2-34	13 Cu	8.4753	1.021	(0.0402)	25.32	(0.997)	6.83	(0.269)	76.20	(3.000)
N2-35	13 Cu	8.2382	1.054	(0.0415)	25.35	(0.998)	7.62	(0.300)	76.35	(3.006)
N2-36	Beta III	8.0910	1.072	(0.0422)	25.37	(0.999)	7.26	(0.286)	76.68	(3.019)
N2-38	13-11-3	8.5357	0.968	(0.0381)	25.45	(1.002)	5.94	(0.234)	76.99	(3.031)
N2-39	13-11-3	8.9651	1.039	(0.0409)	25.43	(1.001)	6.38	(0.251)	76.94	(3.029)
N2-40	Ti_3Al	7.6155	1.021	(0.0402)	25.40	(1.000)	6.17	(0.243)	76.48	(3.011)
N2-41	8-1-1(40)	8.1874	1.087	(0.0428)	25.45	(1.002)	6.93	(0.273)	76.20	(3.000)

C. TEST FACILITIES

The titanium combustion test rig used for these studies is a small wind tunnel driven from a 2.41 MPa (350 psi) compressed air supply. Ancillary conditioning equipment permits the simulation of a wide range of environmental combinations of air pressure — up to 0.97 MPa (140 psia), temperature — up to 550°C (1022°F) and velocity — up to 335 m/sec (1100 ft/sec). Test specimens are mounted in a rectangular test chamber. Instrumentation is provided to monitor pressure and temperature at strategic locations in/on the rig.

The overall arrangement of the test rig is shown in Figure 5.

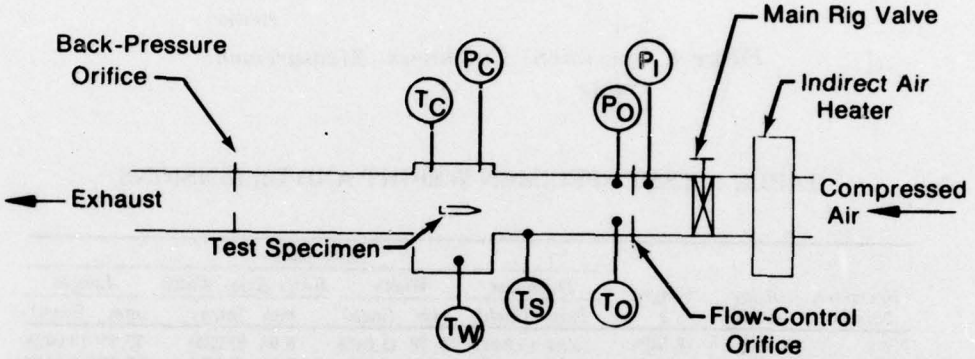

P_I = Orifice Upstream Pressure
P_O = Orifice Downstream Pressure
P_C = Test Chamber Pressure
T_O = Orifice Air Temperature
T_S = Rig Skin Temperature
T_C = Test Chamber Temperature
T_W = Window Temperature

FD 139565

Figure 5. Titanium Combustion Test Rig Schematic

Air, supplied from a large compressor, is passed through a gas-fired indirect heater and a flow-measuring orifice prior to entering the test section. The test section, shown schematically in Figure 6, is a 19.1 mm by 50.1 mm (0.75 in. by 2.0 in.) rectangular channel with a bellmouth inlet and 75 mm (3.0 in.) of straight section upstream of the airfoil leading edge. The test specimen mounts in a cylindrical carrier which is inserted into the test section. (See Figure 7.) Orifice plates, upstream and downstream of the test section, provide control of the flowrate and pressure level. Thermocouples are positioned to provide temperatures at the flow-measuring orifice, in the specimen test chamber, on the rig skin, and at the laser and camera windows. Points are provided to measure flow-control orifice upstream and downstream pressure as well as static pressure in the test chamber. (See Figure 5.) Airstream velocity is determined by calculation using the differential pressure (ΔP) across the flow-control orifice.

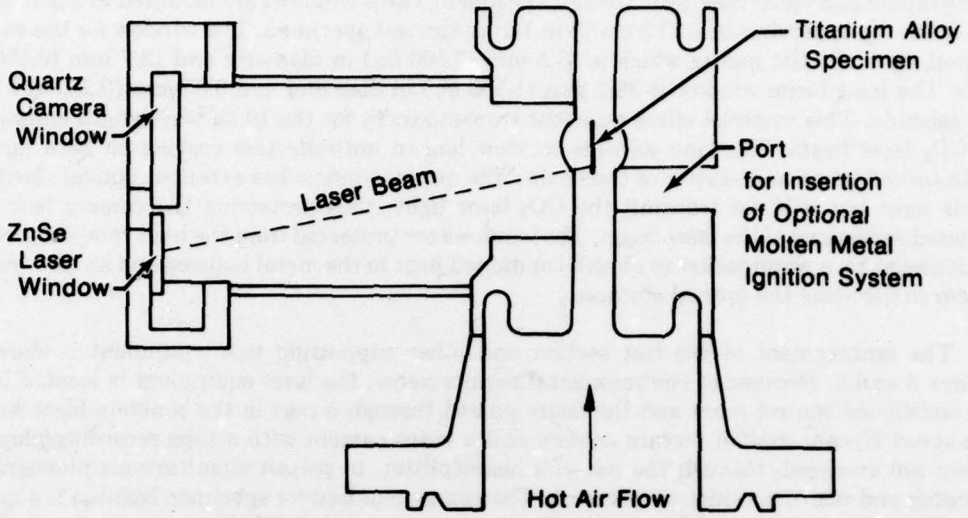

Figure 6. Titanium Combustion Rig Test Section

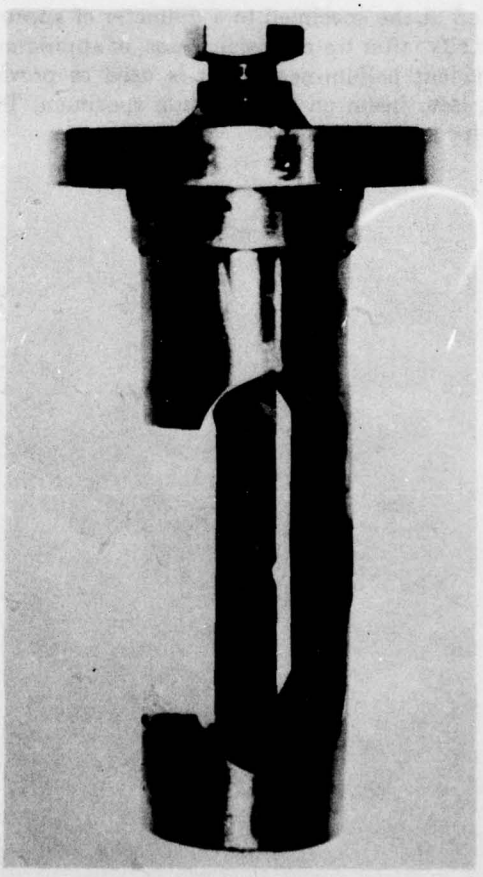

Figure 7. Test Specimen Holder

The test section has two windows, one for laser irradiation of the specimen and one for photographic and video viewing of the test specimen. These windows are mounted in a port on the side of the rig approximately 20.3 cm (8 in.) from the test specimen. The window for the camera is fused, optically flat quartz which is 63.5 mm (2.500 in.) in diameter and 12.7 mm (0.500 in.) thick. The laser beam window is 38.1 mm (1.500 in.) in diameter and 6.35 mm (0.250 in.) thick zinc selenide. This material offers excellent transmissivity for the 10.6μ wavelength emission of the CO_2 laser beam. The zinc selenide window has an antireflective coating on both faces to minimize reflection and scatter of the beam. The quartz window has excellent optical clarity for visible light but will not transmit the CO_2 laser light, thus protecting the camera lens from scattered reflections of the laser beam. The windows are protected from the high-temperature test environment by a water jacket to absorb conducted heat in the metal housing and an air injection system to film-cool the optical surfaces.

The arrangement of the test section and other supporting test equipment is shown in Figures 8 and 9. Because of environmental requirements, the laser equipment is located in the air-conditioned control room and the beam passed through a port in the concrete blast wall. A high-speed Hycam motion picture camera and a video camera with a tape recording/playback system are arranged, through the use of a beamsplitter, to permit simultaneous photographic recording and real-time video observation. The energy required for specimen ignition is supplied by a CRL Model 41 laser. This electric-discharge, water-cooled CO_2 laser system is capable of providing an output of approximately 250 watts in the Transverse Electromagnetic Mode (TEM) 00 at a transmission frequency of 10.6μ.

The beam is defocused at the specimen to a diameter of approximately 2 mm to yield an incident average power density, after transmission losses, of approximately 2.5 Kw/cm^2 absorbed by the specimen. A coincident helium-neon laser is used to provide a visible red beam for alignment of the hot CO_2 laser beam on the titanium specimen. This red alignment beam is observed using the videotape system.

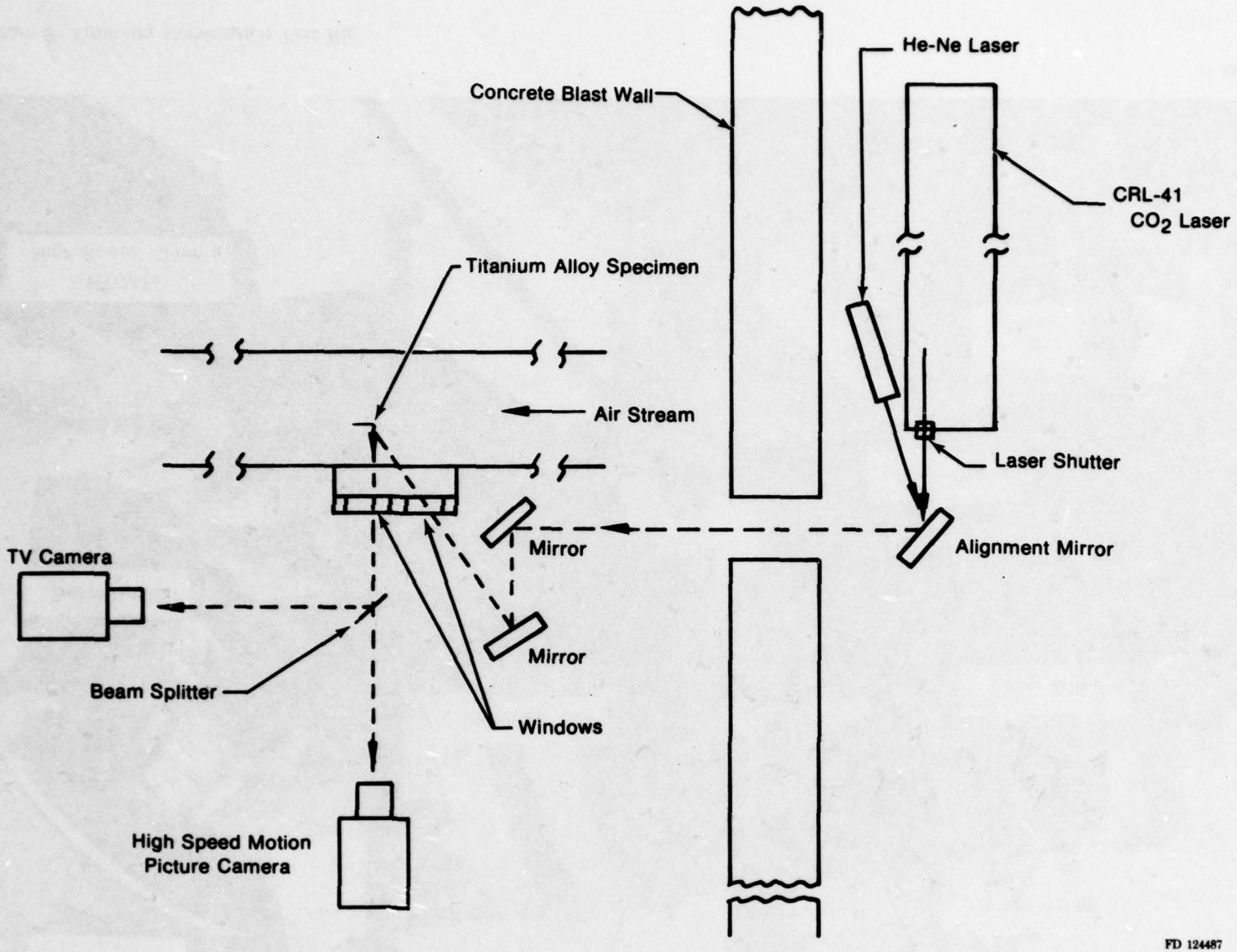

Figure 8. Arrangement of Laser Ignition and Photographic Recording Systems

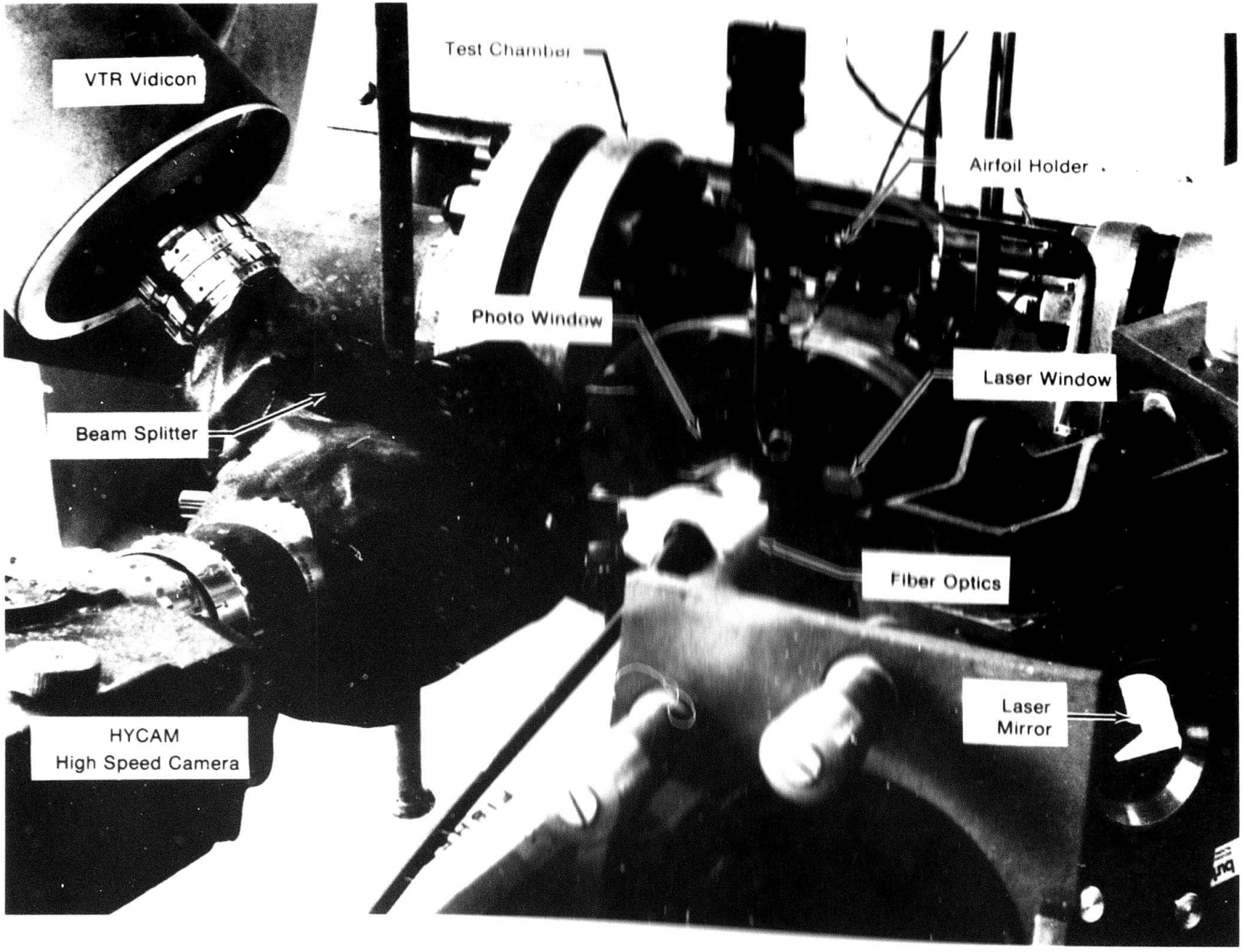

Figure 9. Titanium Combustion Test Rig

EC 42608B

D. TEST RUN PROCEDURE

Prior to a test run, the test specimen is secured in the specimen holder and mounted in the test chamber. Run values for air velocity and chamber pressure are established by installing a specific combination of flow-control and backpressure orifices in the test rig. After setting the heater to the desired temperature, airflow is introduced into the system and the test chamber allowed to come to thermal equilibrium. Near thermal equilibrium the laser optics are aligned using the visible helium-neon laser beam and the videotape system. Specimen illumination during laser, video and high-speed camera alignment and focusing is provided by a high intensity light transmitted from its source by fiber optics. During the run, light from the specimen ignition and burning is sufficiently intense to permit photodocumentation of burn propagation and melt transportation. An event marker (light pulse) is recorded on the side of the film on all runs to annotate the start and finish of the laser action during the run. The high-speed films are also marked with light pulses from a 1000-Hz timing generator to provide an absolute time reference for event sequences.

Just prior to the start of a run, final temperature and pressure adjustments are made by judicious throttling of the hot air valve and a cold air bleed input valve. Simultaneously, a final adjustment, if required, is made to the laser alignment. Final run parameters are then recorded and the test is initiated by a time-sequenced switch which, when actuated, starts the high-speed camera. Approximately 2 sec after camera start the sequencer opens the laser shutter to irradiate the specimen, thereby starting the run. The laser remains on for 5 sec before the sequencer closes the shutter. This time can be manually overridden when ignition occurs before the 5 sec has elapsed. The camera is allowed to run out of film at about 16 sec and is sequenced off at approximately 20 sec. The video system remains on at all times in a closed circuit television (CCTV) mode. Video tape recording is controlled manually during a run sequence. The instant replay and slow-motion/stop-frame capability of the color video recording permits immediate review of the test run for its potential impact on the next test run.

SECTION III

TEST RESULTS AND ANALYSIS

This section begins with a detailed assessment of the accuracy of the primary and derived data obtained during the course of the program. This is followed by a description of the procedure used in acquiring the various combustion parameters subsequently used as the basis for an analysis of the observed test performance. The final subsection presents an analysis of test results in terms of the effect of specimen thickness, specimen alloy and the test environmental conditions.

A. DATA ACCURACY ASSESSMENT

1. Time Data Accuracy

The accuracy of ignition and combustion time data is controlled by two factors. The first, and most significant, is the establishment of an accurate, reference time base. This reference point was taken as the first photographic frame containing the "laser on" annotation. The validity of this point as an accurate time reference is dependent upon defining its relationship to the actual opening of the laser shutter. A disparity between the occurrence of the event and the event marker can occur as a result of the difference in time between the corresponding relay closures in the automatic sequencer and upon camera geometry. These relays are manually set, using a stop-watch, to occur simultaneously and thus are subject to errors introduced by human perception and reaction time. In a separate test, employing a power source and an O-graph, the laser shutter relay was found to be closing 0.016 sec earlier than the event marker relay. In addition, due to camera film path geometry, the annotating light source placed the event marker on the film five frames behind the frame being exposed at the camera shutter.

Since the nominal film exposure was 1000 frames per sec, the above considerations established that the laser shutter opened 0.021 sec prior to the appearance of the "laser on" event marker. This event/marker time correlation is depicted diagramatically in Figure 10. Throughout data acquisition this event/marker displacement of approximately 0.021 sec was treated as 21 frames for purposes of establishing the zero setting of the Vanguard frame counter. On the average, the absolute error introduced by failing to consider individual frame-rate variations over this short interval was approximately 0.001 sec. Although this error would primarily impact the determination of ignition time, the subjective nature of the ignition event identification would tend to make this effect insignificant.

The second factor affecting ignition and combustion event timing is the true camera film transport rate. This rate was initially set on the camera indication of 1000 frames per sec. This was subsequently increased when a check of the run film indicated that actual rates were approximately 900 frames per sec after the initial 2-sec ramp up to equilibrium speed. This change resulted in achieving a range of 1000 to 1050 frames per sec for the balance of the test runs. Because film transport rate tended to vary slightly from run to run, it was necessary to determine the actual time interval of an individual frame on the photographic record of each test run. This was accomplished by counting the number of 1000 Hertz, pulse generator annotations recorded on a 100-frame segment selected from the burn portion of the run film. From this actual time for the occurrence of 100 frames the true frame rate can be readily calculated. The accuracy of this frame rate data is estimated to be 2 frames per sec or approximately 0.2%

In summary consideration of the foregoing accuracy factors, ignition and combustion event time data acquired from the high-speed motion picture films was shown to be accurate to within ±0.6% (maximum).

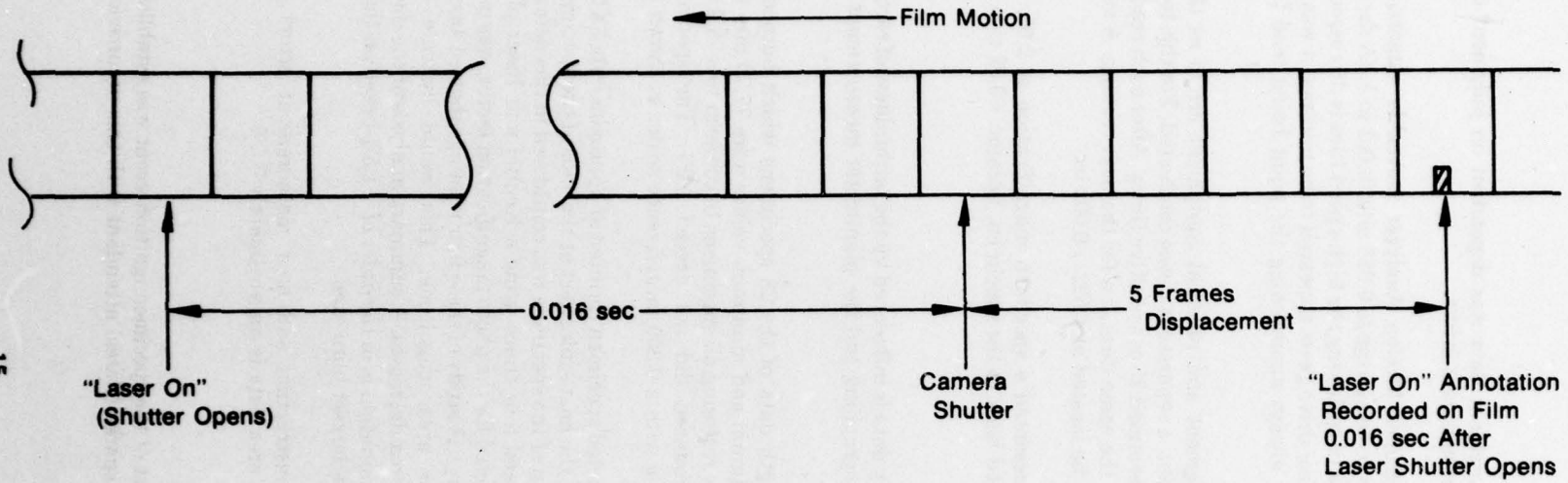

Laser Irradiation of Specimen Begins 0.016 sec + 5 Frames Prior to the Appearance of the "Laser On" Annotation at the Camera Shutter

FD 145913

Figure 10. Correlation of "Laser On" Annotation With True Laser On Event

2. Distance Data Accuracy

The accuracy of distance measurement data was dependent on judgment considerations and to a lessor extent on physical measurement errors.

Position indicators for the Vanguard Motion Analyzer moveable cursors permit direct readout of "X" and "Y" points on the screen image to 0.025 mm (0.001 in.). (A description of the Vanguard Motion Analyzer and its use in reviewing the high-speed film is discussed in paragraph III.B.3.) Although backlash in the cursor drive gears appeared to be minimal it was, nevertheless, eliminated as an accuracy factor by always approaching the point being read from the same direction.

To evaluate the combined judgment and physical equipment errors as they affect the repeatability of a distance measurement, a separate test was conducted. For this test the location of a representative melt front was determined 25 consecutive times. After each reading the cursor was backed off and approached from the same direction for the next reading. A summary of the 25 readings showed the melt front to be located at 4.022 $\pm$0.002 in.

Since the Vanguard image represented a specimen magnification of 2.65, the combined position reading error, when referenced back to the specimen, became $<$0.02 mm ($<$0.0008 in.).

3. Area Data Accuracy

The accuracy of the burn severity data is influenced by the faithfulness of reconstructing the burned specimen fragments for photographing and the planimeter measurement of the burned area.

An analysis of the original length data of the 28 specimens which burned indicated an average of 76.5 mm (3.012 in.). Maximum and minimum values were 77.70 mm (3.059 in.) and 75.95 mm (2.990 in.), respectively. By restoring all specimens to conform to a 76.2 mm (3.000 in.) template, the maximum error introduced did not exceed 2.0%. The specimens, thus reconstructed, were photographed along with a 0.250 in. reference scale, as shown in Figure 11.

The photograph of the reconstructed specimen (printed at approximately 3X) was then used to determine area burned. Because of the heat-sink effect at the ends of the specimen holder, only the 53.3 mm (2.10 in.) exposed portion of the specimen was considered in this determination. The burn area of each specimen was traced four times using a Keuffel and Esser planimeter. The average of these readings, when corrected for the photo magnification factor, was used to compute the percent area burned (burn severity). A study of these four readings showed an expected, fairly constant range independent of the area magnitude. This would indicate that the area measurement error increases as the area decreases. A summary analysis of the data showed that the maximum error of the area determination is in the order of $\pm$1.5% based on the smallest burn area and decreasing to $\pm$0.5% for the largest burn area.

Combining the specimen reconstruction and area measurement errors the maximum probable error of the specimen burn area data is approximately 3.5%.

4. Ignition Event Accuracy

Criteria for identifying the onset of the specimen ignition event was established as the first discernible condition of melt or the sparks (flares) attendant with this occurrence.

For most specimens, sparks represented the criteria governing detection of the ignition event since they occurred prior to the appearance of melt quantities sufficient to ascertain movement. In a few cases a detectable melt movement did occur prior to a spark. In these instances two frames (approximately 0.002 sec) were required to verify motion and, therefore, the existence of a melt condition.

Thus, it is concluded that the error associated with identification of the ignition event does not exceed one frame (approximately 0.001 sec) and then only for a small number of specimens.

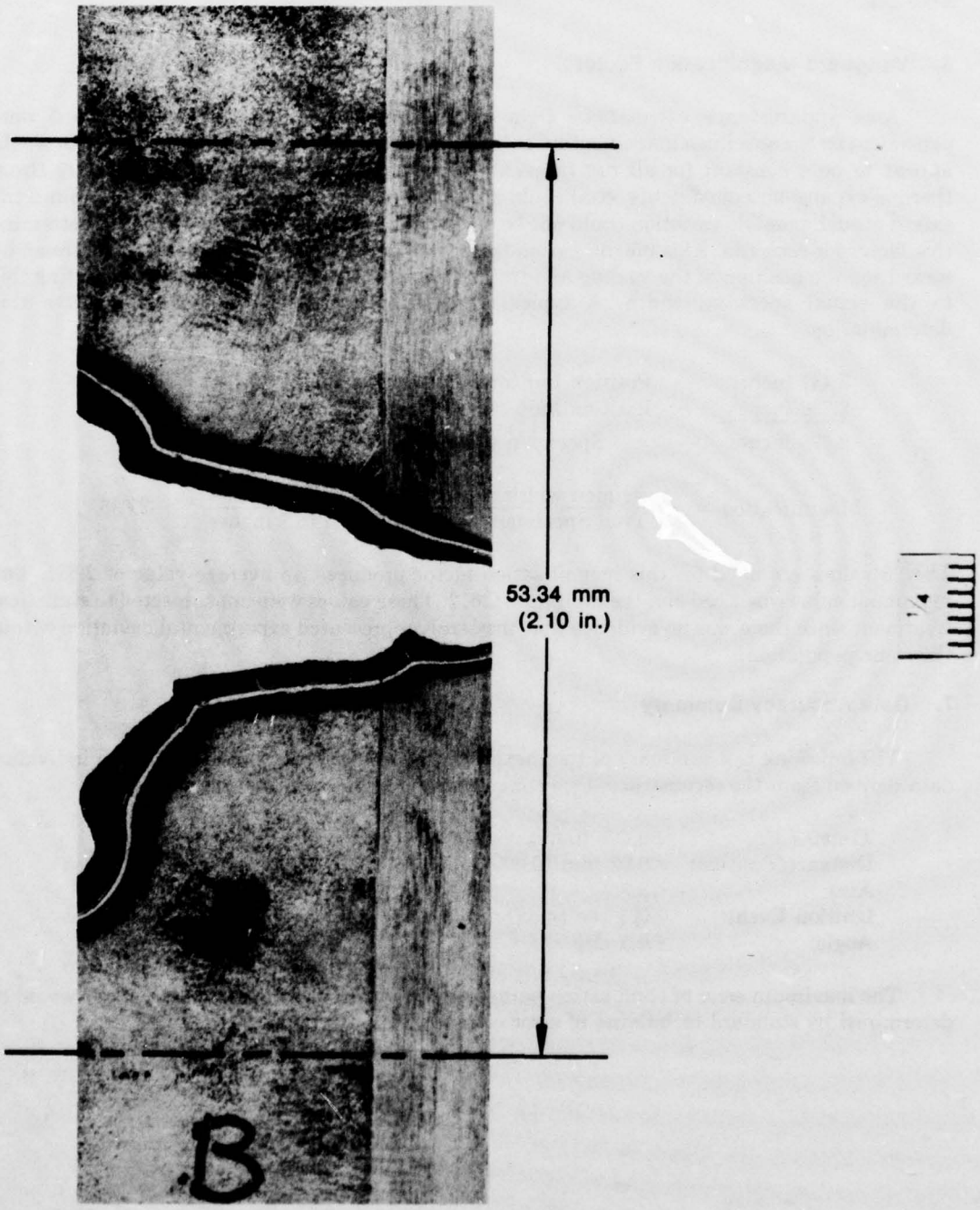

FD 145914

Figure 11. Reconstructed Specimen

5. Angular Data Accuracy

An angular setting on the Vanguard Motion Analyzer permits a direct vernier readout to the nearest ¼ deg. The accuracy of angular data, however, is determined primarily by human judgment in deciding where to locate the cursor on a typical, slightly-curved burnfront. Repeated test readings of a single angular spanwise burnfront established that the maximum range of these readings did not exceed one degree. Thus, angular measurements are assumed to be accurate to ±0.5 deg.

6. Vanguard Magnification Factor

Area and distance calculations from still photographs taken off the Vanguard were dependent on the specimen magnification at the screen. Although this magnification factor would appear to be a constant for all run films, slight variations in camera set-up geometry (from thermal expansion, adjustments, etc.) could affect the relative image size on the film. Since the extent of such possible variation could not be assessed, the only valid approach was to determine this factor for each run. This magnification factor was determined for each burned specimen by measuring the position of the leading and trailing edges of the specimen image and relating this to the actual specimen width. A typical calculation for specimen N2-1 illustrates this determination:

5.441 inches	—	Position Indicator at Leading Edge
−2.766 inches	—	Position Indicator at Trailing Edge
2.675 inches	—	Specimen width on screen

$$\text{Magnification} = \frac{\text{Specimen width on Screen}}{\text{True Specimen Width}} = \frac{2.675 \text{ inches}}{1.015 \text{ inches}} = 2.635$$

The 26 values obtained for this magnification factor produced an average value of 2.651. The maximum value was 2.686 and the minimum 2.612. These values were not subjected to statistical treatment since there was no evidence that they truly represented experimental deviation within the same population.

7. Data Accuracy Summary

The following is a summary of the maximum parameter error to be expected in individual data derived from the reconstructed specimen and the high-speed motion picture film:

Time:	±0.6% (max)
Distance/Position:	<0.02 mm (0.0008 in.)
Area:	<3.5%
Ignition Event:	0.001 sec (max)
Angle:	±0.5 deg

The maximum error of combustion parameters involving two or more of the above would be determined by standard techniques of error combination.

B. DATA ACQUISITION PROCEDURE

This subsection contains a detailed description of the procedures used in converting the basic raw data into forms suitable for use in the subsequent analysis and interpretation of test performance.

Table 2 contains a correlation between the basic data obtained from the test program and the data derived from it.

TABLE 2. CORRELATION OF BASIC AND DERIVED DATA

Basic Data		*Derived Data*	
Data Item	*Included in Table*	*Data Item*	*Included in Table*
Environmental run conditions	3	Summary of run conditions	4
Specimen weight loss	5	% Weight loss	5
% Specimen area burned	5	Burn severity	5
Time to first melt	6	Ignition time	6
Time for melt front to reach 0.4, 0.5, 0.6, 0.7, 0.8, 0.9 and 1.0 in. from leading edge	7	Burn-through time Average chordwise burn velocity Incremental burn velocity Incremental melt front velocity	6 6 7 7
Melt photographs at the above distances	—	Incremental melt area Maximum melt area (at 1.0 in.)	10 10
Spanwise burn distance (after burn-through) at various frame intervals	8	Spanwise incremental burn velocity Spanwise average burn velocity Spanwise burn angle	8 6 9
Combustion photographs at equal time intervals	—	Burn comparison photo-matrices	Various figures

Test program data emanated from three sources; test chamber environmental conditions, the specimen itself and the high speed film coverage of the test run.

1. Test Run Data

Test chamber environmental temperature and pressure data, recorded just prior to the test run, served only to permit calculation of airstream velocity and to verify compliance with the established run parameters. This test run environmental data is included in Table 3 and summarized in Table 4. Since chamber temperature changes influenced the attained airstream velocity, Table 4 summarizes only the data representing the two environmental run conditions initially established for the test program. An analysis of this summary shows the following maximum and minimum variations from the average:

Parameter	*Deviation From Average (%)*
Pressure	+0.9
	−1.1
Temperature	+0.8
	−0.6
Velocity	
Low	+3.9
	−4.5
High	+0.8
	−0.8

TABLE 3. TEST RUN ENVIRONMENTAL DATA

Specimen Number	Alloy (mils)	Temperature °C	Temperature (°F)	Pressure MPa	Pressure (psia)	Velocity m/sec	Velocity (ft/sec)
N2-1	13-11-3	456	(853)	0.69	(100)	141	(464)
N2-2	13-11-3	456	(853)	0.68	(99)	247	(810)
N2-3	6-2-4-6	459	(859)	0.70	(101)	141	(462)
N2-4	6-2-4-6	457	(855)	0.70	(101)	246	(807)
N2-5	13 Cu	454	(850)	0.69	(100)	138	(454)
N2-6	13 Cu	457	(854)	0.69	(100)	245	(803)
N2-7	Beta III	457	(854)	0.69	(100)	141	(463)
N2-8	Beta III	457	(854)	0.69	(100)	246	(808)
N2-9	Ti_6Al	457	(854)	0.69	(100)	141	(463)
N2-10	Ti_6Al	457	(854)	0.69	(100)	246	(806)
N2-11	8-1-1 (40)	460	(860)	0.70	(101)	136	(445)
N2-12	8-1-1 (40)	456	(852)	0.70	(101)	245	(803)
N2-13	8-1-1 (20)	454	(850)	0.69	(100)	148	(484)
N2-14	8-1-1 (70)	456	(852)	0.69	(100)	141	(464)
N2-17	5 Ni	458	(856)	0.69	(100)	141	(464)
N2-18	5 Ni	456	(853)	0.69	(100)	243	(797)
N2-19	10 Ni	454	(849)	0.68	(99)	145	(475)
N2-20	10 Ni	457	(854)	0.69	(100)	244	(800)
N2-21	20 Ni	459	(859)	0.70	(101)	143	(470)
N2-21-1	20 Ni	514	(958)	0.69	(100)	254	(832)
N2-22	20 Ni	455	(851)	0.68	(99)	244	(801)
N2-22-1	20 Ni	509	(949)	0.69	(100)	152	(498)
N2-23	8-1-1 (70)	455	(851)	0.69	(100)	141	(462)
N2-24	8-1-1 (20)	458	(857)	0.69	(100)	142	(465)
N2-25	8-1-1 (40)	454	(849)	0.69	(100)	142	(465)
N2-26	8-1-1 (70)	456	(852)	0.69	(100)	244	(799)
N2-27	8-1-1 (20)	456	(852)	0.69	(100)	245	(804)
N2-28	8-1-1 (55)	458	(856)	0.69	(100)	246	(806)
N2-29	8-1-1 (55)	456	(852)	0.69	(100)	144	(472)
N2-30	8-1-1 (30)	453	(848)	0.69	(100)	244	(801)
N2-31	8-1-1 (30)	454	(850)	0.69	(100)	146	(480)
N2-32	Ti_6Al	429	(804)	0.48	(70)	237	(777)
N2-33	Ti_6Al	424	(795)	0.69	(100)	240	(789)
N2-34	13 Cu	509	(948)	0.70	(101)	148	(487)
N2-35	13 Cu	510	(950)	0.70	(101)	252	(828)
N2-36	Beta III	426	(799)	0.48	(70)	237	(776)
N2-38	13-11-3	509	(948)	0.69	(100)	151	(497)
N2-39	13-11-3	511	(952)	0.69	(100)	255	(835)
N2-40	Ti_6Al	511	(952)	0.28	(40)	245	(804)
N2-41	8-1-1 (40)	429	(804)	0.69	(100)	141	(463)

TABLE 4. SUMMARY OF RUN CONDITIONS

Test Run Parameter	Established Value	Values Obtained: Highest	Lowest	Average
Chamber Pressure MPa (psia)	0.69 (100)	0.70 (101)	0.68 (99)	0.69 (100.1)
Specimen Temperature °C (°F)	454 (850)	460 (860)	453 (848)	456 (853.2)
Airstream Velocity m sec (ft/sec)	137 (450)	148 (484)	136 (445)	142 (465.8)
	244 (800)	247 (810)	243 (797)	245 (803.5)

This close control allowed the elimination of variations in environmental conditions as a factor in the subsequent analysis of run data.

2. Burn Severity Data

Data for the determination of burn severity was obtained by reconstructing and photographing the burned specimen. Using a planimeter, the area burned was measured from the enlarged photograph. Burn severity was calculated in the manner described in paragraph III.A.3. Table 5 shows the burn severity value for all specimens.

TABLE 5. TEST SPECIMEN BURN SEVERITY DATA

Specimen Number	Alloy (mils)	Reaction to Laser	Weight (gms)			Wt Loss (%)	Area Burned (%)
			Initial	After Burn	Loss		
N2-1	13-11-3	B	8.5424	7.6061	0.9363	11.0	13.8
N2-2	13-11-3	N	8.0490	8.0472	0.0018	~0	—
N2-3	6-2-4-6	B	8.0282	2.6357	5.3925	67.2	100.0
N2-4	6-2-4-6	B	7.7567	1.9944	5.7623	74.3	100.0
N2-5	13 Cu	N	8.4429	8.4423	0.0006	~0	—
N2-6	13 Cu	N	8.3421	8.3412	0.0009	~0	—
N2-7	Beta III	B	8.7194	7.4171	1.3023	14.9	20.5
N2-8	Beta III	B	8.5955	7.4288	1.1667	13.6	17.8
N2-9	Ti_6Al	B	8.3310	7.8443	0.4867	5.8	7.0
N2-10	Ti_6Al	B	8.4120	7.5453	0.8657	10.3	11.9
N2-11	8-1-1 (40)	B	8.2954	5.3502	2.9452	35.5	46.9
N2-12	8-1-1 (40)	B	8.3132	3.9504	4.3628	52.5	72.1
N2-13	8-1-1 (20)	B	3.8824	1.0172	2.8652	73.8	100.0
N2-14	8-1-1 (70)	B	14.0320	4.7866	9.2454	65.9	92.5
N2-17	5 Ni	B	8.3171	2.9861	5.3310	64.1	92.8
N2-18	5 Ni	B	8.2281	4.8017	3.4264	41.6	53.9
N2-19	10 Ni	B	8.2365	5.0037	3.2340	39.3	53.1
N2-20	10 Ni	B	8.1224	6.9768	1.1456	14.1	17.6
N2-21	20 Ni	N	8.5157	8.5159	~0	~0	—
N2-21-1	20 Ni	N	8.5146	8.5144	~0	~0	—
N2-22	20 Ni	N	8.6686	8.6661	0.0025	~0	—
N2-22-1	20 Ni	N	8.6650	8.6629	0.0021	~0	—
N2-23	8-1-1 (70)	B	14.0374	5.2526	8.7848	62.6	86.1
N2-24	8-1-1 (20)	B	4.0298	1.0948	2.9350	72.8	100.0
N2-25	8-1-1 (40)	B	7.6588	6.0573	1.6015	20.9	25.2
N2-26	8-1-1 (70)	B	14.0908	4.2586	9.8322	69.8	98.8
N2-27	8-1-1 (20)	B	3.9871	1.6092	2.3779	59.6	70.7
N2-28	8-1-1 (55)	B	10.6185	3.1193	7.4992	70.6	99.4
N2-29	8-1-1 (55)	B	10.3577	5.1751	5.1826	50.0	63.9
N2-30	8-1-1 (30)	B	6.3625	4.8922	1.4703	23.1	28.1
N2-31	8-1-1 (30)	B	6.0406	2.0021	4.0385	66.9	93.5
N2-32	Ti_6Al	N	8.1586	8.1589	~0	~0	—
N2-33	Ti_6Al	B	8.0455	7.3708	0.6747	8.4	9.9
N2-34	13 Cu	N	8.4753	8.4756	~0	~0	—
N2-35	13 Cu	N	8.2382	8.2380	~0	~0	—
N2-36	Beta III	B	8.6910	7.9096	0.7814	9.0	9.7
N2-38	13-11-3	N	8.5357	8.5362	~0	~0	—
N2-39	13-11-3	N	8.9551	8.9550	~0	~0	—
N2-40	Ti_6Al	B	7.6155	6.8120	0.8035	10.6	12.9
N2-41	8-1-1 (40)	B	8.1874	4.0723	4.1151	50.3	66.5

N = Notch: Energy input from the laser was sufficient, in these cases, to ignite the specimens over some limited area, however, the energy being generated from the combustion process was less than the combined heat losses so the burning processes ceased before reaching midspan.

B = Burn: The specimen ignited and sustained combustion propagated across the width of the airfoil.

3. High-Speed Film Data

The majority of test data was obtained from the high-speed film coverage of each test run. This data took the form of:

- Time to first sign of heating
- Time to ignition
- Time for the melt front and burn front to reach predetermined increments during chordwise burn
- Time vs incremental spanwise burn distance
- Melt photographs at specific times or locations.

Review and analysis of the high-speed film was performed using a Vanguard Motion Analyzer Model M-16C, Vanguard Instrument Corporation, New York. (See Figure 12.) This apparatus is a continuously variable frame-rate (0 to 24 frames/sec) motion picture projector which back-projects a magnified frame to an integral ground glass screen. This screen contains moveable X and Y axis cursors geared to position indicators which permit a readout to the nearest 0.001 in. In addition, a superimposed clear screen face containing parallel fixed cursors (0.75 in. apart) is rotatable and calibrated to permit reading angles to the nearest 0.25 deg.

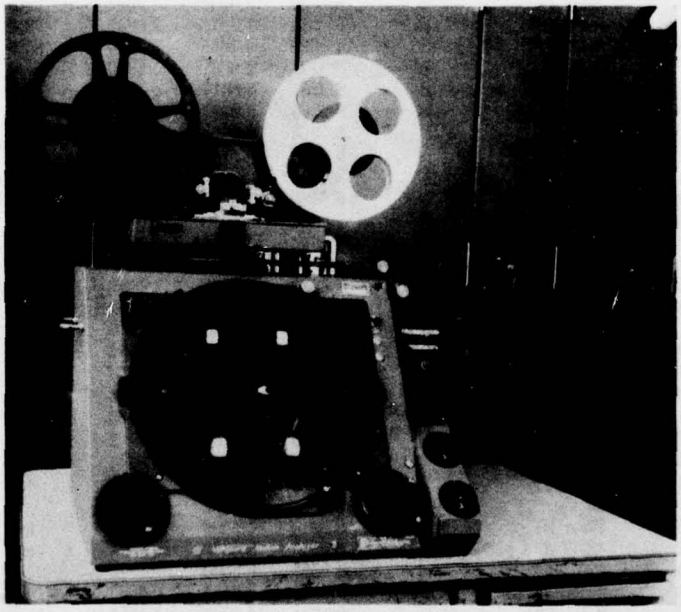

FE 341234

Figure 12. Vanguard Motion Analyzer

The balance of this subsection is a description of the typical data acquisition sequence used in extracting the primary test run data from the film.

The film was threaded on the Vanguard Motion Analyzer and advanced to display the first frame containing the "laser on" annotation. The film was then reversed for 21 frames and the

frame counter set to zero. As discussed in paragraph III.A.1, this corresponded to the time at which the laser shutter opened to irradiate the specimen. From this point the film was advanced by single frames until the visible, red helium-neon laser beam first showed a change to yellow indicating heating by the "hot" CO_2 laser beam. This frame number was recorded as the first visible heat. Single frame advance was continued until the ignition event (as defined in paragraph III.A.4) was located and recorded. This data is shown in Table 6.

TABLE 6. TEST SPECIMEN IGNITION AND BURN VELOCITY DATA

Specimen Number	Alloy (mils)	Time (ms) First Vis. Heat	Time (ms) Ignition	Time (ms) Burn Through	Time (ms) Total Burn	Average Burn Velocity Chord cm/sec	Average Burn Velocity Chord (in/sec)	Average Burn Velocity Span cm/sec	Average Burn Velocity Span (in/sec)
N2-1	13-11-3	19	47	831	4288	3.25	(1.28)	0.64	(0.25)
N2-2	13-11-3	18	22	—	1963	—	—	—	—
N2-3	6-2-4-6	59	90	589	3297	5.08	(2.00)	1.57	(0.62)
N2-4	6-2-4-6	8	25	343	3959	7.98	(3.14)	1.45	(0.57)
N2-5	13 Cu	10	22	—	93	—	—	—	—
N2-6	13 Cu	7	14	—	75	—	—	—	—
N2-7	Beta III	11	44	722	4067	3.73	(1.47)	0.84	(0.33)
N2-8	Beta III	7	34	393	2320	7.09	(2.79)	2.34	(0.92)
N2-9	Ti_3Al	13	37	903	2763	2.92	(1.15)	0.25	(0.10)
N2-10	Ti_3Al	8	42	480	2000	5.79	(2.28)	1.57	(0.62)
N2-11	8-1-1(40)	19	34	638	4203	4.22	(1.66)	1.27	(0.50)
N2-12	8-1-1(40)	18	45	432	5457	6.55	(2.58)	1.55	(0.61)
N2-13	8-1-1(20)	— Film Ruined —							
N2-14	8-1-1(70)	16	35	1029	6621	2.57	(1.01)	0.94	(0.37)
N2-17	5 Ni	— Film Ruined —							
N2-18	5 Ni	5	20	349	3880	7.72	(3.04)	2.69	(1.06)
N2-19	10 Ni	12	23	754	8557	3.48	(1.37)	1.14	(0.45)
N2-20	10 Ni	5	15	2921	4961	6.05	(2.38)	1.12	(0.44)
N2-21	20 Ni	24	32	—	40	—	—	—	—
N2-21-1	20 Ni	21	22	—	133	—	—	—	—
N2-22	20 Ni	4	8	—	40	—	—	—	—
N2-22-1	20 Ni	2	9	—	45	—	—	—	—
N2-23	8-1-1(70)	8	36	955	5496	2.77	(1.09)	0.91	(0.36)
N2-24	8-1-1(20)	9	42	396	3393	7.16	(2.82)	1.55	(0.61)
N2-25	8-1-1(40)	7	13	672	4016	3.68	(1.45)	1.30	(0.51)
N2-26	8-1-1(70)	5	43	574	3734	4.78	(1.88)	1.55	(0.61)
N2-27	8-1-1(20)	3	26	243	3318	11.71	(4.61)	1.85	(0.73)
N2-28	8-1-1(55)	5	26	453	5485	5.94	(2.34)	1.30	(0.51)
N2-29	8-1-1(55)	5	35	737	7495	3.61	(1.42)	1.35	(0.53)
N2-30	8-1-1(30)	4	14	313	2115	8.48	(3.34)	—	—
N2-31	8-1-1(30)	3	36	466	4168	5.92	(2.33)	1.32	(0.52)
N2-32	Ti_3Al	22	48	—	2711	—	—	—	—
N2-33	Ti_3Al	27	83	608	1613	4.83	(1.90)	1.45	(0.57)
N2-34	13 Cu	6	22	—	656	—	—	—	—
N2-35	13 Cu	12	17	—	228	—	—	—	—
N2-36	Beta III	23	42	582	2160	4.70	(1.85)	3.33	(1.31)
N2-38	13-11-3	9	30	—	1185	—	—	—	—
N2-39	13-11-3	9	25	—	202	—	—	—	—
N2-40	Ti_3Al	18	50	1034	3197	2.59	(1.02)	0.84	(0.33)
N2-41	8-1-1(40)	4	31	585	6042	4.60	(1.81)	1.30	(0.51)

The next task was to establish the location of the specimen leading edge and trailing edge in terms of the Vanguard position indicator dial reading. Location of the leading edge is evident very early in the burn when the ignited area burned back to the leading edge and then began consuming the specimen in a spanwise direction. The moveable cursor was set on this point and the dial reading recorded. The trailing edge was most readily identified from a frame containing sparks or flares which produced sufficient light to permit specimen definition. Again its location in terms of Vanguard dial reading was recorded. From the location of the leading and trailing edges, the Vanguard magnification factor was calculated in accordance with the method described in paragraph III.A.6.

Knowledge of the magnification factor permitted locating discrete points on the specimen. For the first analysis effort these points were established as 0.25 cm (0.1 in.) increments 1.02 to 2.54 cm (0.4 to 1.0 in.) from the leading edge. The 1.02 cm (0.4 in.) location was selected as the initial data point to eliminate the potential influence of the knife edge on combustion propagation data. When correlated with the Vanguard magnification factor and leading edge location these points could then be identified on the screen image.

For example, if the magnification factor is 2.635 and the leading edge is at 5.441 in. on the Vanguard "X" cursor dial, then the 0.4 in. location (on the screen) is at $5.441 - (0.4 \times 2.635) = 4.387$ in. Successive points are located at dial setting increments of 0.264 in. (0.1×2.635).

Once this "calibration" of the screen image was complete, data analysis was able to proceed. This phase of the analysis consisted of determining the time at which the melt front and burn front reach the increments identified above. In addition, through the use of the ancillary still camera setup shown in Figure 13, photographs were taken of the melt area displayed on the screen at these points.

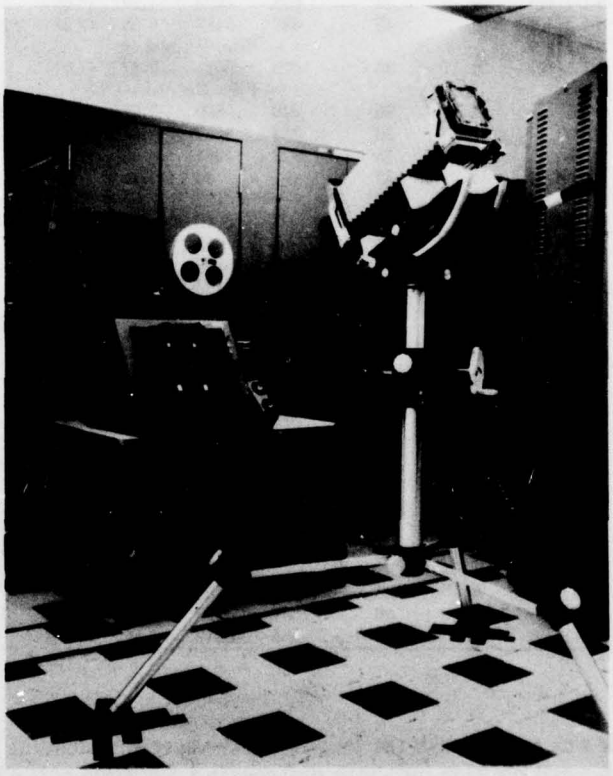

FE 341233

Figure 13. Vanguard-Camera Setup for Still Photographic Documentation

Data acquisition began by setting the "X" cursor to the position indicator setting previously calculated to represent the desired location. The film was then advanced until the melt front came into alignment with the cursor. The frame counter was read and recorded for eventual

conversion into time (per paragraph III.A.1) and the film frame photographed. Figure 14 shows a typical example of this photograph. The film was then advanced until the burn front aligned with the cursor. The frame counter was read and recorded. This process was repeated at each increment until the specimen was severed when the burn front reached the trailing edge. The final data point taken for this acquisition phase was to identify and record the last frame in which combustion was discernible. This constituted the raw data for total burn time.

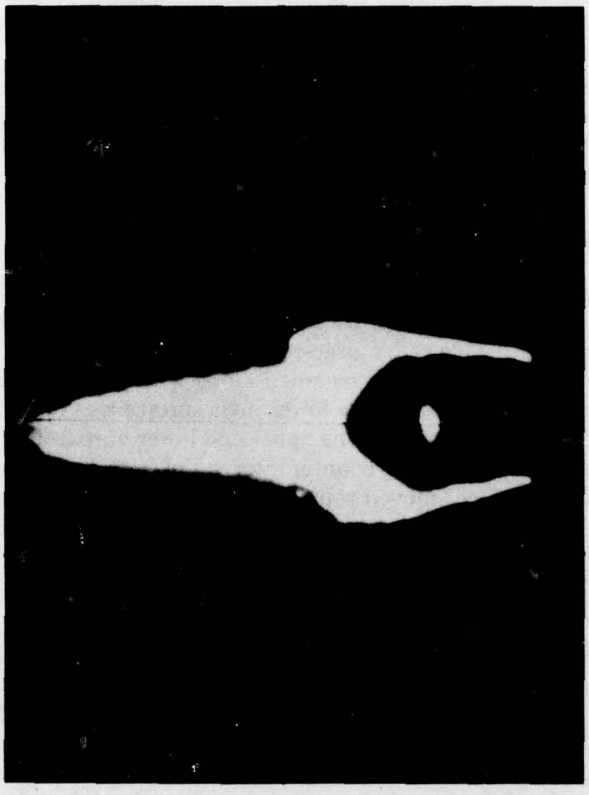

FE 342473A

Figure 14. Typical Melt Area Photographed from Vanguard Motion Analyzer

Data obtained during this sequence was treated per paragraph III.A.1 and resulted in derived data of total burn time, incremental chordwise melt and burn front transit times and average chordwise burn velocity. This data is included in Tables 6 and 7.

A variation of the above data acquisition technique was then conducted to gather pictorial data for the visual comparison of burn rate and burn severity among alloys and among specimens of varying thickness. This technique consisted of photographing the combustion process, of those specimens which burned, at equal and common time intervals. These intervals were selected as 0.1, 0.2, 0.3, 0.4, 0.5 and 0.7 sec into the burn (after ignition). The 0.6 sec interval was omitted as a compromise to maximize visual impact and minimize the quantity of photographs required. Using the film frame/time relationship determined for each film record, the selected time intervals were converted to frame counter readings. The data collection process consisted of advancing the film to this frame counter setting, photographing the frame and continuing to the next interval until complete. Figure 15 shows the use of data thus obtained in depicting the relative burn characteristics of Ti 8-1-1 at various thicknesses. Similarily, Figure 16 compares the relative burn characteristics of the various alloys and Ti 8-1-1 thicknesses at the low airstream velocity.

Another measure of the sustained combustion of titanium is its burning characteristics in a spanwise direction after chordwise burn-through. Generally, the extent of this stage of the total combustion process determines the severity of the resultant burn. Therefore, a study of this property is an important aspect in achieving a total understanding of the alloy's combustion characteristics.

With no prior knowledge or experience for guidance, it was decided to evaluate spanwise burn at specimen midchord. Ultimately this selection appeared to have been adequate to achieve the objectives of the analysis.

To begin this analysis the X cursor was preset at the specimen midchord on the Vanguard image. This point was readily retrieved as the position indicator reading at the 0.5 in. point which was used for the melt/burn front data acquisition. The Y axis cursor was then set to bisect the red laser alignment beam or, alternately, the yellow glow denoting CO_2 laser impingement of the specimen. At this setting the Y axis readout was recorded as the best estimate of the centerline of spanwise burn propagation.

For the first data reading the film was advanced until the burn front passed the preset X cursor by approximately 5 mm. The Y cursor was next adjusted to the point at which it was tangent to the upper melt surface at its intersection with the X cursor as shown diagramatically in Figure 17. This position reading was recorded along with the frame counter reading. In the same manner the spanwise progress of the lower melt surface was determined. The above data was collected and recorded separately for the upper and lower burn fronts. These upper and lower readings were taken at successive frame counter intervals of 50 to 400 frames per data point. Early in the burn the combustion front moved rapidly and frequent readings produced better velocity definition. Later, as the movement slowed down, the data intervals were increased to 100 to 400 frames. Data was accumulated until either one of the melt fronts had receded to the point where it no longer intersected the X cursor.

TABLE 7. INCREMENTAL CHORDWISE MELT AND BURN FRONT TRANSIT TIMES

Specimen Number	Alloy (mils)	Time (ms) — Melt and Burn Front Distances From Leading Edge in mm (inch)													
		10.2 (0.4)		12.7 (0.5)		15.2 (0.6)		17.8 (0.7)		20.3 (0.8)		22.9 (0.9)		25.4 (1.0)	
		Melt	Burn	Melt	Burn	Melt	Burn	Melt	Burn	Melt	Burn	Melt	Burn	Melt	Burn
N2-1	13-11-3	366	516	437	619	534	668	613	705	678	790	705	825	732	831
N2-3	6-2-4-6	249	408	294	452	352	501	379	529	404	563	417	582	418	589
N2-4	6-2-4-6	126	224	152	260	168	291	193	308	212	323	219	338	221	343
N2-7	Beta III	367	540	437	577	470	638	528	662	553	689	565	717	609	722
N2-8	Beta III	167	268	220	299	240	328	280	354	293	379	297	393	308	393
N2-9	Ti_6Al	299	564	371	661	413	720	491	777	559	824	638	883	672	903
N2-10	Ti_6Al	175	340	229	383	264	418	288	444	296	457	312	472	322	480
N2-11	8-1-1(40)	283	479	337	522	383	552	413	588	437	614	465	635	491	638
N2-12	8-1-1(40)	214	338	245	363	262	385	276	408	310	421	319	430	330	432
N2-14	8-1-1(70)	393	768	491	830	555	918	609	969	656	987	692	1028	716	1029
N2-18	Ti 5Ni	157	232	188	259	218	291	238	313	247	325	255	329	280	349
N2-19	Ti 10Ni	268	413	404	514	473	611	492	668	527	715	565	753	598	754
N2-20	Ti 10Ni	2678	2764	2739	2804	2772	2843	2790	2874	2812	2900	2830	2917	2844	2921
N2-23	8-1-1(70)	345	710	439	787	512	843	561	924	613	931	635	953	675	955
N2-24	8-1-1(20)	201	271	239	300	277	327	300	350	321	373	347	386	363	396
N2-25	8-1-1(40)	268	469	315	527	372	570	422	614	460	654	500	670	529	672
N2-26	8-1-1(70)	187	427	226	451	270	500	295	546	323	561	341	574	357	574
N2-27	8-1-1(20)	128	176	150	194	167	209	177	221	199	235	205	242	208	243
N2-28	8-1-1(55)	167	334	202	349	227	395	251	426	278	445	296	452	316	453
N2-29	8-1-1(55)	261	541	322	597	382	639	406	700	472	710	498	731	526	737
N2-30	8-1-1(30)	134	232	155	251	161	272	194	290	205	303	217	311	232	313
N2-31	8-1-1(30)	237	358	285	399	325	432	343	450	354	457	389	461	424	466
N2-33	Ti_6Al	209	434	250	469	289	510	333	555	362	582	373	603	383	608
N2-36	Beta III	239	389	331	465	363	485	377	535	431	579	453	581	468	582
N2-40	Ti_6Al	439	695	527	784	560	853	630	914	657	957	706	1018	728	1034
N2-41	8-1-1(40)	248	441	302	483	336	526	390	545	392	571	401	584	435	585

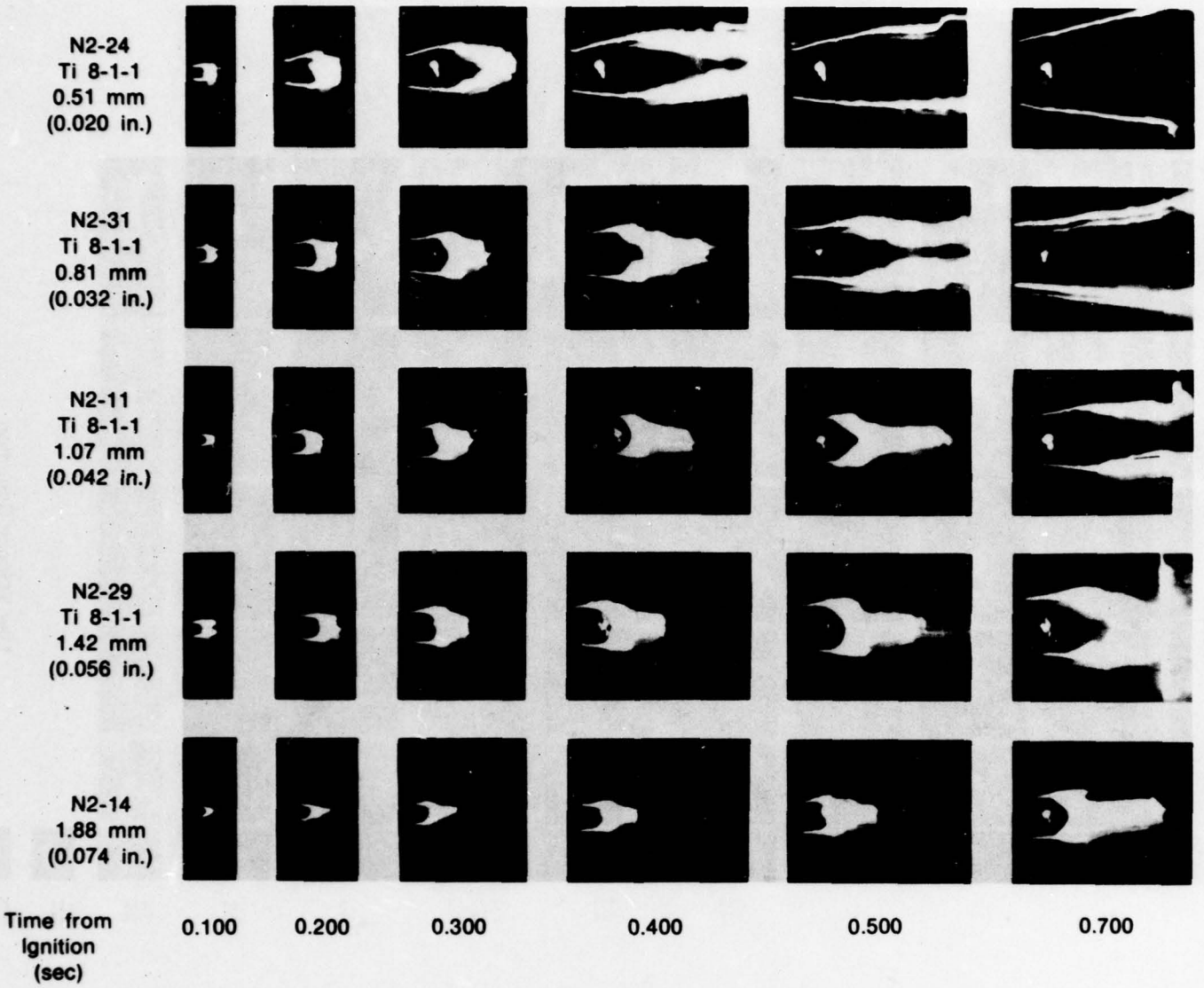

Figure 15. Burn Appearance of 5 Thicknesses of Ti 8-1-1 at Increasing Time Intervals

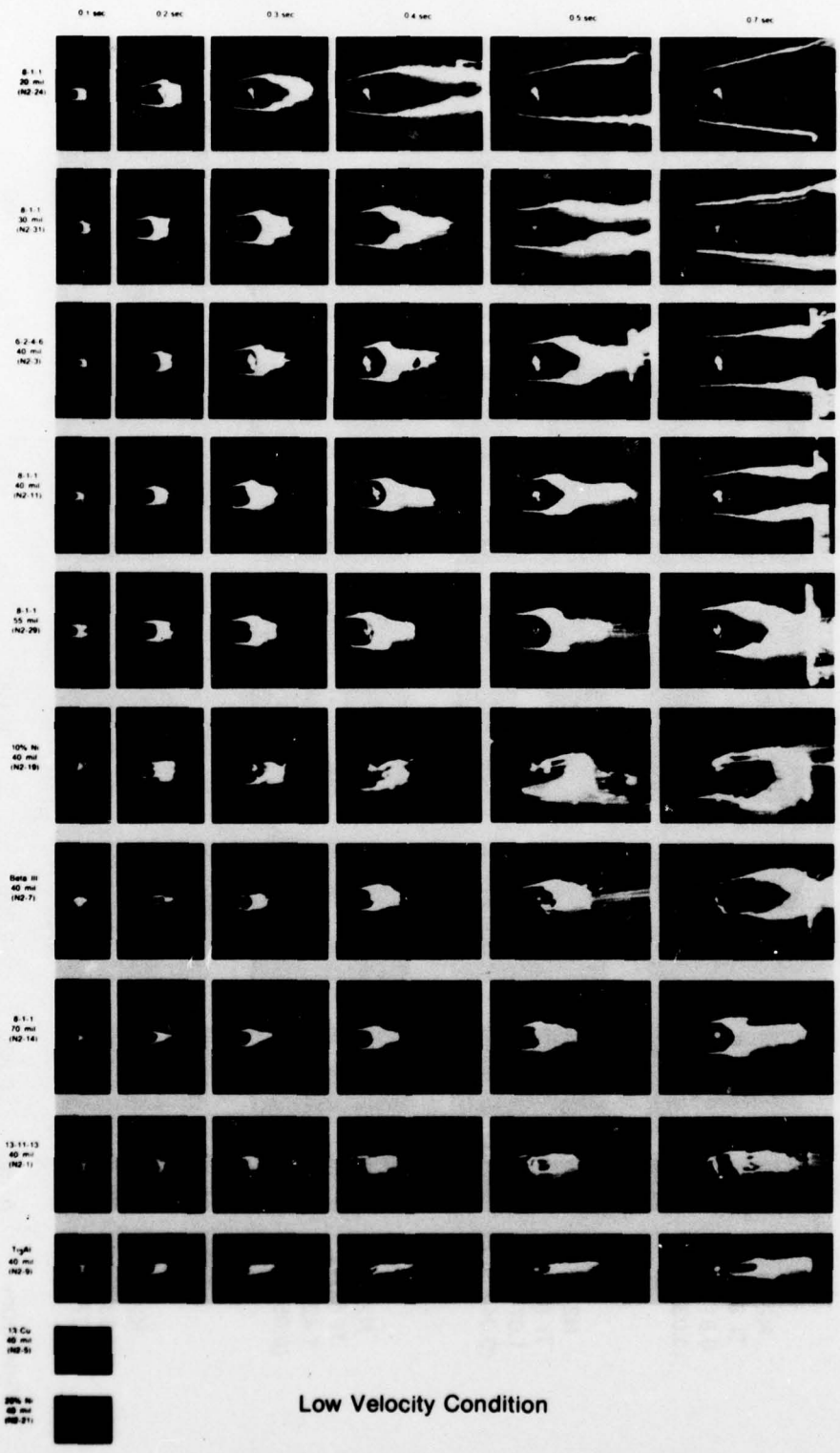

Figure 16. Burn Appearance of Alloys at Increasing Time Intervals

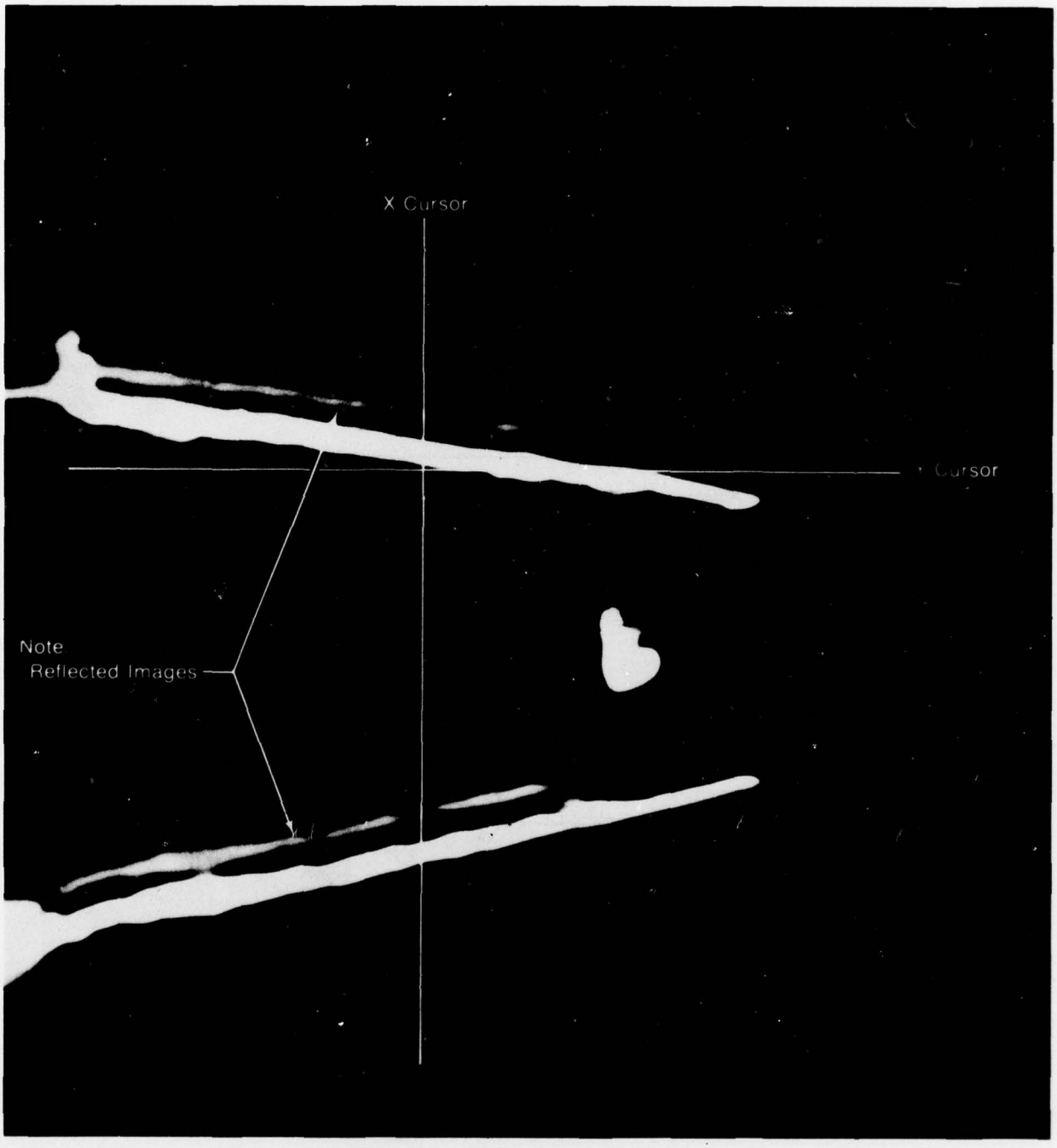

FD 145915

Figure 17. Cursor Alignment for Obtaining Spanwise Burn Data

In the subsequent treatment of this raw data, frame counts were converted to time and the Y axis readings into equivalent inches at the specimen. This derived data is contained in Table 8. The resultant time and distance data permitted calculation of incremental and average spanwise velocity.

In reviewing the high-speed films, it was frequently noted that the angle of the spanwise burn front appeared to vary with specimen alloy material and thickness. Since this observed phenomenon potentially could be related to some combustion characteristic, burn front angle was measured for 15 specimens. The specimens selected for this data were those which exhibited significant combustion in the spanwise direction.

During the initial period of developing a standardized measurement technique, it was observed that the angle of the burn front changed as the burn progressed away from the spanwise centerline. For this reason the data was taken immediately after the normal chordwise burn-through perturbances had subsided.

TABLE 8. MIDCHORD SEPARATION DISTANCE VS TIME AFTER BURN THROUGH

Specimen Number	*Alloy*	*Time (ms)*	*Separation Distance*	
			mm	*(inch)*
N2-1	13-11-3	49	2.41	(0.095)
		86	3.40	(0.134)
		171	4.55	(0.179)
		206	4.75	(0.187)
		212	4.75	(0.187)
		298	5.49	(0.216)
		410	5.87	(0.231)
		522	6.15	(0.242)
		634	6.83	(0.269)
		746	6.83	(0.269)

Specimen Number	*Alloy*	*Time (ms)*	*Separation Distance*	
			mm	*(inch)*
N2-3	6-2-4-6	49	3.96	(0.156)
		76	5.72	(0.226)
		110	7.54	(0.297)
		130	8.28	(0.326)
		137	8.56	(0.337)
		224	10.13	(0.399)
		333	11.56	(0.455)
		442	13.00	(0.512)
		551	14.33	(0.564)
		661	16.10	(0.634)
		770	17.55	(0.691)
		879	19.02	(0.749)
		988	20.40	(0.803)
		1097	21.95	(0.864)
		1207	23.14	(0.911)
		1316	25.12	(0.989)
		1425	26.85	(1.057)
		1534	28.24	(1.112)
		1643	29.67	(1.168)
		1753	30.81	(1.213)
		1841	32.21	(1.268)

TABLE 8. MIDCHORD SEPARATION DISTANCE VS TIME AFTER BURN THROUGH (Continued)

Specimen Number	Alloy	Time (ms)	Separation Distance mm	Separation Distance (inch)
N2-4	6-2-4-6	30	4.22	(0.166)
		48	5.11	(0.201)
		63	5.77	(0.227)
		77	6.71	(0.264)
		83	6.88	(0.271)
		153	8.31	(0.327)
		251	10.29	(0.405)
		349	11.81	(0.465)
		447	13.79	(0.543)
		545	15.37	(0.605)
		643	17.12	(0.674)
		741	18.72	(0.737)
		839	20.17	(0.794)
		937	21.46	(0.845)
		1035	22.86	(0.900)
		1133	23.95	(0.943)
		1231	25.12	(0.989)
		1329	26.31	(1.036)
		1427	27.48	(1.082)
		1525	28.55	(1.124)
		1623	29.46	(1.160)
		1721	30.35	(1.195)
		1819	31.80	(1.252)
		1917	32.77	(1.290)
		2015	33.55	(1.321)
		2113	34.85	(1.372)
		2211	36.07	(1.420)

Specimen Number	Alloy	Time (ms)	Separation Distance mm	Separation Distance (inch)
N2-7	Beta III	61	5.92	(0.233)
		85	6.65	(0.262)
		112	6.78	(0.267)
		139	7.21	(0.284)
		145	7.42	(0.292)
		218	8.10	(0.319)
		328	8.76	(0.345)
		439	9.07	(0.357)
N2-8	Beta III	28	2.08	(0.082)
		55	4.88	(0.192)
		79	5.66	(0.223)
		94	6.55	(0.258)
		114	6.88	(0.271)
		212	7.39	(0.291)
		261	7.52	(0.296)
N2-9	Ti_3Al	59	1.60	(0.063)
		116	1.85	(0.073)
		163	2.01	(0.079)
		222	1.98	(0.078)
		242	2.36	(0.093)
		367	2.36	(0.093)
N2-10	Ti_3Al	34	2.98	(0.117)
		60	3.89	(0.153)
		73	4.67	(0.184)
		89	4.67	(0.184)
		97	4.67	(0.184)
		126	5.03	(0.198)
		224	5.94	(0.234)

TABLE 8. MIDCHORD SEPARATION DISTANCE VS TIME AFTER BURN THROUGH (Continued)

Specimen Number	Alloy (mils)	Time (ms)	Separation Distance mm	Separation Distance (inch)
N2-20	Ti 10Ni	39	4.37	(0.172)
		70	5.05	(0.199)
		96	5.28	(0.208)
		113	5.28	(0.208)
		117	5.44	(0.214)
		187	6.15	(0.242)
		286	7.11	(0.280)
N2-23	8-1-1(70)	56	2.84	(0.112)
		137	6.30	(0.248)
		144	6.55	(0.258)
		166	7.24	(0.285)
		222	8.84	(0.348)
		321	10.72	(0.422)
		420	11.66	(0.459)
		519	12.90	(0.508)
		618	13.72	(0.540)
		716	14.78	(0.582)
		815	15.57	(0.613)
		914	16.48	(0.649)
		1013	17.20	(0.677)
		1112	17.93	(0.706)
		1210	19.08	(0.751)
		1309	19.66	(0.774)
		1408	20.55	(0.809)
		1507	21.56	(0.849)
		1606	22.35	(0.880)
		1704	23.01	(0.906)
		1803	23.80	(0.937)
		1902	24.79	(0.976)
		2001	25.43	(1.001)
		2100	25.58	(1.007)
		2198	26.72	(1.052)

Specimen Number	Alloy (mils)	Time (ms)	Separation Distance mm	Separation Distance (inch)
N2-23	8-1-1(70)	2297	27.18	(1.070)
		2396	27.76	(1.093)
		2594	29.29	(1.153)
		2791	30.53	(1.202)
		2989	31.83	(1.253)
		3186	32.99	(1.299)
		3384	34.54	(1.360)
		3582	35.69	(1.405)
		3779	36.96	(1.455)
		3878	37.52	(1.477)
N2-24	8-1-1(20)	29	3.86	(0.152)
		54	5.51	(0.217)
		75	6.40	(0.252)
		89	7.11	(0.280)
		91	7.34	(0.289)
		125	8.69	(0.342)
		181	10.36	(0.408)
		293	12.47	(0.491)
		406	14.07	(0.554)
		518	15.95	(0.628)
		630	17.68	(0.696)
		743	19.05	(0.750)
		855	20.62	(0.812)
		968	21.87	(0.861)
		1080	23.42	(0.922)

TABLE 8. MIDCHORD SEPARATION DISTANCE VS TIME AFTER BURN THROUGH (Continued)

Specimen Number	Alloy (mils)	Time (ms)	Separation Distance mm	Separation Distance (inch)
		1190	24.77	(0.975)
		1305	26.19	(1.031)
		1417	27.84	(1.096)
		1530	28.75	(1.132)
		1640	30.56	(1.203)
		1754	31.55	(1.242)
		1867	32.89	(1.295)
		1980	34.26	(1.349)
N2-25	8-1-1(40)	43	2.29	(0.090)
		88	3.71	(0.146)
		128	4.57	(0.180)
		143	4.95	(0.195)
		146	4.95	(0.195)
		161	5.16	(0.203)
		272	6.10	(0.240)
		383	6.71	(0.264)

Specimen Number	Alloy (mils)	Time (ms)	Separation Distance mm	Separation Distance (inch)
N2-26	8-1-1(70)	50	5.36	(0.211)
		95	7.75	(0.305)
		110	8.59	(0.338)
		124	8.89	(0.350)
		164	9.83	(0.387)
		263	11.20	(0.441)
		362	12.47	(0.491)
		461	13.89	(0.547)
		560	15.21	(0.599)
		659	16.36	(0.644)
		758	17.83	(0.702)
		857	19.23	(0.757)
		956	20.78	(0.818)
		1055	22.20	(0.874)
		1154	23.57	(0.928)
		1253	25.17	(0.991)
		1352	26.59	(1.047)
		1451	27.53	(1.084)
		1550	29.44	(1.159)
		1649	30.45	(1.199)
		1748	32.13	(1.265)
		1847	33.58	(1.322)
		1946	35.08	(1.381)
		2045	36.25	(1.427)
		2144	37.64	(1.482)
N2-27	8-1-1(20)	15	2.72	(0.107)
		27	3.99	(0.157)
		41	5.23	(0.206)
		48	5.51	(0.217)
		124	8.31	(0.327)
		223	10.16	(0.400)
		322	11.84	(0.466)

TABLE 8. MIDCHORD SEPARATION DISTANCE VS TIME AFTER BURN THROUGH (Continued)

Specimen Number	Alloy (mils)	Time (ms)	Separation Distance mm	Separation Distance (inch)
N2-27	8-1-1(20)	421	13.67	(0.538)
		520	15.16	(0.597)
		619	16.56	(0.652)
		718	17.81	(0.701)
		817	19.00	(0.748)
		916	19.86	(0.782)
		1015	21.29	(0.838)
N2-28	8-1-1(55)	46	5.41	(0.213)
		76	6.91	(0.272)
		96	7.82	(0.308)
		103	8.00	(0.315)
		113	8.36	(0.329)
		162	9.55	(0.376)
		260	11.05	(0.435)
		358	12.24	(0.482)
		456	13.74	(0.541)
		554	15.11	(0.595)
		652	16.18	(0.637)
		750	17.42	(0.686)
		848	18.77	(0.739)
		946	20.24	(0.797)
		1044	21.31	(0.839)
		1142	22.73	(0.895)
		1240	24.21	(0.953)
		1338	25.15	(0.990)
		1436	26.26	(1.034)
		1534	27.58	(1.086)
		1632	28.91	(1.138)
		1730	30.18	(1.188)
		1828	31.24	(1.230)
		1926	32.41	(1.276)
		2024	33.55	(1.321)

Specimen Number	Alloy (mils)	Time (ms)	Separation Distance mm	Separation Distance (inch)
N2-28	8-1-1(55)	2122	34.16	(1.345)
		2220	34.90	(1.374)
		2318	35.74	(1.407)
		2416	36.58	(1.440)
		2514	37.34	(1.470)
N2-29	8-1-1(55)	42	3.07	(0.121)
		103	5.77	(0.227)
		113	5.77	(0.227)
		134	6.78	(0.267)
		140	7.01	(0.276)
		166	8.05	(0.317)
		216	9.09	(0.358)
		315	10.90	(0.429)
		414	11.86	(0.467)
		513	12.93	(0.509)
		612	13.72	(0.540)
		711	14.73	(0.580)
		810	15.62	(0.615)
		909	16.28	(0.641)
		1008	17.15	(0.675)
		1107	17.88	(0.704)
		1206	18.67	(0.735)

TABLE 8. MIDCHORD SEPARATION DISTANCE VS TIME AFTER BURN THROUGH (Continued)

Specimen Number	Alloy (mils)	Time (ms)	Separation Distance mm	Separation Distance (inch)
N2-30	8-1-1(30)	22	3.38	(0.133)
		40	5.16	(0.203)
		53	6.25	(0.246)
		60	6.73	(0.265)
		62	6.88	(0.271)
		117	9.27	(0.365)

Specimen Number	Alloy (mils)	Time (ms)	Separation Distance mm	Separation Distance (inch)
N2-31	8-1-1(30)	33	3.61	(0.142)
		51	4.52	(0.178)
		58	4.67	(0.184)
		62	5.05	(0.199)
		67	5.21	(0.205)
		122	8.26	(0.325)
		222	10.77	(0.424)
		322	12.07	(0.475)
		422	13.41	(0.528)
		522	14.71	(0.579)
		622	15.32	(0.603)
		722	16.38	(0.645)
		822	18.24	(0.718)
		922	18.72	(0.737)
		1022	20.12	(0.792)
		1122	21.34	(0.840)
		1222	22.20	(0.874)
		1322	23.04	(0.907)
		1422	24.56	(0.967)
		1522	25.48	(1.003)
		1622	26.80	(1.055)
		1722	27.76	(1.093)
		1822	28.88	(1.137)
		1922	29.77	(1.172)
		2022	30.81	(1.213)
		2122	31.88	(1.255)
		2222	32.97	(1.298)
		2322	33.91	(1.335)
		2422	35.46	(1.396)

Specimen Number	Alloy	Time (ms)	Separation Distance mm	Separation Distance (inch)
N2-33	Ti_3Al	41	2.57	(0.101)
		86	3.76	(0.148)
		113	4.24	(0.167)
		134	4.47	(0.176)
		139	4.52	(0.178)
		189	4.72	(0.186)
N2-36	Beta III	20	1.04	(0.041)
		70	4.27	(0.168)
		114	4.67	(0.184)
		144	5.18	(0.204)

TABLE 8. MIDCHORD SEPARATION DISTANCE VS TIME AFTER BURN THROUGH (Continued)

Specimen Number	Alloy	Time (ms)	Separation Distance mm	Separation Distance (inch)
N2-40	Ti_6Al	69	3.78	(0.149)
		129	4.93	(0.194)
		172	5.49	(0.216)
		233	5.89	(0.232)
		250	6.20	(0.244)
		364	6.40	(0.252)
		413	6.53	(0.257)

Specimen Number	Alloy (mils)	Time (ms)	Separation Distance mm	Separation Distance (inch)
N2-41	8-1-1(40)	43	2.74	(0.108)
		62	3.94	(0.155)
		89	5.87	(0.231)
		101	6.50	(0.256)
		109	6.88	(0.271)
		205	9.96	(0.392)
		300	11.81	(0.465)
		395	12.93	(0.509)
		490	13.59	(0.535)
		586	14.50	(0.571)
		681	15.29	(0.602)
		776	16.36	(0.644)
		871	16.99	(0.669)
		967	17.73	(0.698)
		1062	18.49	(0.728)
		1157	19.56	(0.770)
		1252	19.96	(0.786)
		1348	20.78	(0.818)
		1443	21.01	(0.827)

Once the data frame was selected, the outer screen of the Vanguard was rotated until one of the parallel cursors could be moved into alignment with the upper combustion front. The angle was read and recorded and the procedure repeated for the lower combustion front. The specimens analyzed and the resultant data are shown in Table 9.

TABLE 9. SPANWISE BURN ANGLE

Alloy (mils)	*Specimen Number*	*Velocity H=High L=Low*	*Spanwise Burn Front Angle (deg)①*	
			Bottom	*Top*
10% Ni	N2-19	L	13.5	10.3
10% Ni	N2-20	H	13.0	10.5
8-1-1(70)	N2-23	L	2.5	7.3
8-1-1(20)	N2-24	L	6.5	10.0
8-1-1(40)	N2-25	L	4.0	12.6
8-1-1(70)	N2-26	H	4.7	8.9
8-1-1(20)	N2-27	H	4.8	11.9
8-1-1(55)	N2-28	H	4.5	11.4
8-1-1(55)	N2-29	L	2.7	6.2
8-1-1(30)	N2-30	H	9.6	9.5
8-1-1(30)	N2-31	L	6.1	6.4
Ti_6Al	N2-33	H	6.7	8.8
Beta III	N2-36	H	9.2	13.8
Ti_6Al	N2-40	H	8.2	13.1
8-1-1(40)	N2-41	L	6.4	8.1

① Angles measured after perturbance of burn-through had subsided.

For the planned data analysis, the area of the molten alloy preceding the burn front was needed for possible correlation with other combustion parameters. Thus, a melt area parameter was required. Because of the lack of precedence, the melt area to be measured was arbitrarily chosen at the point where the melt front reached the trailing edge of the specimen. This was designated as the *maximum melt area*.

The maximum melt area was contained on the photograph previously taken at the 25.4 mm (1.0 in.) point during the 2.54 mm (0.1 in.) increment series. The photograph was enlarged to 20.3 by 25.4 cm (8 by 10 in.) for area determination. This enlargement represented a magnification of the Vanguard image which had been previously calculated. The photograph magnification was then calculated based on the known 1.91 mm (0.75 in.) separation of the Vanguard fixed cursors shown on the photograph.

The melt area of the photograph was determined with a planimeter and converted into actual area at the specimen in accordance with the following example:

Maximum Melt Area — Specimen N2-41
(See Figure 18)

Specimen Magnification at Vanguard Screen = 2.675X

Magnification of Screen Image on Photograph = 1.76X

Specimen Magnification on Photograph = $2.675 \times 1.76 = 4.708X$

Melt Area Measured on Photograph = 26.7 cm^2 (4.14 in^2)

$$\text{Melt Area at Specimen} = \frac{26.7\ cm^2}{4.708^2} = 1.20\ cm^2 \left(\frac{4.14\ in^2}{4.708^2} = 0.19\ in^2 \right)$$

In addition to the maximum melt area, the melt area at the 10.2 to 22.9 mm (0.4 to 0.9 in.) increments were also determined for all specimens. This data is included in Table 10.

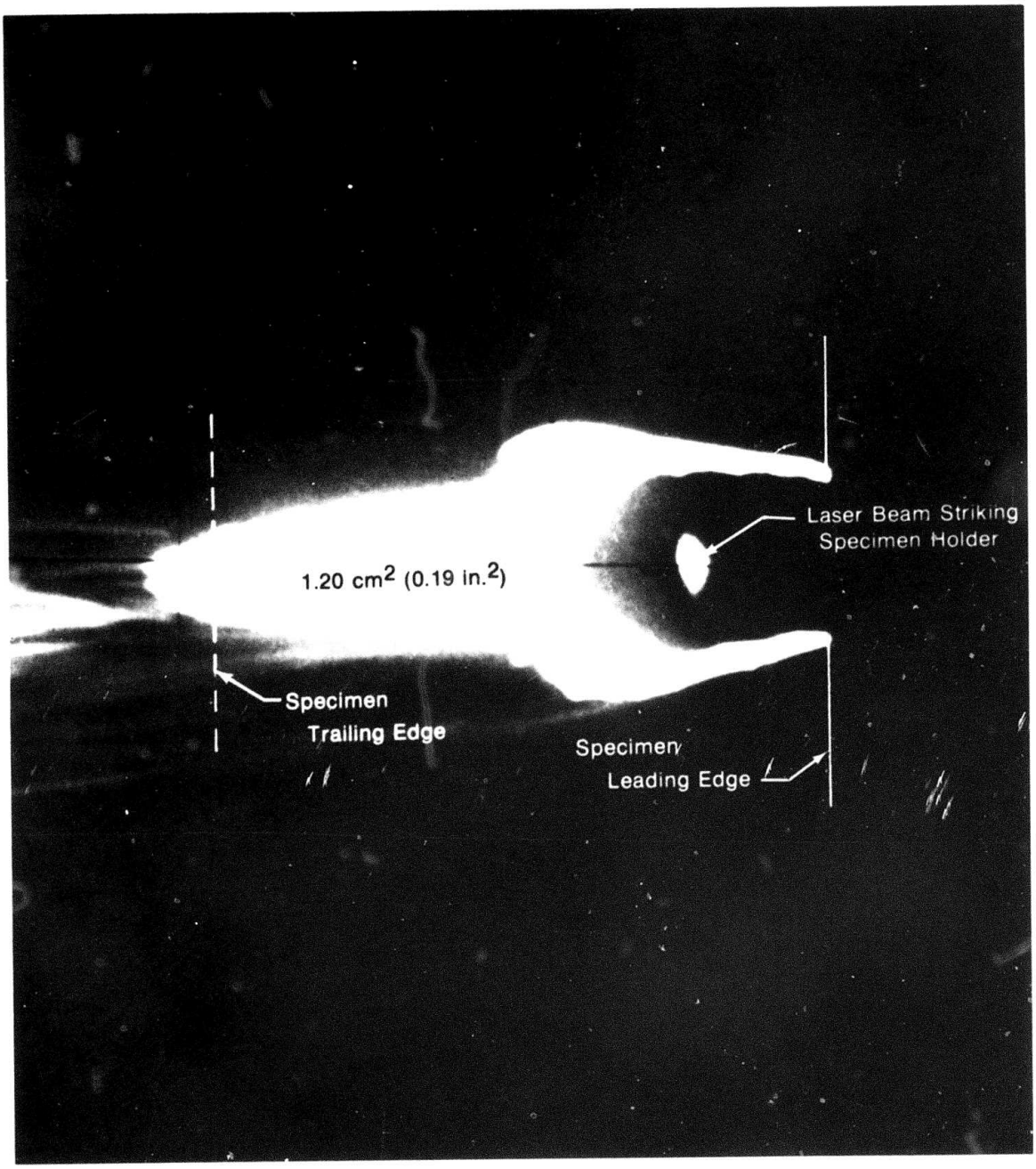

FD 145916

Figure 18. Maximum Melt Area Photograph

TABLE 10. MELT AREA AT EQUAL MELT FRONT INCREMENTS

Alloy (mils)	Specimen Number	Melt Front — Distance From Leading Edge — mm (in.)													
		10.1 (0.4)		12.7 (0.5)		15.2 (0.6)		17.8 (0.7)		20.3 (0.8)		22.9 (0.9)		25.4 (1.0)	
		cm^2	(in^2)	cm^2	(in^2)	cm^2	(in^2)	cm^2	(in^2)	cm^2	(in^2)	cm^2	(in^2)	cm^2	(in^2)
13-11-3	N2-1	0.19	(0.03)	0.32	(0.05)	0.26	(0.04)	0.32	(0.05)	0.58	(0.09)	0.71	(0.11)	0.77	(0.12)
6-2-4-6	N2-3	0.32	(0.05)	0.39	(0.06)	0.58	(0.09)	0.71	(0.11)	0.84	(0.13)	0.97	(0.15)	0.90	(0.14)
6-2-4-6	N2-4	0.19	(0.03)	0.26	(0.04)	0.32	(0.05)	0.45	(0.07)	0.52	(0.08)	0.58	(0.09)	0.65	(0.10)
Beta III	N2-7	0.26	(0.04)	0.45	(0.07)	0.52	(0.08)	0.65	(0.10)	0.77	(0.12)	0.90	(0.14)	1.16	(0.18)
Beta III	N2-8	0.26	(0.04)	0.32	(0.05)	0.39	(0.06)	0.52	(0.08)	0.58	(0.09)	0.65	(0.10)	0.77	(0.12)
Ti_3Al	N2-9	0.13	(0.02)	0.13	(0.02)	0.19	(0.03)	0.19	(0.03)	0.32	(0.05)	0.39	(0.06)	0.39	(0.06)
Ti_3Al	N2-10	0.19	(0.03)	0.32	(0.05)	0.39	(0.06)	0.52	(0.08)	0.58	(0.09)	0.65	(0.10)	0.71	(0.11)
8-1-1 40 mil	N2-11	0.32	(0.05)	0.45	(0.07)	0.52	(0.08)	0.52	(0.08)	0.65	(0.10)	0.77	(0.12)	0.90	(0.14)
8-1-1 40 mil	N2-12	0.32	(0.05)	0.45	(0.07)	0.52	(0.08)	0.58	(0.09)	0.84	(0.13)	0.97	(0.15)	1.16	(0.18)
8-1-1 70 mil	N2-14	0.26	(0.04)	0.45	(0.07)	0.65	(0.10)	0.77	(0.12)	0.90	(0.14)	1.03	(0.16)	1.16	(0.18)
5% Ni	N2-18	0.39	(0.06)	0.45	(0.07)	0.52	(0.08)	0.71	(0.11)	0.97	(0.15)	0.97	(0.15)	1.23	(0.19)
10% Ni	N2-19	0.19	(0.03)	0.32	(0.05)	0.58	(0.09)	0.77	(0.12)	0.71	(0.11)	0.90	(0.14)	1.23	(0.19)
10% Ni	N2-20	0.19	(0.03)	0.26	(0.04)	0.39	(0.06)	0.58	(0.09)	0.71	(0.11)	0.84	(0.13)	1.03	(0.16)
8-1-1 70 mil	N2-23	0.32	(0.05)	0.52	(0.08)	0.71	(0.11)	0.77	(0.12)	0.97	(0.15)	1.10	(0.17)	1.35	(0.21)
8-1-1 20 mil	N2-24	0.26	(0.04)	0.32	(0.05)	0.52	(0.08)	0.58	(0.09)	0.71	(0.11)	0.84	(0.13)	0.97	(0.15)
8-1-1 40 mil	N2-25	0.26	(0.04)	0.32	(0.05)	0.39	(0.06)	0.52	(0.08)	0.71	(0.11)	0.77	(0.12)	0.77	(0.12)
8-1-1 70 mil	N2-26	0.26	(0.04)	0.39	(0.06)	0.58	(0.09)	0.77	(0.12)	0.90	(0.14)	1.16	(0.18)	1.23	(0.19)
8-1-1 20 mil	N2-27	0.19	(0.03)	0.32	(0.05)	0.39	(0.06)	0.45	(0.07)	0.52	(0.08)	0.58	(0.09)	0.77	(0.12)
8-1-1 55 mil	N2-28	0.45	(0.07)	0.65	(0.10)	0.77	(0.12)	0.65	(0.10)	0.71	(0.11)	0.84	(0.13)	1.03	(0.16)
8-1-1 55 mil	N2-29	0.32	(0.05)	0.45	(0.07)	0.58	(0.09)	0.71	(0.11)	0.90	(0.14)	1.03	(0.16)	1.23	(0.19)
8-1-1 30 mil	N2-30	0.26	(0.04)	0.32	(0.05)	0.39	(0.06)	0.58	(0.09)	0.65	(0.10)	0.71	(0.11)	0.90	(0.14)
8-1-1 30 mil	N2-31	0.26	(0.04)	0.39	(0.06)	0.45	(0.07)	0.52	(0.08)	0.77	(0.12)	0.90	(0.14)	1.16	(0.18)
Ti_3Al	N2-33	0.19	(0.03)	0.26	(0.04)	0.32	(0.05)	0.39	(0.06)	0.39	(0.06)	0.45	(0.07)	0.58	(0.09)
Beta III	N2-36	0.26	(0.04)	0.32	(0.05)	0.45	(0.07)	0.58	(0.09)	0.58	(0.09)	0.65	(0.10)	0.71	(0.11)
Ti_3Al	N2-40	0.26	(0.04)	0.32	(0.05)	0.39	(0.06)	0.52	(0.08)	0.58	(0.09)	0.65	(0.10)	0.77	(0.12)
8-1-1 40 mil	N2-41	0.32	(0.05)	0.52	(0.08)	0.65	(0.10)	0.77	(0.12)	0.84	(0.13)	0.97	(0.15)	1.23	(0.19)

C. ANALYSIS OF DATA

This subsection presents an analysis and interpretation of the test results in terms of the run conditions and combustion parameters represented by the program derived data. Although the data quality is excellent and exhibits discrete differences in performance, not all of it can be explained.

1. Thickness Effect

Difficulties inherent in the machining of airfoil-contoured specimens for the first year's combustion tests resulted in midchord thickness variations as great as 2.1 to 1. Since the exact influence of specimen thickness on combustion parameters was not known, the interpretation of the resultant data was difficult. This current program, therefore, included a separate study of specimen thickness as it influenced the various measures of titanium alloy combustibility.

Alloy Ti 8Al-1Mo-1V was selected for this study because of its availability, ease of fabrication and its potential contribution to the compilation of combustion-related data from previous programs.

A total of 14 specimens were tested at the conditions and in the thicknesses shown in Table 11. As indicated on this table, the photographic records for specimens N2-13 and part of N2-30 were lost due to processing errors. Specimen N2-13 was rerun as N2-24. The loss to the N2-30 film occurred on the portion subsequent to burn-through and was not discovered in sufficient time to permit the fabrication and rerun of another specimen.

TABLE 11. Ti 8Al-1Mo-1V THICKNESS VARIATION DATA

Specimen Thickness mm (in)	*Specimen Number ID*	*Test Environ. Conditions*	*Burn Severity (%)*	*Ignition Time (ms)*	*Average Burn Velocity cm/sec (in/sec)*		*Max. Melt Area*
					Chord	*Span*	*cm² (in²)*
0.51 (0.020)	N2-13	LV	100.0	①	—	—	—
0.51 (0.020)	N2-24	LV	100.0	42	7.16 (2.82)	1.55 (0.61)	0.97 (0.15)
0.51 (0.020)	N2-27	HV	70.7	26	11.71 (4.61)	1.85 (0.73)	0.77 (0.12)
0.83 (0.033)	N2-31	LV	93.5	36	5.92 (2.33)	1.32 (0.52)	1.16 (0.18)
0.82 (0.032)	N2-30	HV	28.1	14	8.48 (3.34)	③	0.90 (0.14)
1.07 (0.042)	N2-11	LV	46.9	34	4.22 (1.66)	1.27 (0.50)	0.90 (0.14)
1.09 (0.043)	N2-25	LV	25.2	13	3.68 (1.45)	1.30 (0.51)	0.77 (0.12)
1.09 (0.043)	N2-41	LV ②	66.5	31	4.60 (1.81)	1.30 (0.51)	1.23 (0.19)
1.08 (0.043)	N2-12	HV	72.1	45	6.55 (2.58)	1.55 (0.61)	1.16 (0.18)
1.44 (0.057)	N2-29	LV	63.9	35	3.61 (1.42)	1.35 (0.53)	1.23 (0.19)
1.43 (0.056)	N2-28	HV	99.4	26	5.94 (2.34)	1.30 (0.51)	1.03 (0.16)
1.89 (0.074)	N2-14	LV	92.5	35	2.57 (1.01)	0.94 (0.37)	1.16 (0.18)
1.90 (0.075)	N2-23	LV	86.1	36	2.77 (1.09)	0.91 (0.36)	1.35 (0.21)
1.89 (0.075)	N2-26	HV	98.8	43	4.78 (1.88)	1.55 (0.61)	1.23 (0.19)

① Film lost in processing
② Temperature 427°C (800°F) instead of 454°C (850°F)
③ Span data lost in processing error

LV = Low Velocity
HV = High Velocity

a. *Thickness vs Burn Severity*

The appearance of the reconstructed specimens at each evaluated thickness, along with the calculated burn severity, is shown in Figure 19. Figure 20 shows all 13 reconstructed Ti 8-1-1 specimens, arranged in descending order of burn severity, along with a maximum melt area photograph. The curves resulting from a plot of these burn severity values against specimen thickness, for each environmental condition, are shown in Figure 21.

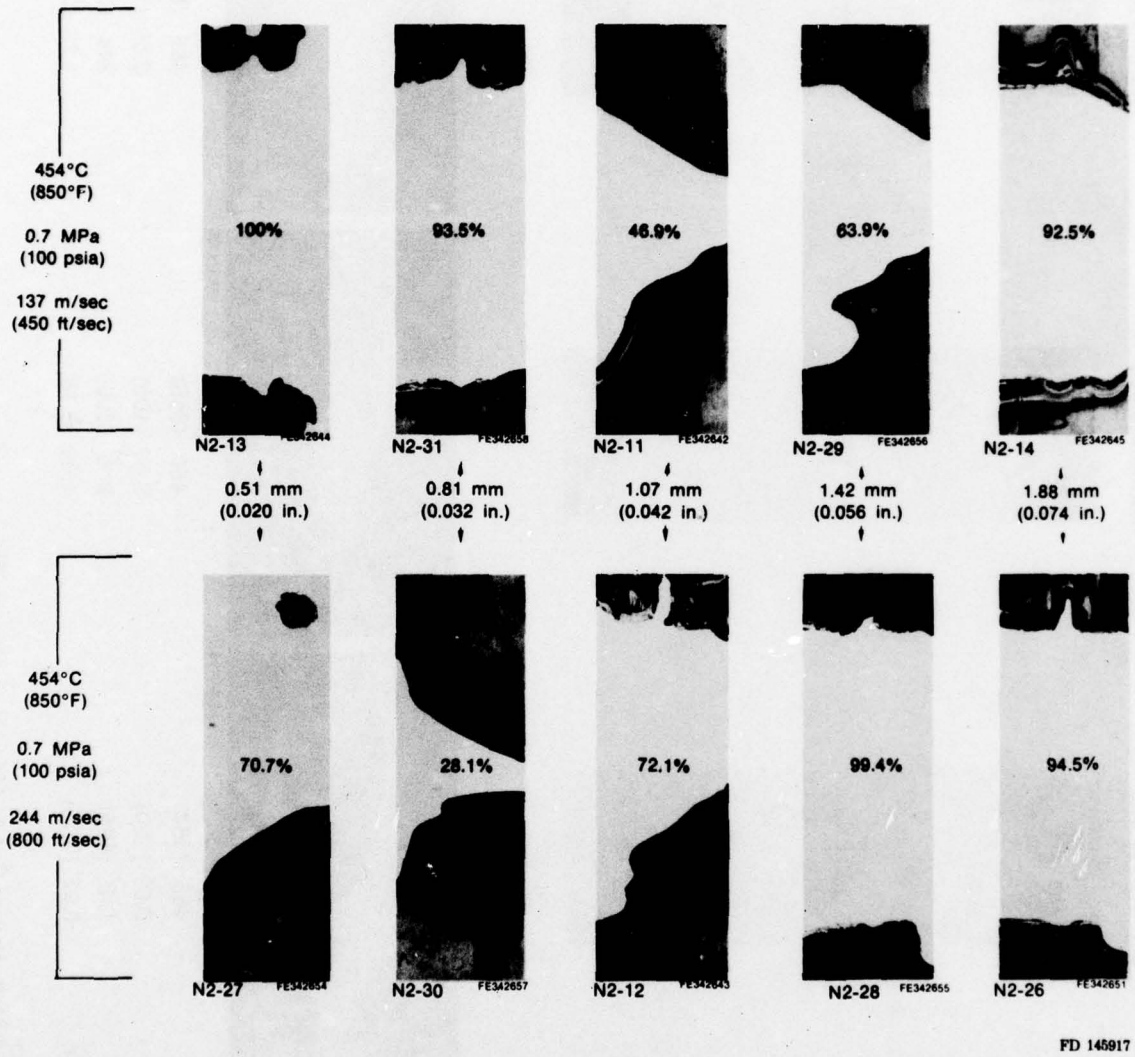

Figure 19. Burn Severity, Alloy Ti 8-1-1 at Various Thicknesses

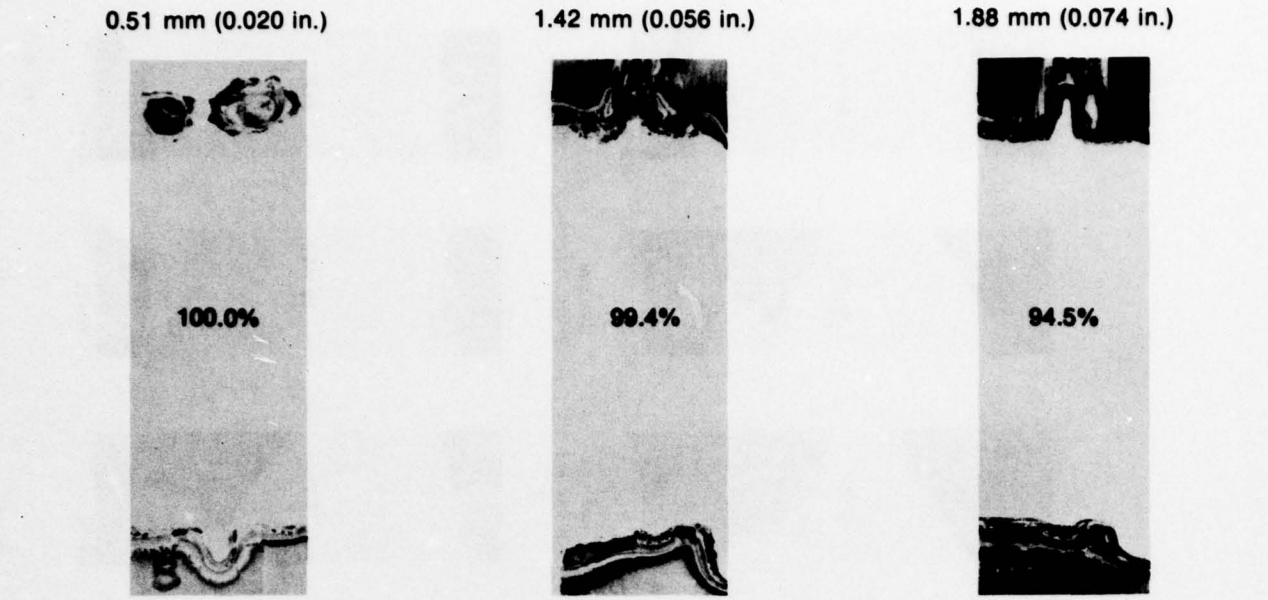

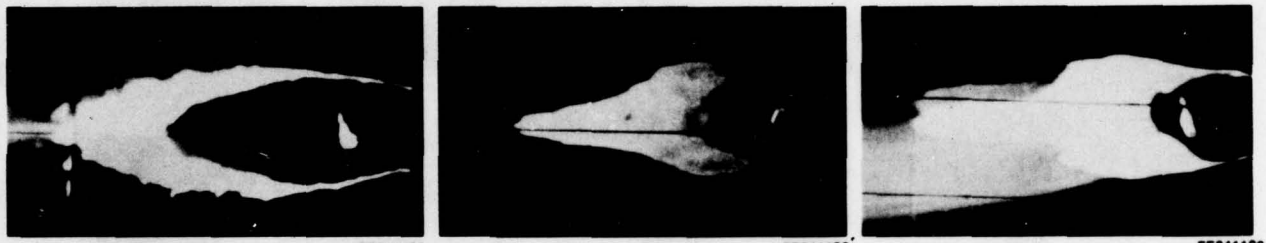

Temperature °C (°F):	458 (857)	458 (856)	456 (852)
Pressure MPa (psia):	0.69 (100)	0.69 (100)	0.69 (100)
Velocity m/sec (ft/sec):	142 (465)	246 (806)	244 (799)
Maximum Melt Area cm^2 ($in.^2$):	0.97 (0.15)	1.03 (0.16)	1.23 (0.19)

FD 145935

Figure 20-A. Burn Severity and Melt Area of Ti 8Al-1Mo-1V at Various Thicknesses

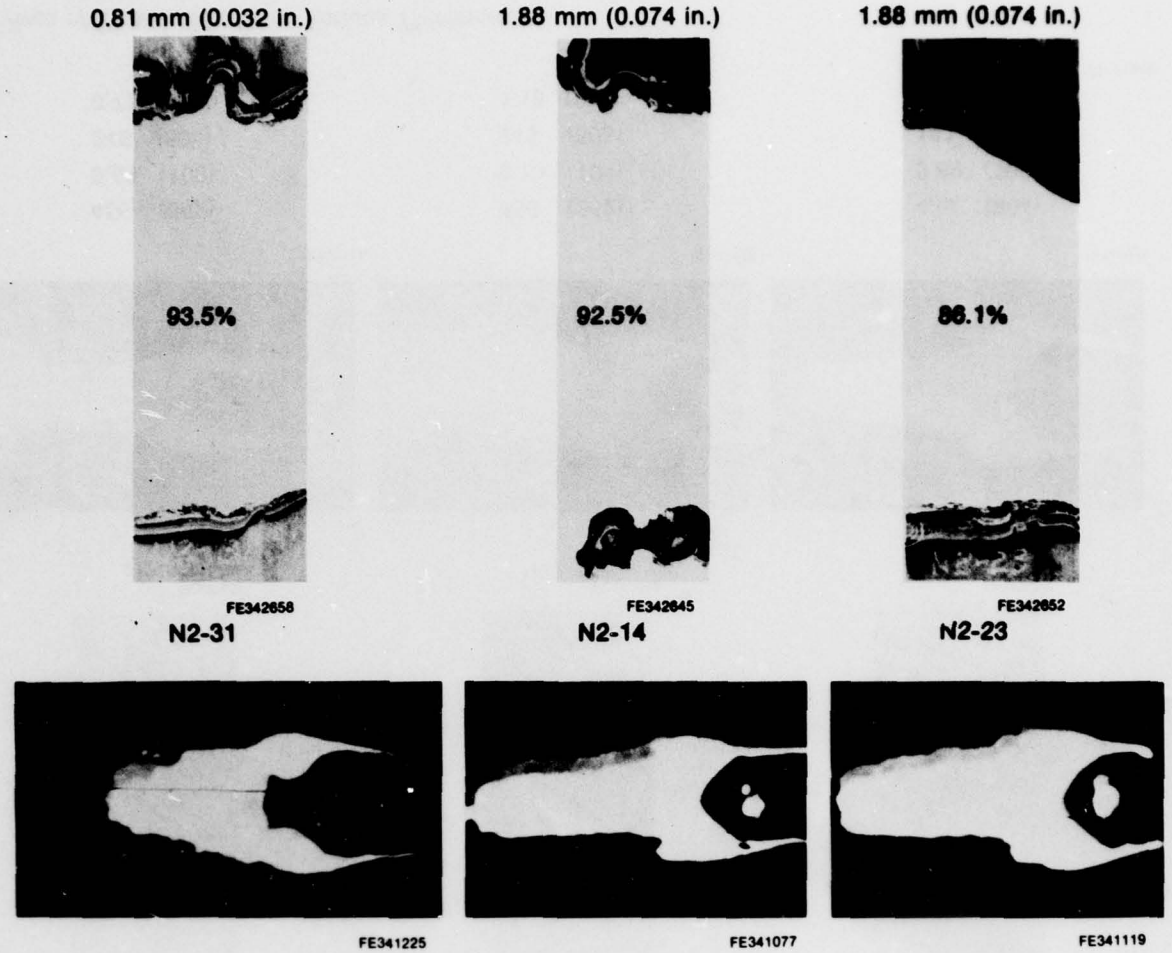

Temperature °C (°F):	454 (850)	456 (852)	455 (851)
Pressure MPa (psia):	0.69 (100)	0.69 (100)	0.69 (100)
Velocity m/sec (ft/sec):	146 (480)	141 (464)	141 (462)
Maximum Melt Area cm^2 ($in.^2$):	1.16 (0.18)	0.16 (0.18)	1.35 (0.21)

FD 145935

Figure 20-B. Burn Severity and Melt Area of Ti 8Al-1Mo-1V at Various Thicknesses

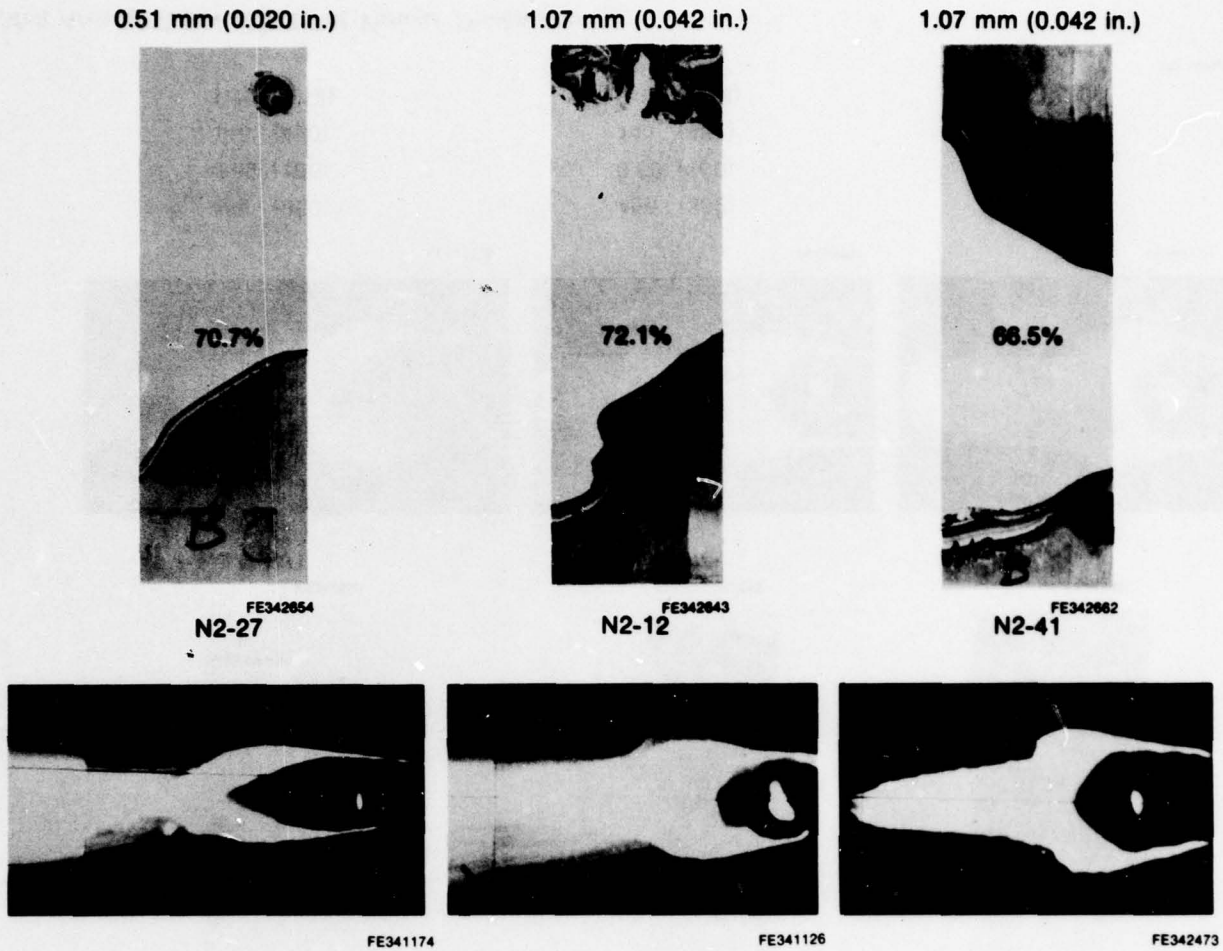

Temperature °C (°F):	456 (852)	456 (852)	429 (804)
Pressure MPa (psia):	0.69 (100)	0.70 (101)	0.69 (100)
Velocity m/sec (ft/sec):	245 (804)	245 (803)	141 (463)
Maximum Melt Area cm^2 ($in.^2$):	0.77 (0.12)	1.16 (0.18)	1.23 (0.19)

FD 145935

Figure 20-C. Burn Severity and Melt Area of Ti 8Al-1Mo-1V at Various Thicknesses

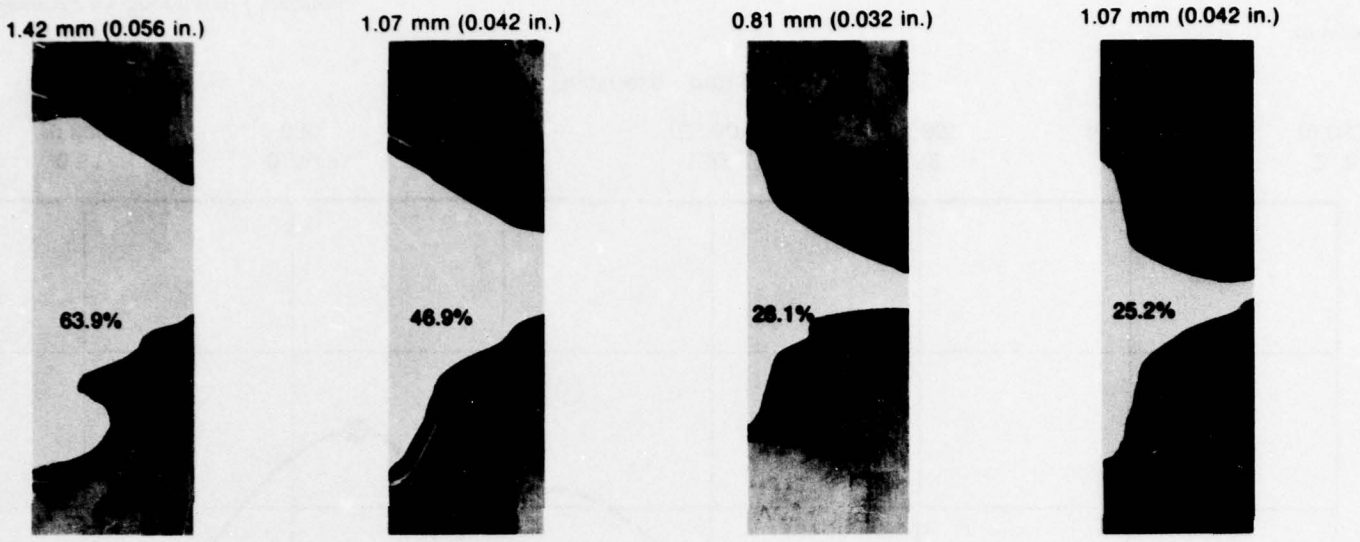

Temperature, °C(°F)	456 (852)	460 (860)	453 (848)	454 (849)
Pressure MPa(psia)	0.69 (100)	0.70 (101)	0.69 (100)	0.69 (100)
Velocity m/sec(ft/sec)	144 (472)	136 (445)	244 (801)	142 (465)
Max Melt Area $cm^2(in.^2)$	1.23 (0.19)	0.90 (0.14)	0.90 (0.14)	0.77 (0.12)

FD 145935

Figure 20-D. Burn Severity and Melt Area of Ti 8Al-1Mo-1V at Various Thicknesses

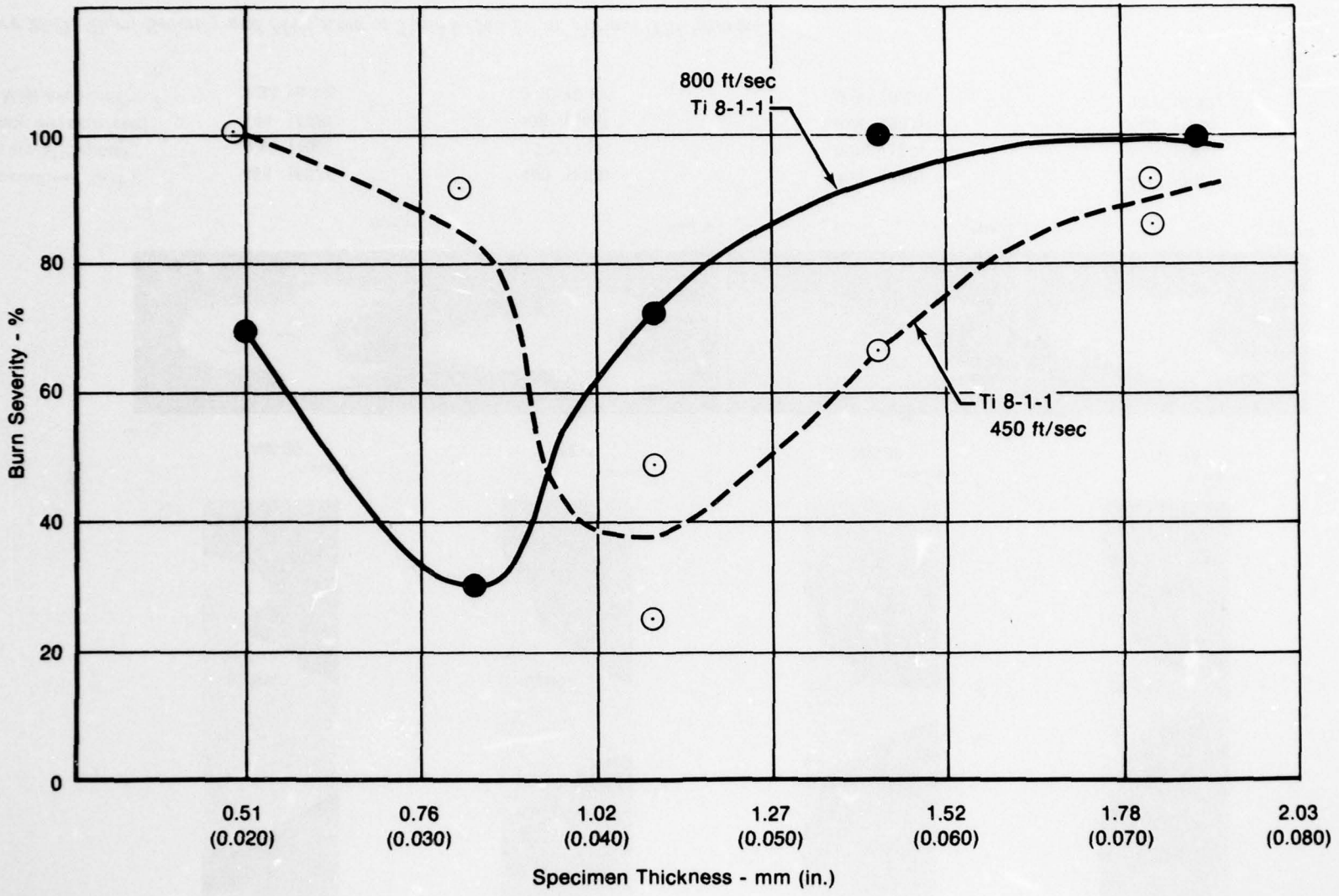

FD 145918

Figure 21. Burn Severity vs Specimen Thickness

These curves indicate a definite relationship in which the severity of burn decreases significantly at an intermediate thickness. Additionally, this intermediate thickness changes as a function of airstream velocity.

In a closer inspection of these overlapping curves, it can be seen that at approximately 0.9 mm (0.036 in.) the burn severity/thickness relationship at the two conditions reverses — that is, at a thickness less than 0.9 mm (0.036 in.) the severity is greater for the low velocity condition. Similarly, for thicknesses greater than 0.9 mm (0.036 in.) the burn severity is greater at the high velocity condition.

b. Thickness vs Chordwise Burn Velocity

A composite plot of burn front distance from the leading edge vs time (burn velocity profile) for Ti 8-1-1 specimens of various thicknesses is shown in Figure 22. These curves indicate that the chordwise burn velocity is correlated with both thickness and airstream velocity. To explicitly define this relationship, a plot of chordwise average burn velocity as a function of specimen thickness was prepared (see Figure 23). A computer-run regression analysis of the points comprising these curves resulted in the following equations for the "best fit" curves:

Low Velocity Condition: $V = 0.134T^{-0.791}$
High Velocity Condition: $V = 0.324T^{-0.674}$

where:

V = Chordwise Average Burn Velocity in in./sec
T = Specimen Thickness in in.

The curves shown in Figure 23 were drawn for these equations and the points then plotted for the actual test results. At each environmental condition these curves show a close correlation in which the average chordwise burn velocity decreases as the thickness increases. A visual interpretation of this thickness/combustion velocity relationship is shown in Figure 15 (see paragraph III.B.3).

c. Thickness vs Spanwise Burn Velocity

Plots of spanwise burning vs time (velocity profile) show an extremely high degree of correlation at each individual specimen thickness. These curves, shown in Figures 24 and 25, all have a correlation coefficient greater than 0.98. As noted in Figure 24, the combustion rate differs significantly among the specimen thicknesses at the low velocity condition while, at the high velocity condition, these curves (Figure 25) are very closely grouped. To provide a comparative illustration of the effect of airstream velocity on this combustion parameter, Figure 24 includes a dotted-line curve representing the average of the closely-grouped high velocity curves. This shows that at the high velocity condition the various thickness specimens burned at a rate between the 0.51 mm (0.020 in.) and 0.81 mm (0.032 in.) specimens at the low velocity condition.

The above observations indicate that, at the lower airstream velocity, thickness has a pronounced influence on the spanwise burn rate and that, as velocity is increased, specimen thickness ceases to be a significant factor.

Because of an encouraging preliminary indication, an attempt was made to correlate spanwise burn velocity with specimen thickness to produce curves and equations similar to those developed for chordwise combustion.

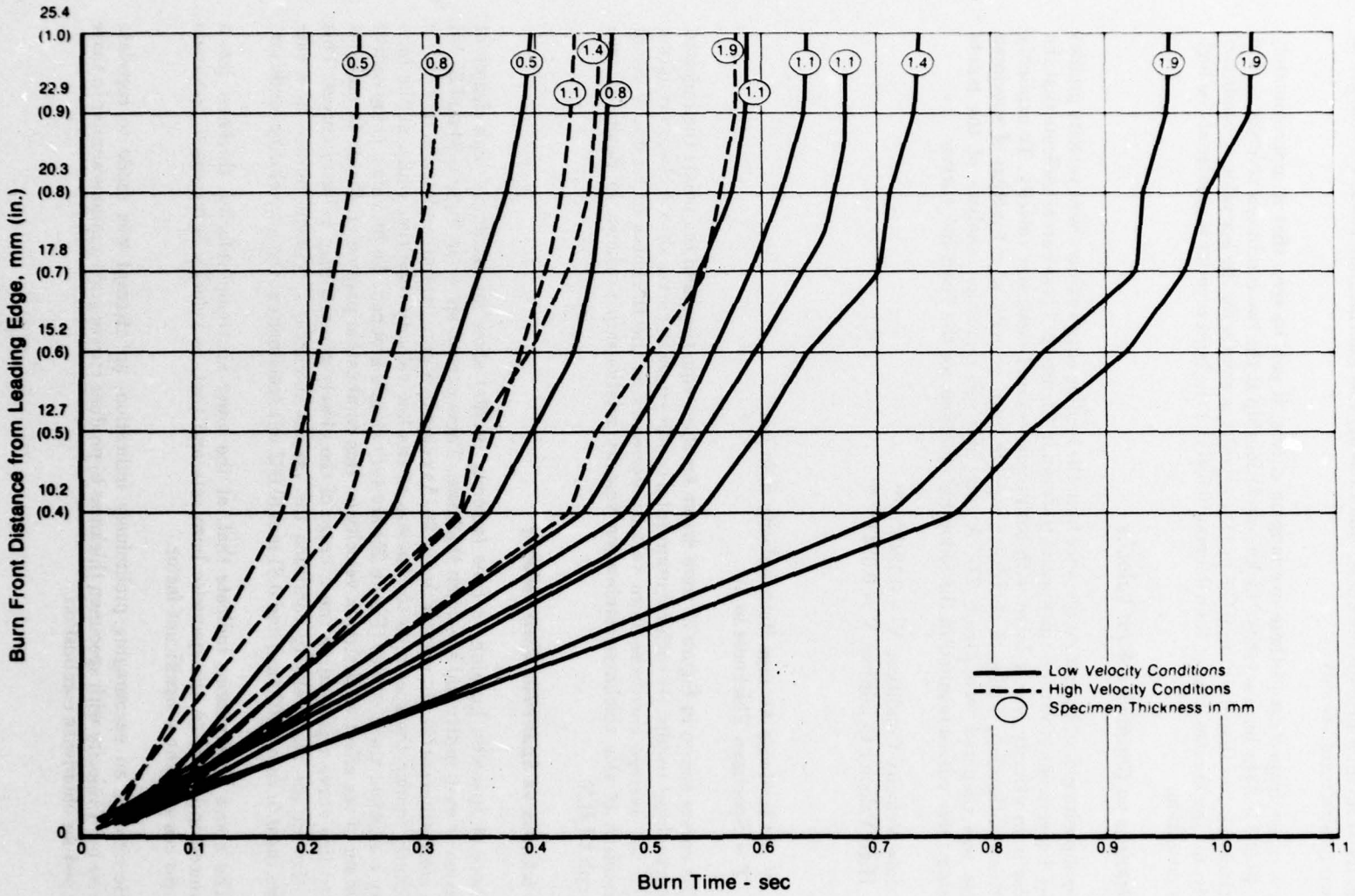

FD 139271

Figure 22. Ti 8-1-1 Burn Velocity Profiles

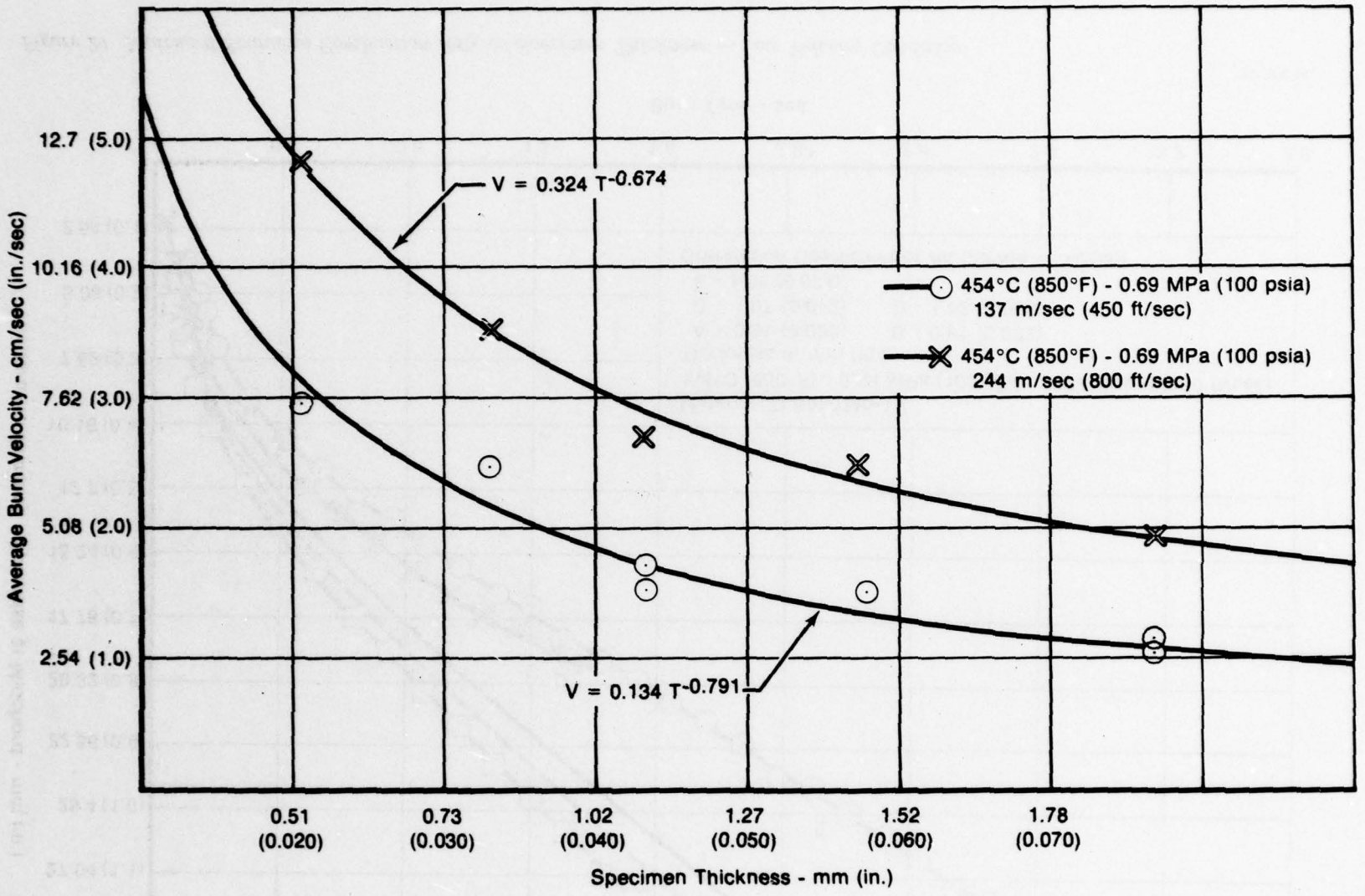

Figure 23. Thickness vs Chordwise Burn Velocity Ti-8Al-1Mo-1V

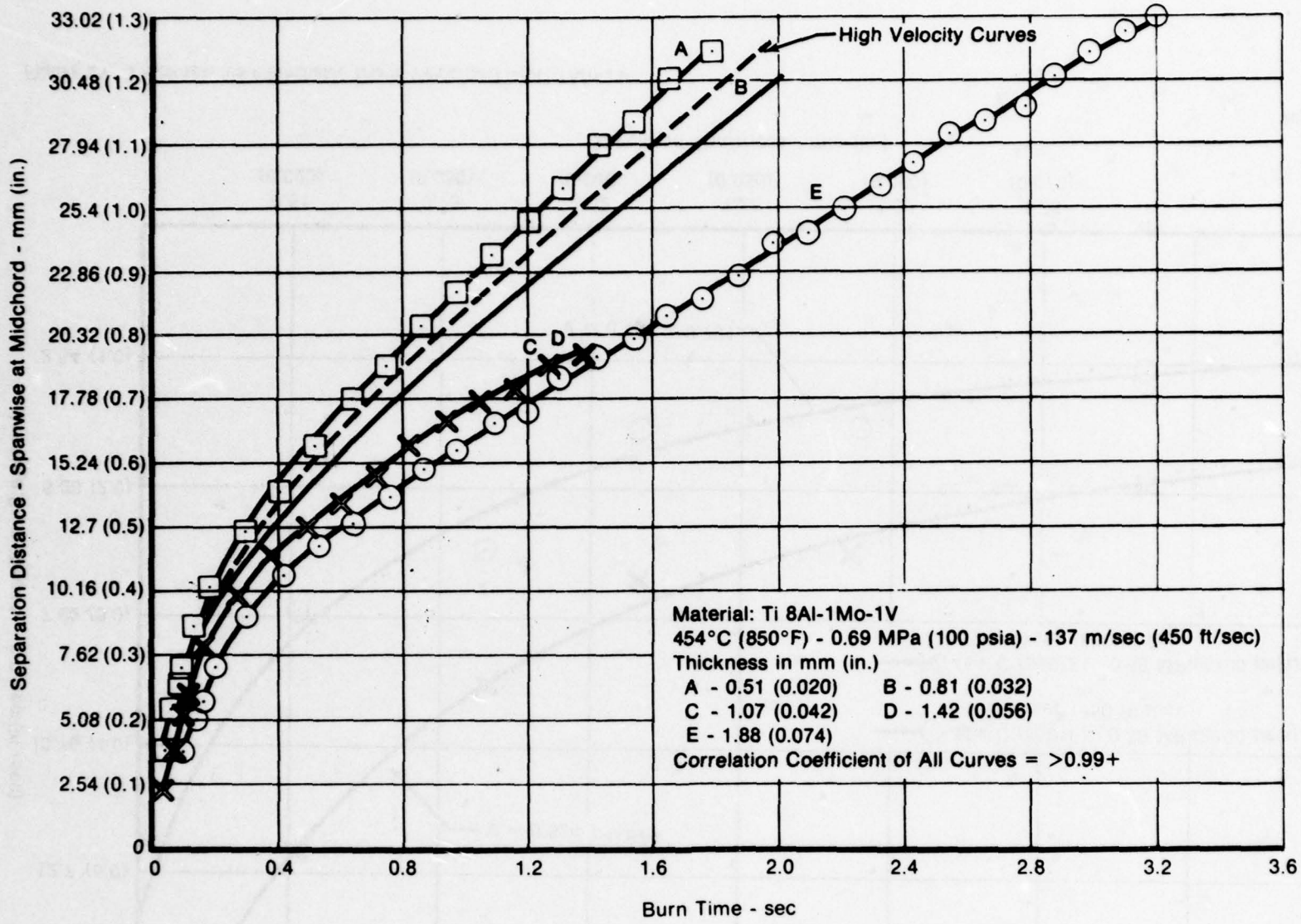

Figure 24. Midchord Spanwise Combustion Rate vs Specimen Thickness — Low Velocity Condition

The nonlinear shape of the velocity profile curves at the early stages of burn (see Figure 24) did not permit the use of an average spanwise velocity. Instead the velocity used for correlation purposes was taken as the slope of the linear portion of the curve. These velocity and thickness data pairs were subjected to a regression analysis. Best fit curves yielded correlation coefficients of 0.18 for the high velocity condition and 0.75 for the low velocity condition. At the high velocity condition, as the thickness increased, the velocity decreased to a minimum at a thickness of 1.07 mm (0.042 in.) and increased again. In contrast to this, at the low velocity condition, the burn velocity continuously decreased as thickness increased.

d. Thickness vs Other Combustion Parameters

Further attempts to correlate thickness with other available combustion parameters failed to establish a relationship which could be considered valid or potentially valid. The parameters evaluated consisted of ignition time, maximum melt area and spanwise burn front angle. In addition, the relationship of a maximum melt length-to-width ratio vs average spanwise burn velocity was investigated. This parameter was considered to be another measure of melt geometry which, potentially, could impact spanwise combustion. The resulting plots showed points having random scatter with a very low correlation coefficient and, thus, no relationship.

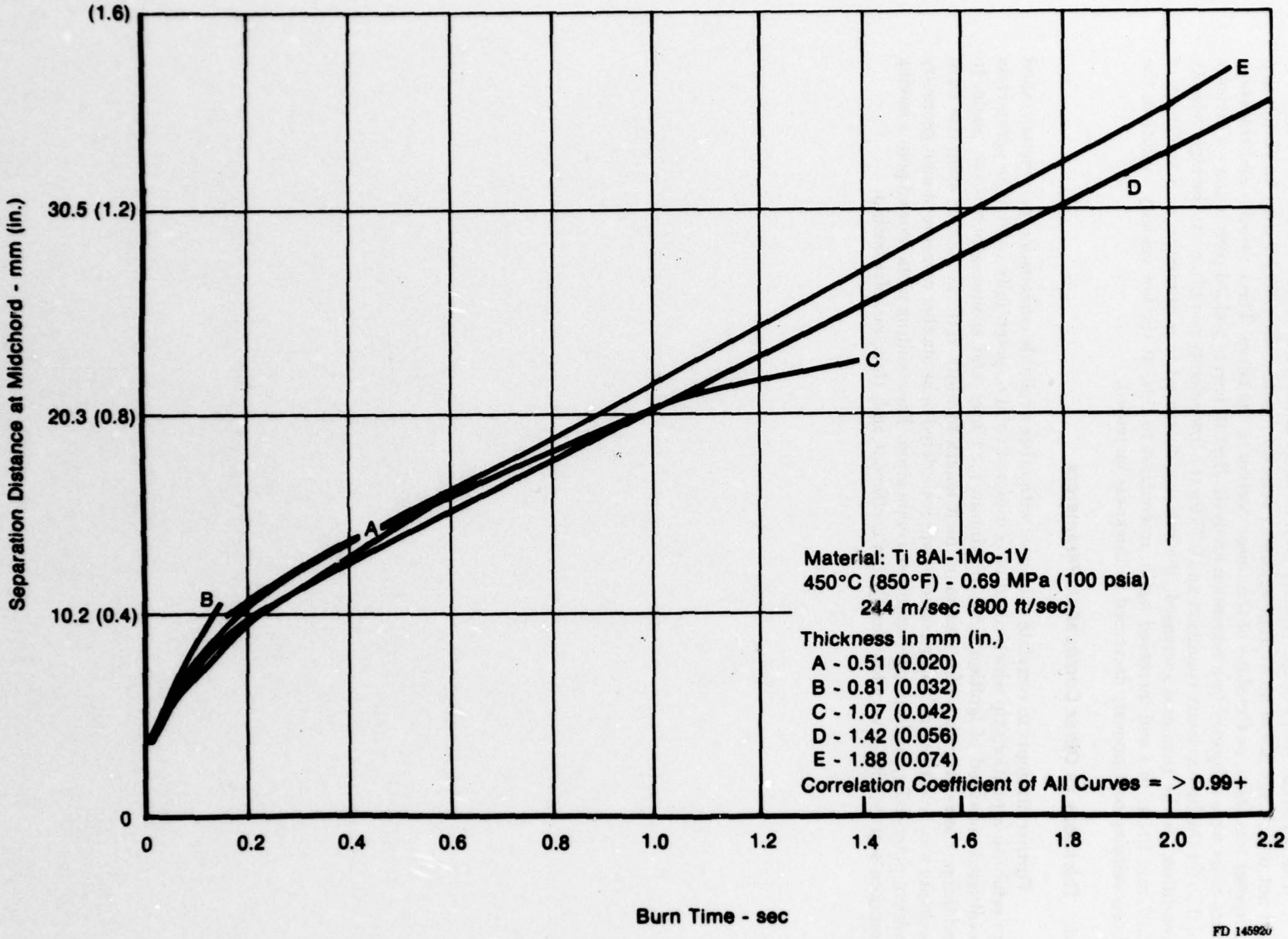

Figure 25. Midchord Spanwise Combustion Rate vs Specimen Thickness — High Velocity Condition

2. Alloy Effect

The following paragraphs delineate the effect that the alloys tested produced on the various combustion parameters.

a. Titanium — Nickel Alloys

The effectiveness of analysis of the Ti-Ni alloys was slightly reduced due to the loss, during processing, of high-speed film coverage for specimen N2-17 (Ti 5Ni). However, burn severity data was available from the reconstructed, burned specimen.

The initial characteristic of the Ti-Ni alloys to command attention was the time to ignition. For the seven specimens for which this data was available, the ignition time range was 0.008 to 0.032 sec with an average of 0.018 sec. This value was consistently and significantly lower than the test series average of 0.033 sec and the baseline Ti 8-1-1 average of 0.032. Further, ignition time did not appear to be a function of the percent nickel. Averages by percent nickel showed the following: Ti 5Ni = 0.020 sec; Ti 10Ni = 0.019 sec; Ti 20Ni = 0.018 sec. These differences are not significant.

These lower ignition times are the result of two general factors. First, the Ti-Ni alloys have a lower specific heat and melting point. Secondly, these properties cause the onset of melting to occur earlier; this first indicated melt represents the defined ignition event.

Subsequent to ignition, the Ti 5Ni and Ti 10Ni alloys experienced sustained combustion. Ignition of the Ti 20Ni specimens, however, only resulted in a small notch in test runs at four environmental conditions. The reconstructed specimens, with the corresponding burn severity values, are shown in Figure 26.

The first observation to be made from Figure 26 is that the burn severity decreased with an increase in percent nickel and an increase in airstream velocity. This burn severity/velocity relationship is a unique characteristic of both a given alloy and its thickness. The thickness effect for Ti 8-1-1 was discussed in paragraph III.C.1 but is currently unknown for Ti-Ni alloys. The graphical relationship of burn severity and percent nickel (shown in Figure 27) indicates that the probable nickel concentration which will not support combustion is between 12% and 17% at the conditions tested.

Considering combustion velocity, the Ti-Ni alloys did not exhibit characteristics significantly different from the average of other alloys of the same thickness. The 5% alloy did burn faster than the 10% alloy as shown in the velocity profiles in Figure 28. Combustion in the spanwise direction for the 5% nickel specimen did not proceed sufficiently to yield reliable velocity results. Values of 1.12 and 1.14 cm/sec (0.44 and 0.45 in./sec) for the 10% Ni specimens did not represent a marked deviation from the baseline Ti 8-1-1 values of 1.27 and 1.30 cm/sec (0.50 and 0.51 in./sec).

The combustion sequence of specimen N2-20 (Ti 10Ni at the high airstream velocity) proved to be the most unusual test of the entire program. This specimen experienced a normal ignition at 0.015 sec which continued glowing until approximately 0.070 sec at which time it appeared to die out. This phenomena was typical of the notch formation of a normal nonburning specimen. However, at approximately 1.0 sec the heat glow reappeared and began to move about slightly, but never enlarging. At about 2.5 sec the glow rapidly began to enlarge. Within a few milliseconds sustained combustion began and propagated to burn-through at 2.921 sec.

The observed sequence, when considered together with the resultant low burn severity, strongly suggests that under these conditions Ti 10Ni is very close to the critical nonburning composition.

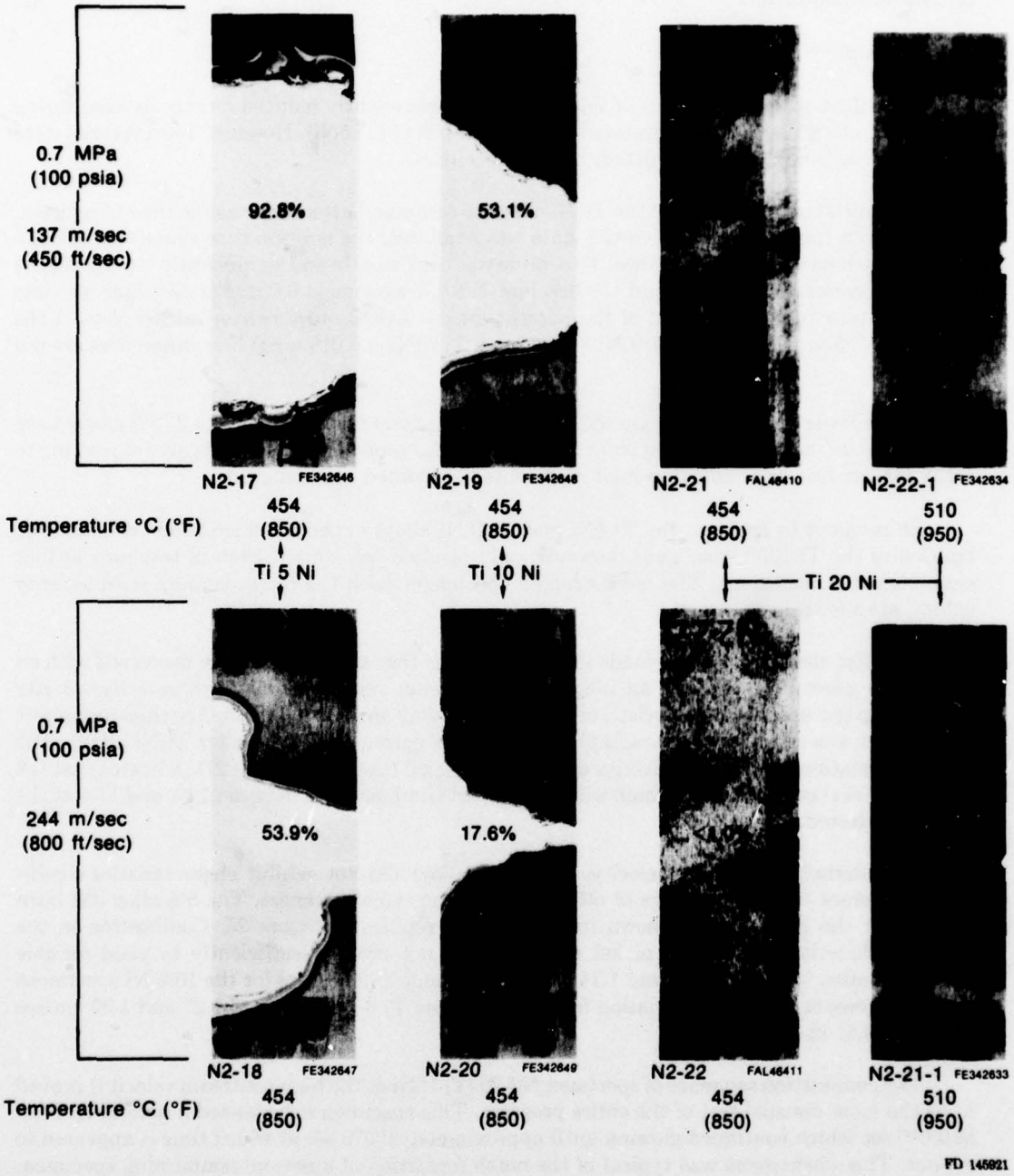

Figure 26. Burn Severity — Ti-Ni Alloys

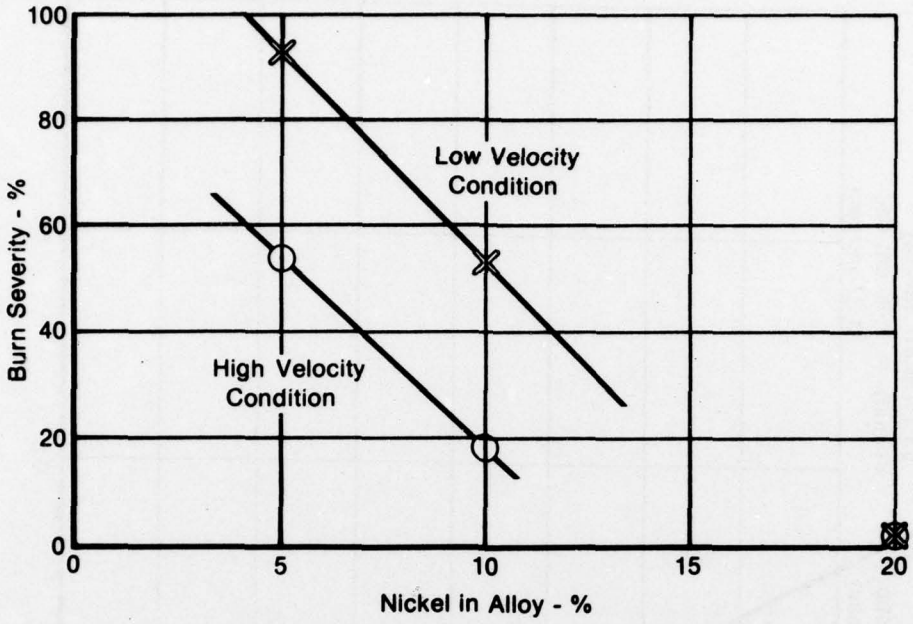

Figure 27. Burn Severity vs Percent Nickel in Alloy

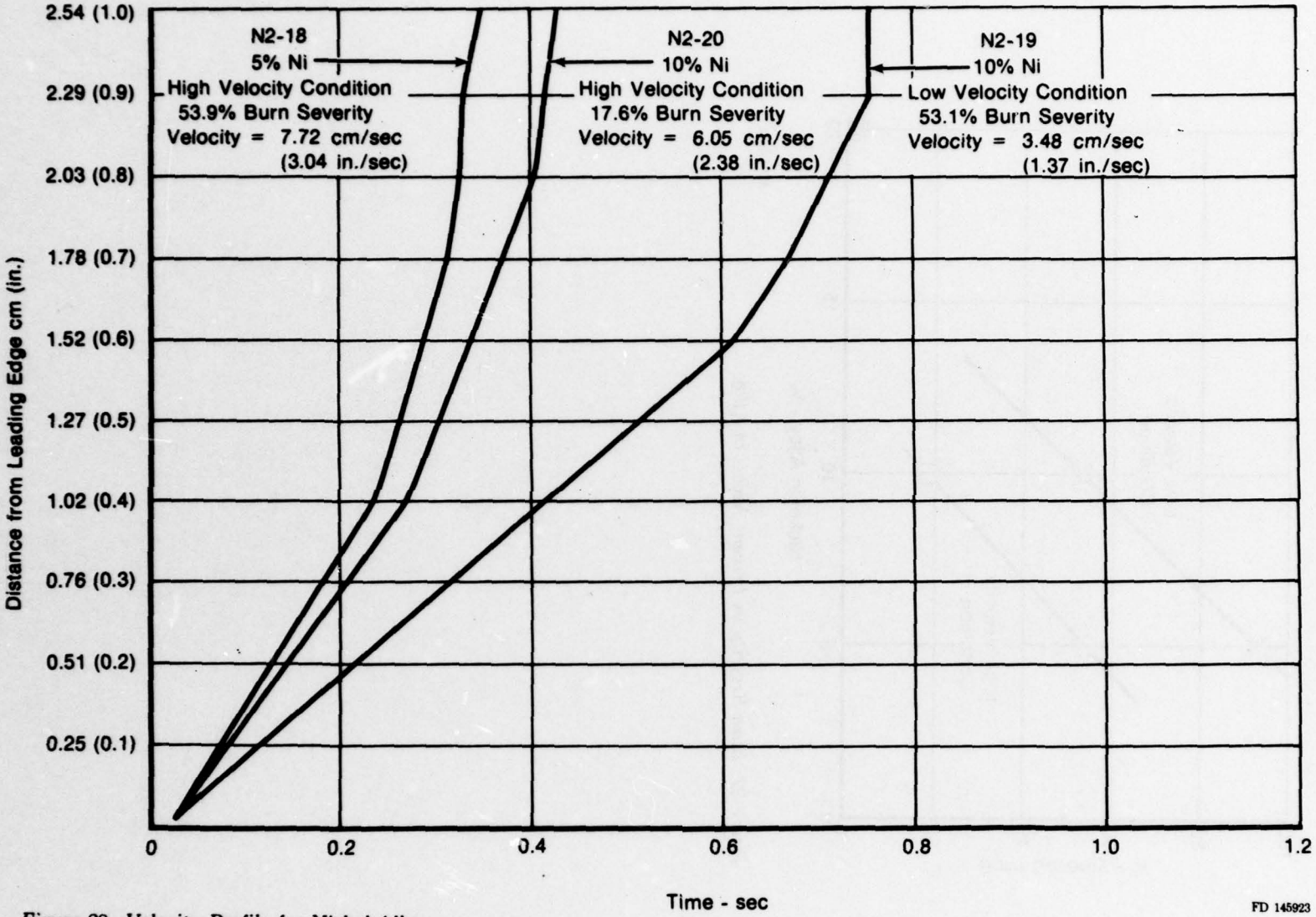

Figure 28. Velocity Profile for Nickel Alloys

b. Ti 13.5Al-21.5Nb (Ti_3Al)

Ti_3Al proved to require, on the average, the most energy to effect ignition of all alloys tested. Times for ignition were consistently greater with a range from 0.037 to 0.083 sec and an average of 0.052 sec. The explanation for this increased ignition time comes from an inspection of the influential physical properties of the alloying constituents. Considering thermal conductivity, the value for niobium is over three times that of titanium. This results in the net heat buildup in the irradiated area, during a normal ignition interval, being significantly reduced thereby requiring a greater time to effect melting. In addition, the heat of fusion of niobium is almost 1.5 times that of titanium. This would have the effect of requiring more energy, and therefore more time, to produce a melt condition (ignition criteria).

Five Ti_3Al specimens were tested and ignited — four experienced sustained combustion. Figure 29 shows the reconstructed specimens along with the associated run conditions. Noteworthy in the appearance of those specimens which burned is the small, relatively constant burn severity. This occurred over a range of environmental conditions which included variations of temperature — 87°C (157°F), pressure — 0.41 MPa (60 psia) and airstream velocity — 105 m/sec (343 ft/sec).

Figure 29 also illustrates the very narrow and small maximum melt areas of this alloy and the general visual correlation of melt area with burn severity. This correlation also exists mathematically with burn severity increasing almost linearly with an increase in melt area.

The velocity profiles for the Ti_3Al alloy are shown in Figure 30. These curves illustrate the expected response — an increase in chordwise burn velocity for an increase in airstream velocity at the two test series environmental conditions. Changes in chordwise burn velocity observed as environmental conditions were varied beyond this are discussed in paragraph III.C.3.

As was true of all specimens experiencing a low burn severity, Ti_3Al did not burn for a sufficiently long interval in the spanwise direction to yield data adequate for establishing a reliable combustion rate.

c. Beta III (Ti 11.5Mo-6Zr-4.5Sn)

Three specimens of alloy Beta III were tested — two at the established environmental conditions and one additional run at a reduced temperature and pressure. All three ignited and experienced sustained combustion.

The 0.034, 0.042 and 0.044 sec ignition times were not significantly greater than the average of 0.032 sec for the baseline Ti 8-1-1 alloy.

As shown in Figure 31, burn severity for the Beta III specimens was moderately low. Like the Ti-Ni alloys, Beta III burn severity decreased (20.5% to 17.8%) with increase in airstream velocity. Additionally, a decrease in temperature and pressure also effected a decreased burn severity (17.8% to 9.7%).

The velocity profile curves of Figure 32 show that at the two standard test conditions Beta III burned at a rate — 3.73 (1.47) and 7.09 (2.79) cm/sec (in./sec) — approximately the same as the baseline alloy Ti 8-1-1 — 3.96 (1.56) and 6.55 (2.58) cm/sec (in./sec). The test run at reduced temperature and pressure resulted in an intermediate value for average chordwise burn velocity.

The extent of spanwise combustion was too short in duration to provide sufficient data for correlation attempts.

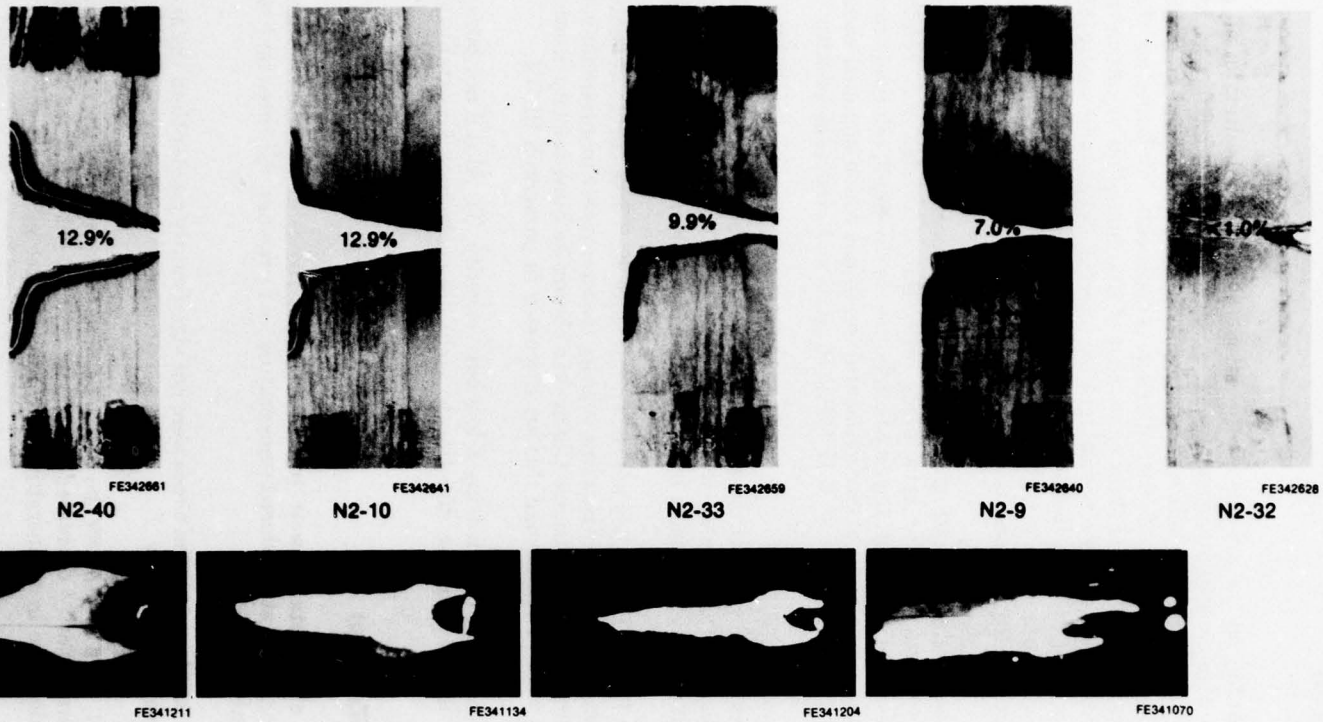

Temperature, °C(°F)	511(952)	457(854)	424(795)	457(854)	429(804)
Pressure MPa(psia)	0.28(40)	0.69(100)	0.69(100)	0.69(100)	0.48(70)
Velocity m/sec(ft/sec)	245(804)	246(806)	240(789)	141(463)	237(777)
Max Melt Area $cm^2(in.^2)$	0.77(0.12)	0.71(0.11)	0.58(0.09)	0.39(0.06)	

FD 145924

Figure 29. Burn Severity of Alloy Ti 13.5Al-21.5Nb

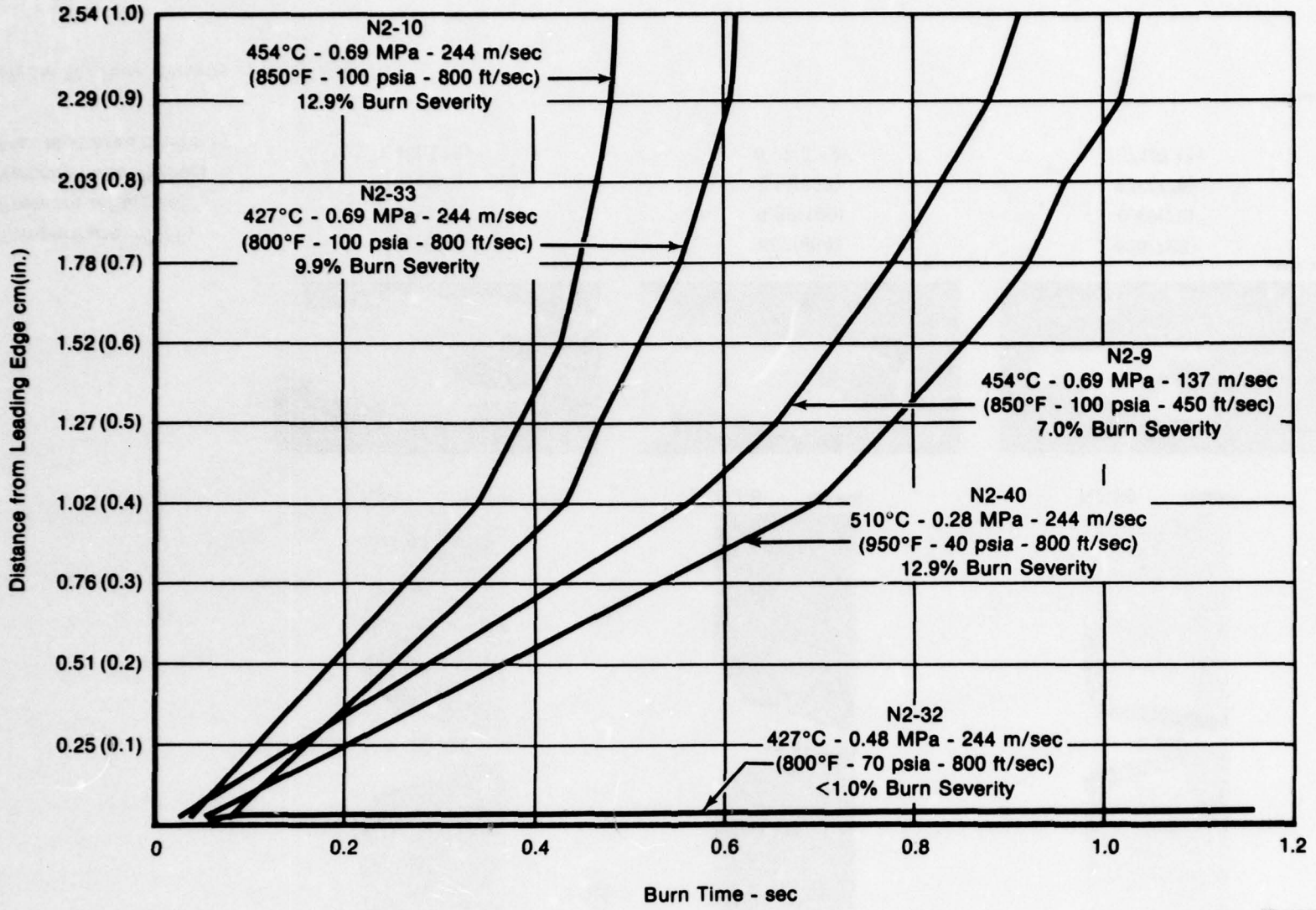

Figure 30. Velocity Profiles for Alloy Ti 13.5Al-21.5Nb

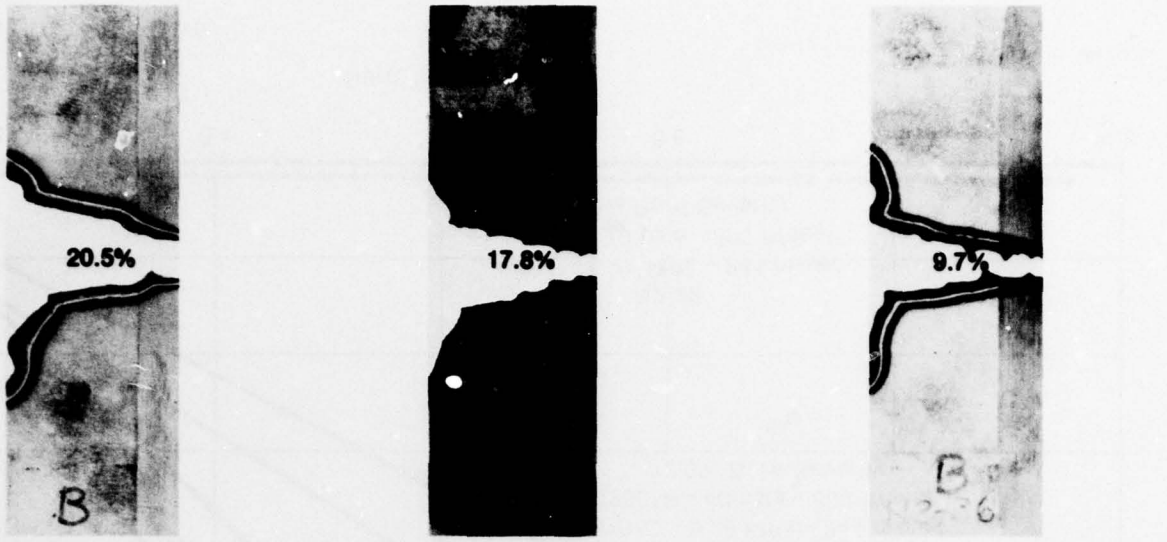

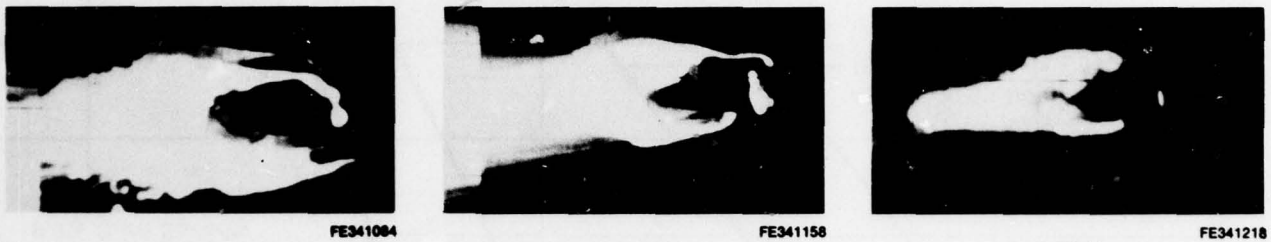

	N2-7	N2-8	N2-36
Temperature, °C(°F)	457(854)	457(854)	426(799)
Pressure MPa(psia)	0.69(100)	0.69(100)	0.48(70)
Velocity m/sec(ft/sec)	141(463)	246(808)	237(776)
Max Melt Area $cm^2(in.^2)$	1.16(0.18)	0.77(0.12)	0.71(0.11)

FD 145926

Figure 31. Burn Severity of Alloy Beta III

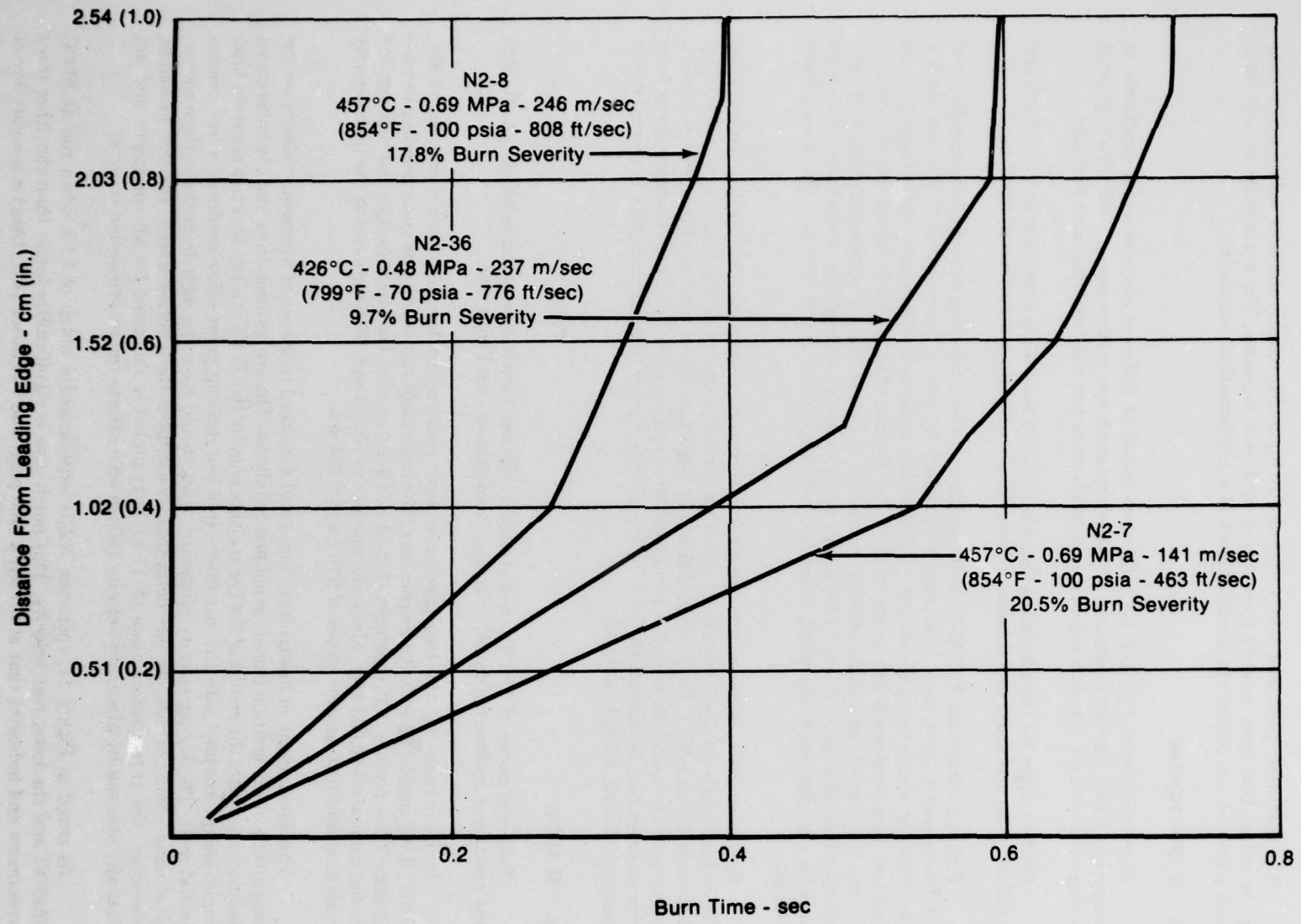

Figure 32. Velocity Profile for Alloy Beta III

The maximum melt area values, included in Figure 31, roughly correlate with burn severity to the extent that burn severity increases as melt area increases. The availability of only three data pairs did not permit the establishment of a mathematical correlation.

d. Ti 13V-11Cr-3Al

Four specimens of Ti 13V-11Cr-3Al were tested at different environmental conditions of temperature and airstream velocity. Chamber pressure was maintained at 0.69 MPa (100 psia) during all four tests. Ignition was achieved in all cases but only one specimen burned.

Ignition times for the specimens that only notched were fairly consistent at 0.022, 0.025 and 0.030 sec. The specimen which burned, however, showed an ignition time of 0.047 sec.

Figure 33 shows the Ti 13V-11Cr-3Al specimens after test along with the corresponding test conditions and ignition time. Specimen N2-1, which burned to the extent of 13.8%, represents a discontinuity which currently cannot be thoroughly explained. The temperature conditions for this test were considered less severe by 53°C (95°F) than those of N2-38 which did not burn. If, on the other hand, airstream velocity represents the more-critical parameter, then specimen N2-39, which also notched, would have burned by reason of temperature and airstream velocity increase. By deductive reasoning, therefore, either specimen N2-38 or N2-39 also should have burned.

Specimen N2-1, however, was unique in one respect — ignition time was 84% greater than the rather closely grouped average of the other three specimens. If the laser beam was slightly defocused for run N2-1, the area heated would be larger. When melt condition was reached, a larger quantity would be available to support sustained combustion. Some evidence exists from this program (see paragraph III.C.2.f) to support the theory that burn severity is related to the quantity of melt initially formed.

e. Ti 13Cu

Four specimens of Ti 13Cu were tested at different environmental conditions. In all cases the specimens ignited but failed to sustain combustion (see Figure 34).

Ignition times for the four specimens were consistently low and closely grouped (0.014, 0.017, 0.022 and 0.022 sec). An inspection of the individual run conditions corresponding to each ignition time reveals that specimens N2-34 and N2-5, run at the low velocity condition, ignited in the same time (0.022 sec). Similarly, specimens N2-35 and N2-6 were run at the high velocity condition and had ignition times of 0.017 and 0.014 sec.

This phenomena of low ignition times and a marked influence of airstream velocity on the magnitude of the ignition time is explained as follows. The low ignition time and the subsequent failure to burn are the results of the low melting point of the Ti 13Cu alloy. Due to a constant laser input energy coupled into the specimen, this low melting point alloy produces a less viscous initial melt. The higher velocity airstream, thus, would blow the melt from the surface sooner, producing sparks which, by our definition, constitutes the ignition event. By this rationale, therefore, the true ignition time of Ti 13Cu is probably the same for all specimens and not actually affected by airstream velocity (which only affects the identification criteria).

As noted in Figure 34, specimen N2-34 experienced a notch of 1.0% when run at 509°C (948°F) and the lower test velocity. This notch area is significantly larger than the other three specimens and indicates that at 0.7 MPa (100 psia) and 148 m/sec (487 ft/sec) a temperature of 509°C (948°F) is very close to that required for self-sustained combustion.

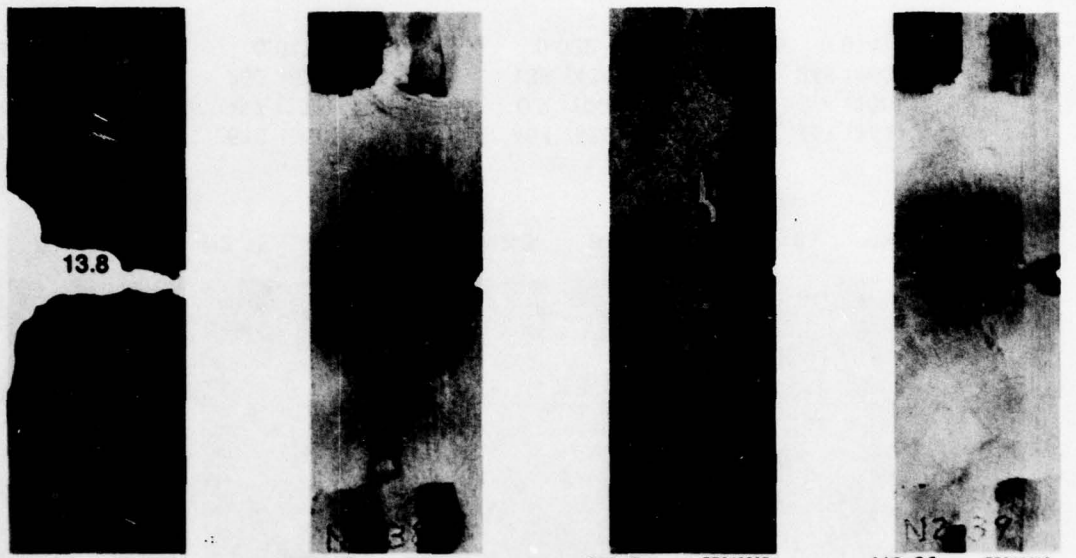

Temperature °C (°F)	:	456 (853)	509 (948)	456 (853)	511 (952)
Pressure MPa (psia)	:	0.69 (100)	0.69 (100)	0.68 (99)	0.69 (100)
Velocity m/sec (ft/sec)	:	141 (464)	151 (497)	247 (810)	255 (835)
Ignition Time (sec)	:	0.047	0.030	0.022	0.025

FD 145928

Figure 23. Burn Severity — Alloy Ti 13V-11Cr-3Al

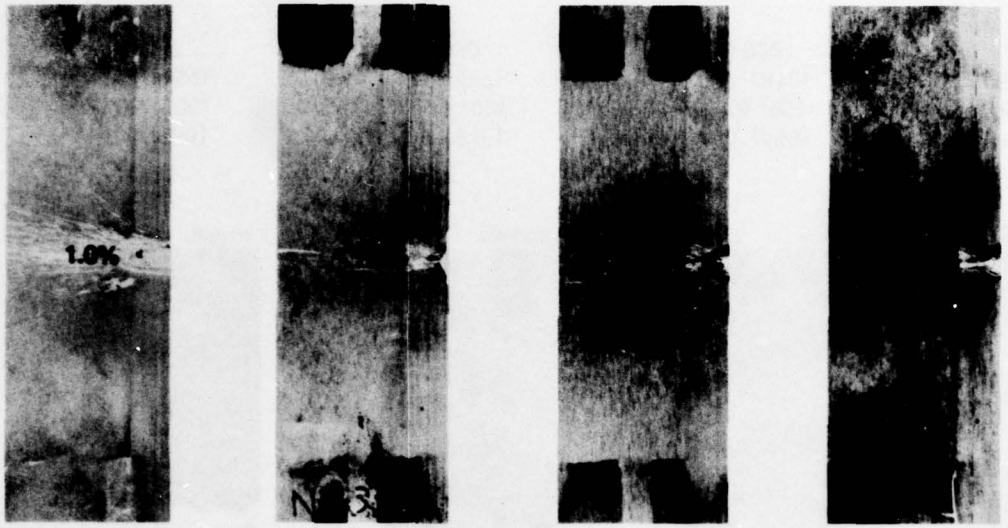

Temperature °C (°F)	:	509 (948)	510 (950)	454 (850)	457 (854)
Pressure MPa (pais)	:	0.7 (101)	0.7 (101)	0.7 (100)	0.7 (100)
Velocity m/sec (ft/sec)	:	148 (487)	252 (828)	138 (454)	245 (803)
Ignition Time (sec)	:	0.022	0.017	0.022	0.014

Figure 34. Burn Severity of Alloy Ti 13Cu

FD 145930

f. Ti 8Al-1Mo-1V

The previous discussion of Ti 8-1-1 was primarily concerned with an evaluation of the effect of specimen thickness and not necessarily of the alloy per se. This subparagraph, therefore, will discuss Ti 8-1-1 ignition and combustion parameters by considering only those specimens of 1.07 mm (0.042 in.) thickness. This subgroup of the Ti 8-1-1 specimens included four test runs — one at the high velocity condition, two at the low velocity condition and a fourth at the low velocity condition in which the temperature was reduced by 28°C (50°F).

Two of the three specimens tested at the low velocity condition (N2-11 and N2-25) were run at close-to-duplicate conditions while the third (N2-41), as pointed out above, was run at a temperature approximately 6% lower than the others. Despite these virtually identical environmental conditions, the combustion results of N2-11 and N2-25 varied considerably. Figure 35 shows burn severity, maximum melt area and test conditions for these specimens.

An analysis of the N2-11 and N2-25 data revealed two outstanding differences. First, the N2-25 specimen was 2.42 cm (0.953 in.) wide instead of the specified 2.54 cm (1.000 in.). This was the narrowest specimen of the entire test series. Secondly, N2-25 experienced ignition in 0.013 sec which is significantly shorter than the 0.034 sec recorded for N2-11 and, coincidentally, the Ti 8-1-1 alloy average. Since these two specimens were run at virtually identical environmental conditions, the almost 2-to-1 ratio of experienced burn severity represented a discontinuity requiring explanation.

One possible explanation involves both of the foregoing differences. The width of specimen N2-25 (almost 1.27 mm (0.050 in.) narrower than the others) may have been responsible for a laser beam "near miss." That is, the laser beam realignment, required to compensate for the narrower specimen, could have resulted in an undetected tracking error between the "hot" (CO_2) beam and the helium-neon alignment beam. This could have placed the "hot" beam straddling the sharp leading edge. This, in turn, would cause heating to occur in a very small area (relative to other specimens). Since under these conditions the specimen was very thin in the impingement area, it required less energy (and thus less time) to effect ignition. As a result, this small ignition area produced less melt to initiate self-sustained combustion thereby effecting less burn severity.

In summary, the N2-25 specimen width, ignition time, burn severity and maximum melt area all tend to support this explanation.

Figure 36 shows the velocity profiles for these three specimens. Here, again, a definite correlation exists between burn severity and average chordwise combustion velocity. The magnitude of the velocity values is in general agreement with the results of previous studies and is only significant in its specimen-to-specimen variation.

Other parameters considered in the combustion of the 1.07 mm (0.042 in.) Ti 8-1-1 specimens included ignition time, spanwise burn velocity and laser power output during the run. Ignition time varied from 0.013 sec to 0.045 sec and exhibited no apparent correlation to either specimen geometry or laser power output. Average spanwise velocity for the three specimens tested at the low velocity condition was extremely constant at 1.27, 1.30 and 1.30 cm/sec (0.50, 0.51 and 0.51 in./sec). This was in contrast to the 25% variation in average chordwise velocity.

In summary, the 1.07 mm (0.042 in.) Ti 8-1-1 specimens reacted as expected based upon previous studies.

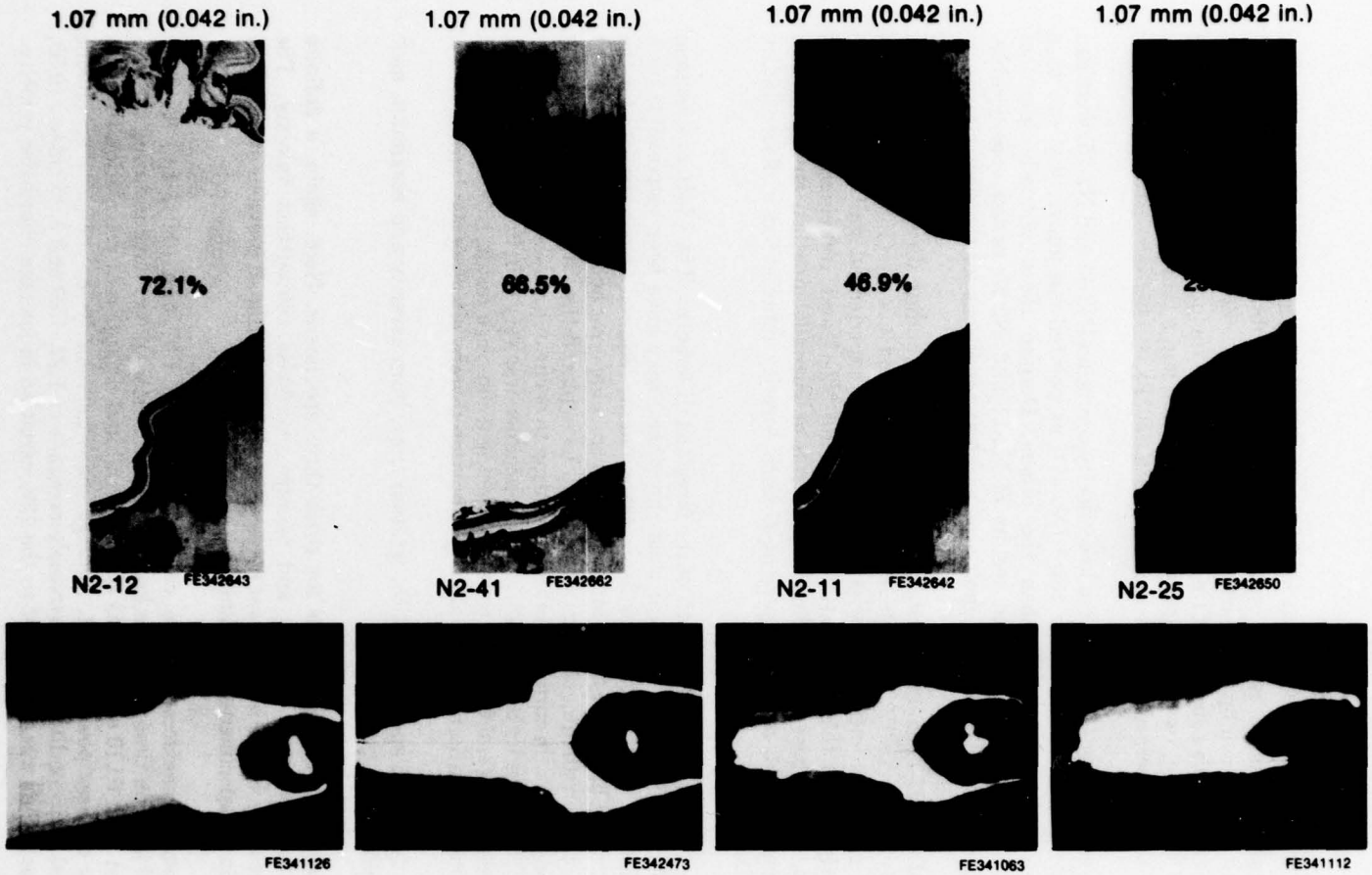

Temperature °C (°F):	456 (852)	429 (804)	460 (860)	454 (849)
Pressure MPa (psia):	0.70 (101)	0.69 (100)	0.70 (101)	0.69 (100)
Velocity m/sec (ft/sec):	245 (803)	141 (463)	136 (445)	142 (465)
Maximum Melt Area cm^2 ($in.^2$):	1.16 (0.18)	1.23 (0.19)	0.90 (0.14)	0.77 (0.12)

FD 145936

Figure 35. Burn Severity — Ti 8-1-1 at 1.07 mm (0.042 in.) Thickness

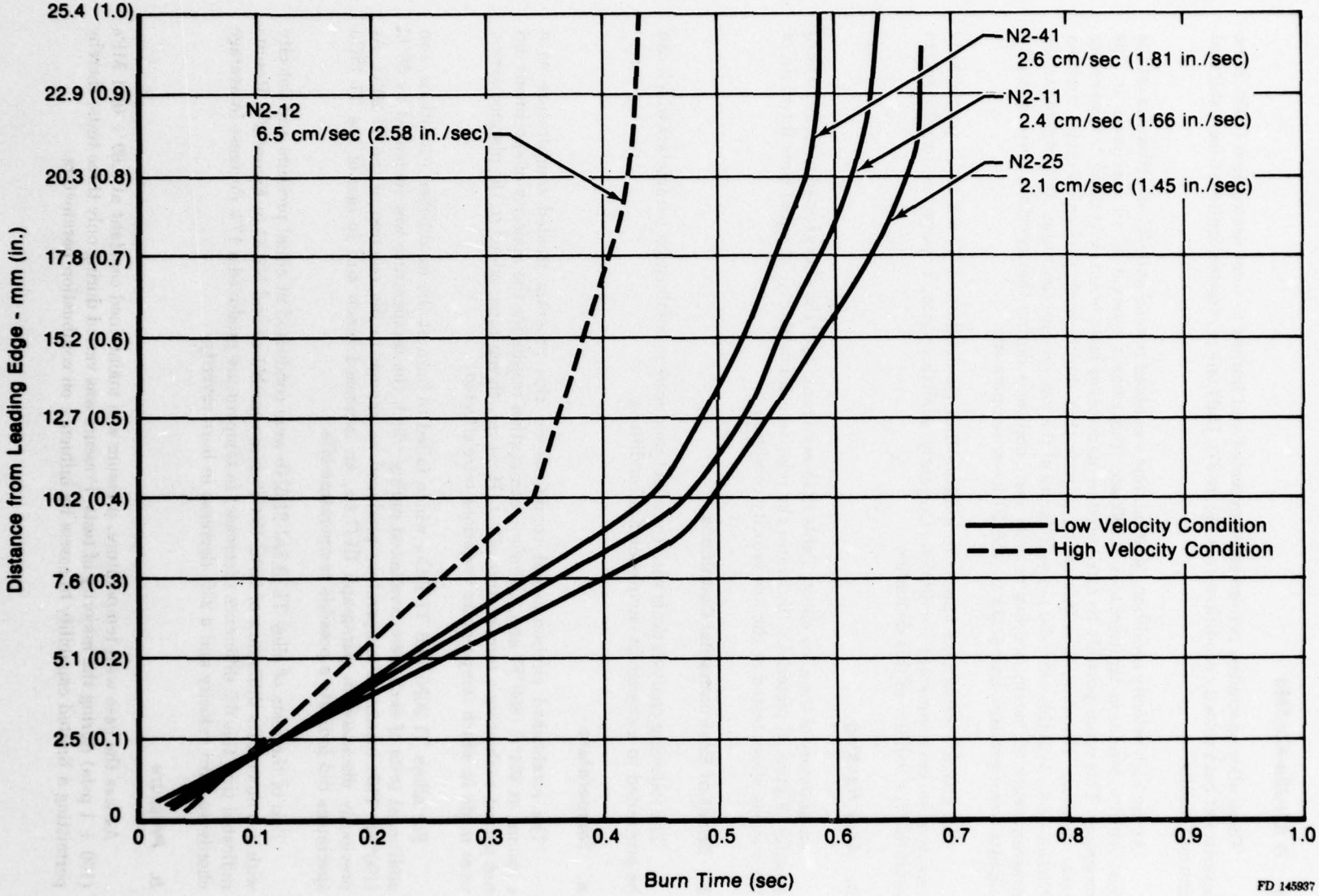

Figure 36. Velocity Profiles — Ti 8-1-1 at 1.07 mm (0.042 in.) Thickness

g. Ti 6Al-2Sn-4Zr-6Mo

These alloy specimens performed as expected and burned to total destruction (100% burn severity) at both velocity conditions (see Figure 37). Only one parameter, ignition time, exhibited unusual results.

At the high velocity condition, ignition time was about normal at 0.025 sec. However, at the low velocity condition ignition took 0.090 sec (the longest interval of all specimens in this program). This could possibly be attributed to inadvertent laser beam defocusing or inadequate laser coupling. However, it is interesting to note that during work performed under contract N62269-76-C-0429 this alloy did not even ignite at the low velocity condition. As compared to the program reported herein, the low velocity test conditions during that program encompassed a slightly lower pressure and a 232°C (450°F) lower temperature.

The above observations appear to indicate that the ignition of Ti 6-2-4-6 is particularly sensitive to environmental conditions. Currently available data, however, is insufficient to establish the validity of this deduction.

h. Alloy Ranking

In summary of the alloy effect, Table 12 shows a ranking of the alloys tested in terms of burn severity. Figure 38 pictorially illustrates the relative combustibility, at equal time intervals, of the various alloys tested at the low velocity condition.

3. Effect of Environmental Conditions

The following analysis deals with the effect produced on combustion parameters which can be attributed to a change in environmental conditions.

a. Temperature

The established environmental conditions for this program treated temperature as a constant at 454°C (850°F) and, therefore, combustion results for the majority of specimens did not permit evaluating a temperature effect. However, eleven runs, added to the planned series, were made in which temperature variations were effected.

For alloys Ti 20Ni and Ti 13Cu, which failed to burn at the established conditions, two additional tests of each were conducted during which the temperature was increased by 56°C (100°F). This increased temperature produced no change to the reaction of the Ti 20Ni. As previously discussed in paragraph III.C.2.e, an increased notch size in one of the Ti 13Cu specimens did indicate a possible temperature effect.

Two of the tests of alloy Ti 13.5Al-21.5Nb were conducted at equal pressure and velocity with a temperature difference of 28°C (50°F) (see runs N2-10 and N2-33 in Figure 30). Results indicated that this 6% difference (decrease) in temperature produced a 17% decrease in average chordwise burn velocity and a 23% decrease in burn severity.

b. Pressure

As was the case with temperature, pressure was maintained constant at 0.69 ± 0.01 MPa (100 ± 1 psia) during the majority of tests. Pressure was varied during only three tests, thereby permitting a limited capability to assess its influence on combustion parameters.

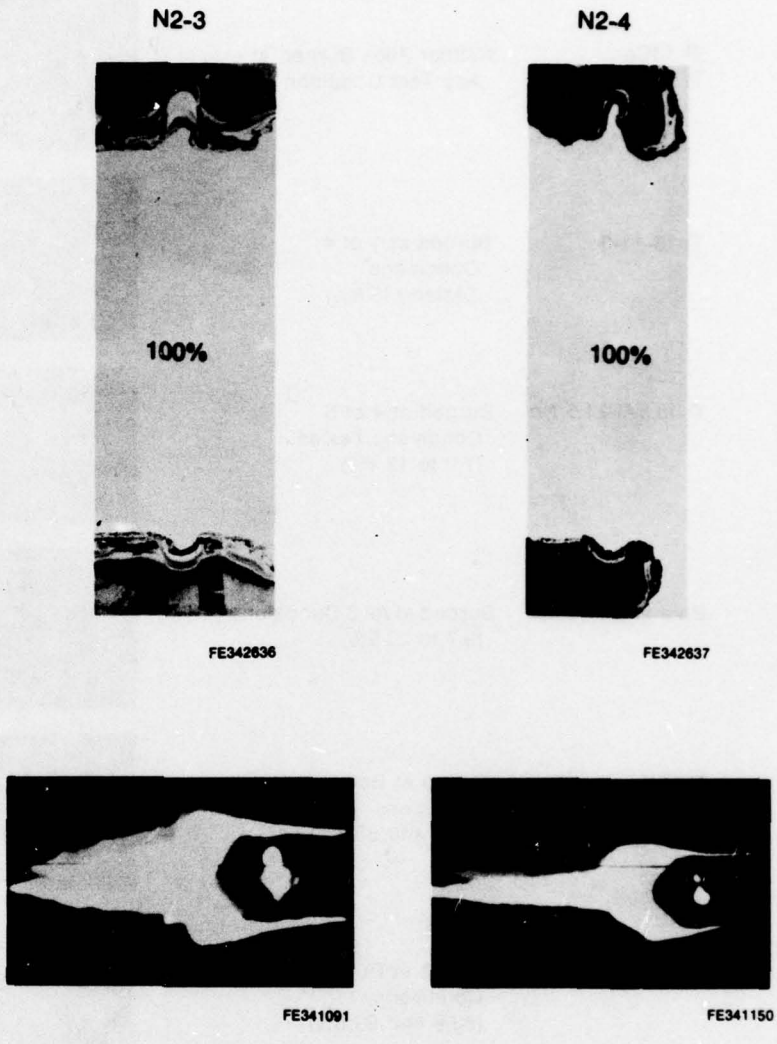

Temperature °C (°F):	459 (859)	457 (855)
Pressure MPa (psia):	0.70 (101)	0.70 (101)
Velocity m/sec (ft/sec):	141 (462)	246 (807)
Maximum Melt Area cm^2 ($in.^2$):	0.90 (0.14)	0.65 (0.10)

D 145938

Figure 37. Burn Severity of Ti 6Al-2Sn-4Zr-6Mo

TABLE 12. ALLOY RANKING BY BURN SEVERITY

Alloy	Overall Results	Burn Severity
Ti 13Cu Ti 20Ni	Neither Alloy Burned at Any Test Condition	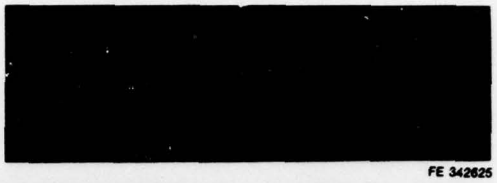 FE 342625
Ti 13-11-3	Burned at 1 of 4 Conditions Tested (13.8%)	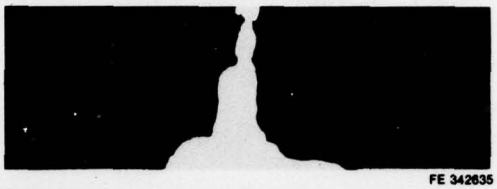 FE 342635
Ti 13.5Al-21.5 Nb	Burned at 4 of 5 Conditions Tested (7.0 to 12.9%)	 FE 342659
Beta III	Burned at All 3 Conditions (9.7 to 20.5%)	 FE 342639
Ti 10Ni	Burned at Both Conditions (17.6 and 53.1%)	 FE 342648
Ti 5Ni	Burned at Both Conditions (53.9 and 92.8%)	 FE 342646
Ti 8-1-1	Burned in All Cases Tested (25.5 to 100%)	 FE 342644
Ti 6-2-4-6	Burned at Both Conditions at 100%	 FE 342638

FD 145941

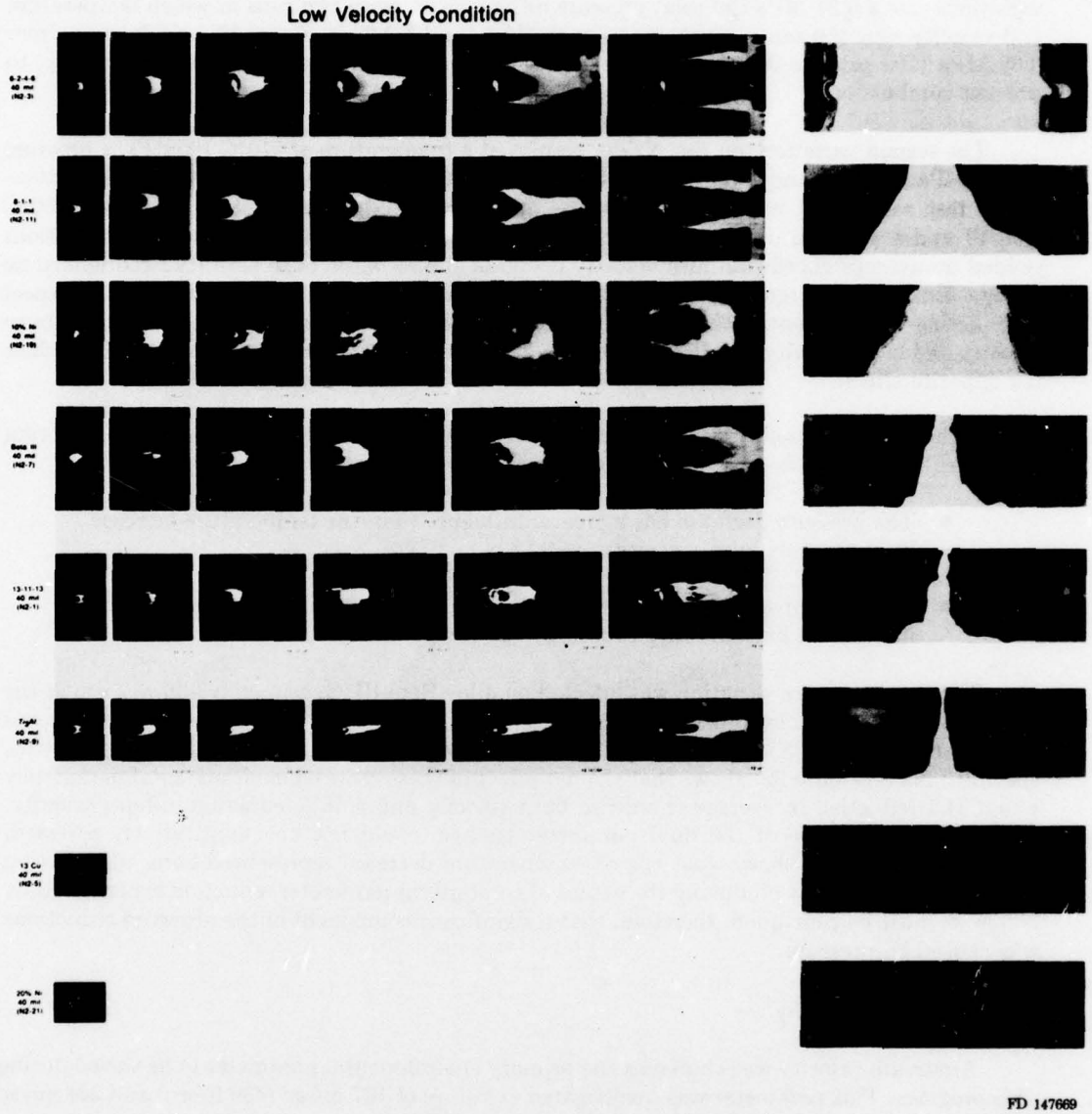

Figure 38. Burn Appearance of Equal-Thickness Alloys at Equal Time Intervals Including Specimen Final Appearance

Two of the pressure variations occurred during tests of Ti 13.5Al-21.5Nb. One of these variations was a 0.21 MPa (30 psia) pressure difference between two runs in which temperature and velocity were the same. As shown by runs N2-32 and N2-33 in Figure 30, this decrease from 0.69 MPa (100 psia) to 0.48 MPa (70 psia) was sufficient, at this temperature and velocity, to prevent combustion.

The second variation, on run N2-40, employed a temperature of 510°C (950°F), a pressure of 0.28 MPa (40 psia) and a velocity of 244 m/sec (800 ft/sec). When compared with run N2-10 — at the test series high velocity condition — this represented a temperature increase of 56°C (100°F) and a pressure decrease of 0.41 MPa (60 psia). Results showed that these conditions yielded an average chordwise burn velocity decrease of 55% while burn severity experienced no change. Based on the temperature effect established in paragraph III.C.3.a, one would expect that, acting independently, the 56°C (100°F) temperature increase would increase both burn velocity and burn severity. As discussed above, however, the decrease in pressure would produce the opposite effect.

Although this amount of data does not permit a quantitative measure of these opposing effects, subjectively it is evident that, for this specific combination of conditions:

- The pressure decrease has a greater influence than the temperature increase by decreasing burn velocity.
- The pressure decrease reduced burn severity by an amount equal to the increase in burn severity caused by the temperature increase.

The third pressure variation was effected on alloy Beta III. Specimen N2-36 was run at the high velocity condition established for the series 244 m/sec (800 ft/sec), but the temperature was reduced by 31°C (55°F) and the pressure by 0.21 MPa (30 psia). Comparing this run with specimen N2-8 (Figure 32) shows that the net affect of these reduced environmental parameters was a 34% reduction in average chordwise burn velocity and a 46% reduction in burn severity. These results, because of the dual parameter change, could not be quantitatively assessed. However, it has been shown that the 6% temperature decrease represented here, when acting alone, is not capable of producing the extent of combustion parameter reduction experienced by N2-36. It must be concluded, therefore, that a significant component of the observed reductions was caused by pressure.

c. Airstream Velocity

Airstream velocity was chosen as the primary environmental parameter to be varied during this program. This parameter was investigated at values of 137 m/sec (450 ft/sec) and 244 m/sec (800 ft/sec).

The effect of airstream velocity on burn severity of the various test alloys is shown visually and numerically in the reconstructed specimens of Figures 39 and 40. Figure 41 is a plot of these results which conveys a clearer picture of the overall airstream velocity effect on burn severity. The dotted-line curve shown in Figure 41 is a typical plot for an expanded velocity range. This curve represents Ti 8-1-1 data taken from previous work and indicates that (for Ti 8-1-1) as airstream velocity increases burn severity increases to some maximum value and then decreases.

From Figure 41 it can be seen that individual alloys differed greatly in their response to a velocity change. First, since alloy Ti 6-2-4-6 burned at 100% in both cases, it must be considered, for this test program, as not being affected by velocity. Previous work, however, has indicated that Ti 6-2-4-6 normally behaves the same as Ti 8-1-1 and increases in burn severity with a velocity increase.

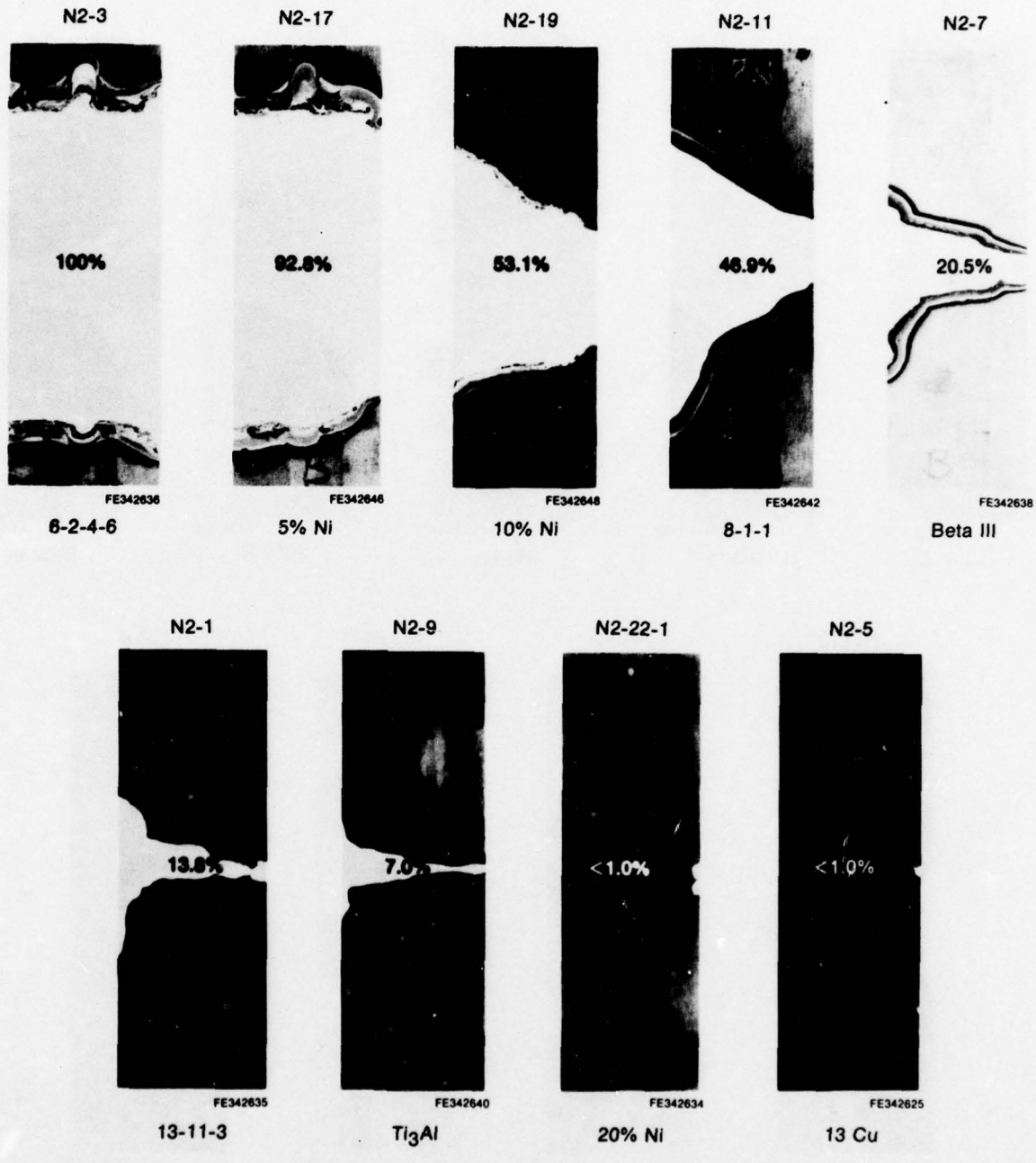

Figure 39. Burn Severity at 454°C (850°F) — 0.7 MPa (100 psia) — 137m/sec (450 ft/sec)

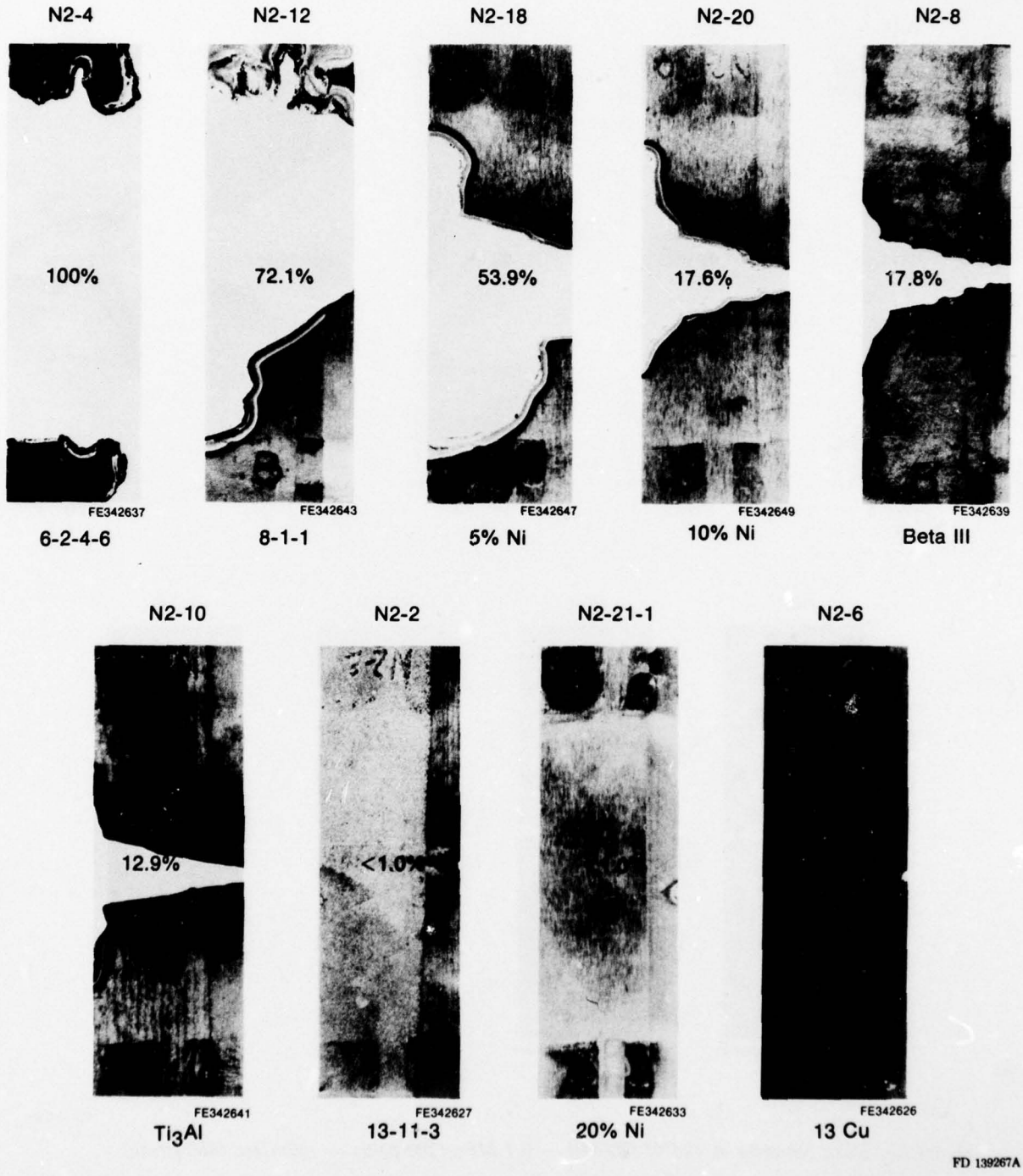

Figure 40. Burn Severity at 454°C (850°F) — 0.7 MPa (100 psia) — 244 m/sec (800 ft/sec)

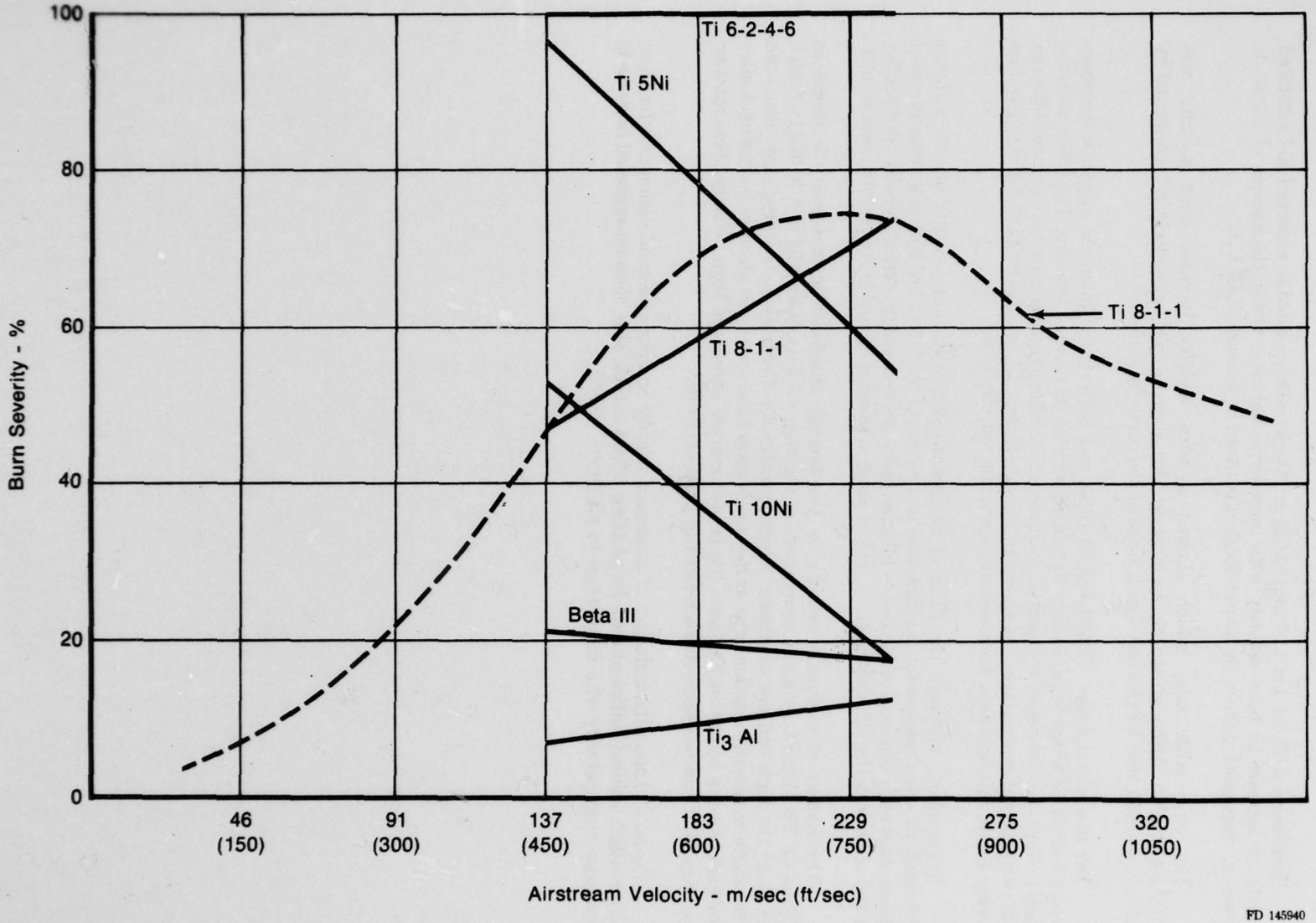

Figure 41. Burn Severity vs Airstream Velocity at Constant Temperature and Pressure

Specimens of Ti 8-1-1 of 1.07 mm (0.042 in.) thickness responded as expected and exhibited a definite increase in burn severity with increase in velocity. Other thicknesses of Ti 8-1-1, however, responded differently as previously discussed in paragraph III.C.1.

The only other alloy which showed a burn severity increase with velocity was Ti 13.5Al-215Nb. Although strictly an increase, this alloy was very close to being unaffected by velocity as indicated by the very small slope of the curve in Figure 41.

The two nickel alloys, Ti 5Ni and Ti 10Ni, and Beta III exhibited the opposite airstream velocity effect in which burn severity decreased with an increase in velocity. The effect with the nickel alloys was the greatest observed with any of the alloys tested and was consistent between the two different percentages. As shown in Figure 41, Beta III, similar to Ti 13.5Al-21.5Nb, had a very small, but opposite, burn severity/airstream velocity effect.

In summary, although the effect of airstream velocity on burn severity has been shown definitely to exist, reasons for the direction and extent of the effect are still unknown. It would appear that alloy physical properties — melting point, melt viscosity, surface tension, wettability of the melt with the substrate, etc. — are in some manner responsible for the observed results.

The impact of airstream velocity on the average chordwise burn velocity is shown in Figure 42. This figure permits a comparison of the burn velocity of all 1.02 mm (0.040 in.) thick alloys at the high and low airstream velocity conditions. Contrary to the previously discussed velocity/burn severity relationships, these curves show no reversals. In all cases and for each alloy the high velocity condition produced the largest average chordwise burn velocity. This reaction was expected and has been characterized in previous work.

Figure 43 shows the influence of airstream velocity on spanwise combustion rate for those alloys which yielded sufficient data for plotting. These curves, also, show an expected increase in spanwise burn velocity with an increase in airstream velocity.

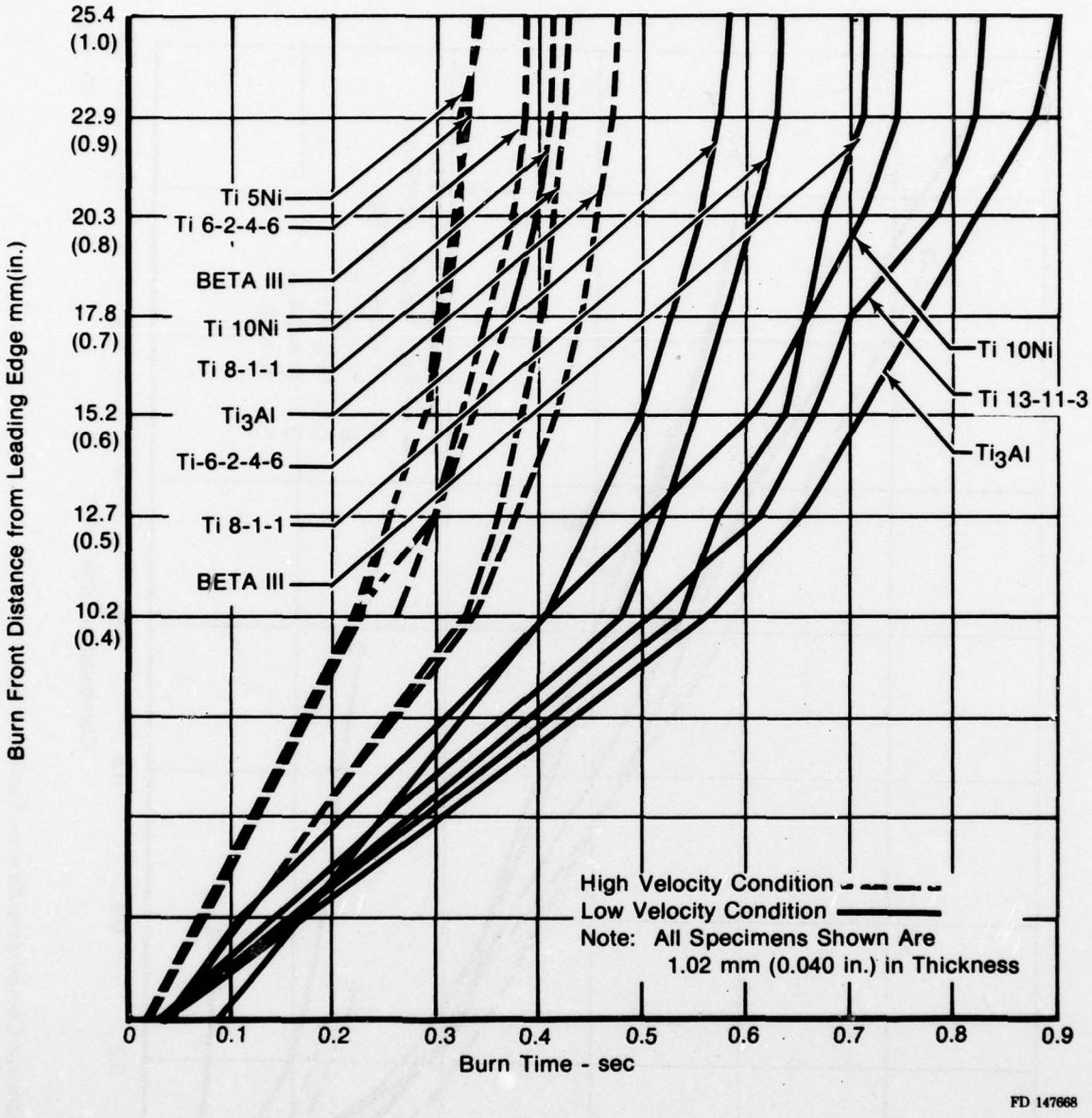

Figure 42. Velocity Profiles for All Alloys Tested

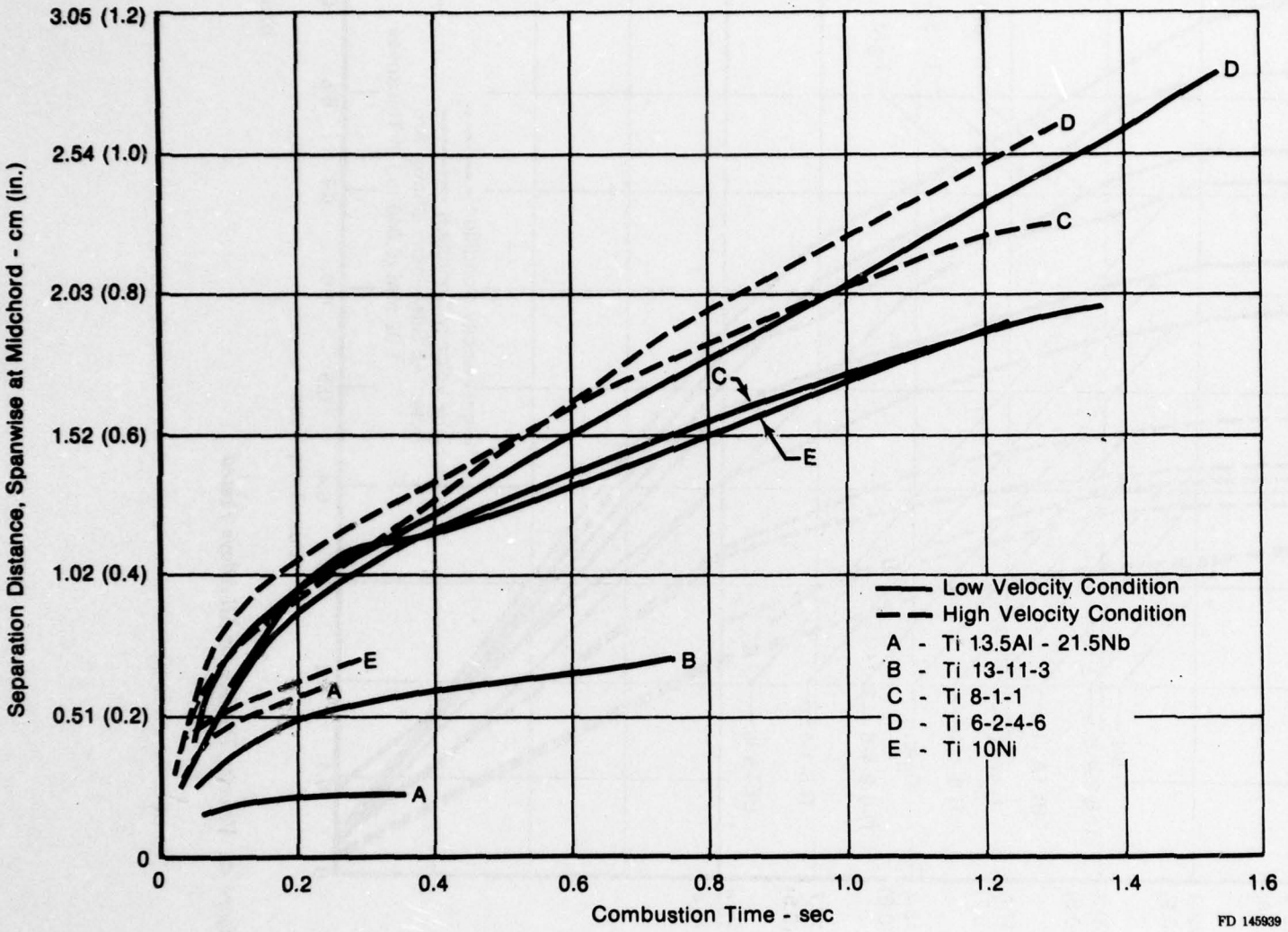

Figure 43. Midchord Spanwise Combustion Rate — Various Alloys

SECTION IV

ANALYTICAL SIMULATION

A short, complementary effort at the completion of the data analysis phase was the development of a titanium combustion computer simulation program based on experimental results. A laboratory SOL Terminal computer with 64K memory and a North Star Extended Basic language was used. Data output was by means of a video display with hard copy possible using an IBM Selectric typewriter tied into the SOL Terminal.

The resulting titanium fire computer simulation (Table 13) utilizes empirical equations formulated from data obtained during the titanium ignition and combustion test program. For the Ti 8-1-1 alloy used in this simulation, the parameters that determine chordwise and spanwise burn velocities are temperature, pressure, airstream velocity and specimen thickness. Empirical equations for the determination of burn severity were generated from relationships between airstream velocity and specimen thickness. The simulation can be used to show the shape of the burn front at various times, time to burn-through and percent burn severity.

To start the simulation program the following inputs are required:

1. PLATE THICKNESS, INCHES: Enter plate thickness (Figure 44) in inches.

2. MAG FACTOR: Enter the number of lines per inch in print-out (typically 19).

3. LENGTH, INCHES: Enter length of specimen exposed in holder in inches.

4. TOTAL WIDTH, INCHES: Enter specimen width (Figure 44) in inches.

5. WIDTH OF KNIFE EDGE, INCHES: Enter specimen knife edge width (Figure 44) in inches.

6. PRESSURE, PSIA: Enter pressure, in psia, at which the test run was conducted.

7. TEMPERATURE, °F: Enter temperature, in degrees Fahrenheit, at which run was conducted.

8. AIRSTREAM VELOCITY, FT/SEC: Enter airstream velocity, in foot/second, at which run was conducted.

9. DISTANCE OF LASER INPUT FROM THE TOP, INCHES: Enter laser input location. For all specimens laser input was at the middle (spanwise) of the specimen (1.05 inches from the top).

10. TOTAL RUN TIME, SEC: Enter the length of burn time, in seconds, for which observation is desired.

11. AT WHAT TIME INTERVAL IS A DISPLAY DESIRED, SEC: Enter the time, in seconds, at which an intermediate display of combustion progress is desired.

12. IS A HARD COPY DESIRED: An affirmative entry will result in display being typed for permanent record.

TABLE 13. TITANIUM COMBUSTION COMPUTER PROGRAM

```
LIST

10 F$="TIFIL"
20 REM                TITANIUM FIRE MODEL
30 DIM S1(50),D7(50)
110 INPUT "PLATE THICKNESS,INCHES ",T1
120 INPUT "MAG. FACTOR ",M1
130 M2=1.67*M1
140 INPUT "LENGTH,INCHES ",L1
150 INPUT"TOTAL WIDTH,INCHES ",W1
160 INPUT "WIDTH OF KNIFE EDGE,INCHES ",W2
170 INPUT "PRESSURE,PSIA ",P1
200 INPUT "TEMPERATURE,F ",T
230 INPUT "AIRSTREAM VELOCITY,FT/SEC",V1
290 INPUT"DISTANCE OF LASER INPUT FROM THE TOP,INCHES ",D2
360 INPUT "TOTAL RUN TIME,SEC LET",T2
370 INPUT "AT WHAT TIME INTERVAL DO YOU WANT A PRINT-OUT ",T3
371 INPUT"DO YOU WANT A HARD PRINT-OUT ",X$
376 T8=T3
377 FOR I=1 TO G2
378 D7(I)=0
379 NEXT I
380 G1=INT(L1*M1+.5) G2=INT(W1*M2+.5)
383 D5=0  S1=0  S3=0
385 A=INT( D2       *M1+.5)
390 T4=0  X=0  T5=0  T6=0  U=0  U1=0
400 FOR I=1 TO G2
410 GOSUB 5000
420 S1(I)=S3
430 NEXT I
431 U1=0
435 X=X+1
440 T4=0.01
450 GOSUB 4000
460 D5=D5+(C1*T4*M2)
465 T5=T5+T4  T6=T6+T4
470 IF D5<X THEN 460
475 IF T6>=T3 THEN U=1
476 IF D5>G2 THEN X1=G2
478 IF D5<=G2 THEN X1=INT(D5+.5)
480 FOR I=1 TO X1
490 D7(I)=D7(I)+(S1(I)*T5*M1)
500 NEXT I
501 IF U1=1 THEN 505
502 IF D5<G2 THEN 505
503 GOSUB 3000
505 T5=0
510 GOSUB 5500
515 IF U=1 THEN 540
517 IF B2>=B1 THEN 560
530 GOTO 435
540 !!!!
```

TABLE 13. TITANIUM COMBUSTION COMPUTER PROGRAM (Continued)

```
542 IF X$(1,1)<>"Y" THEN 550
544 FILL 51207,2
545 !!!!
550 IF U=1 THEN 570
560 !"Fire stopped at",INT(T6*1000+.5)/1000," seconds."U=2
565 GOTO 580
570 !"Elasped time is",INT(T6*1000+.5)/1000," seconds."
580 FOR I=1 TO G1
590 FOR J=1 TO G2
600 D7=    D7(J)         D7=INT(D7+.5)  Q=A-D7Q1=A+D7
610 IF Q<=0 THEN Q=0  IF Q1>=G1 THEN Q1=G1
615 IF J>D5 THEN 640
620 IF I<Q OR I>Q1 THEN 640
630 !"-",GOTO 650
640 !"X",
650 NEXT J
660 !" "
670 NEXT I
671 !
672 !"The burn area shown is ",INT(B2*100)/100," percent."
673 !"The burn area calculated is ",INT(B1*100)/100," percent."
674 IF X$(1,1)<>"Y" THEN 680
675 FILL 51207,0
680 IF T6>=T2 THEN 915
685 IF U=2 THEN 915
690 T3=T3+T8  U=0
700 GOTO 435
915 INPUT"ANOTHER TIME AT THE SAME CONDITIONS ",Y$
920 IF Y$="Y" THEN 360
930 INPUT" ANOTHER RUN ",Y$
940 IF Y$(1,1)="Y" THEN 20
950 GOTO 6000
2000 REM   SUBROUTINE TO CALCULATE IGNITION TIME
2005 REM D4 IS LASER DIAMETER
2010 A1=3.14*D4*D4/4
2020 T7=T1*(.5*D4+D1)/W2
2030 H1=((8.7+V1*.0111)/(A1*T7))*P/135
2040 T9=3000/H1
2050 !"Ignition occurs at ",T9," seconds."
2060 RETURN
2070 REM  END OF SUB
3000 REM SUBROUTINE TO STORE SPANWISE VELOCITIES
3010 FOR I=1 TO G2
3020 S1(I)=(I+50)/(G2+50)
3030 NEXT I
3040 U1=1
3050 RETURN
3060 REM END OF SUB
4000 REM    SUBROUTINE TO CALCULATE CHORDWISE VEL. & DIST.
4010 IF V1 > 400 THEN 4030
4020 C1=((P1+50)/150)*(V1/450*.134*T1^(-.791))  GOTO 4040
4030 C1=((P1+50)/150)*((5.43E-04)*V1-.1103)*T1^((3.34E-04)*V1-.941)
```

TABLE 13. TITANIUM COMBUSTION COMPUTER PROGRAM (Continued)

```
4040 C1=C1*1.00       C2=C2*1.00
4050 RETURN
4060 REM END OF SUB
5000 REM    SUBROUTINE TO CALCULATE SPANWISE VEL. & DIST.
5010 S1=.121*T1^(-.344)
5020 S2=-7.54E-02+(1.25E-03)*P1+(1.03E-04)*V1+(3.61E-06)*P1*V1
5030 S2=S2*(T+2350)/3200
5035 S1=S1*S2/0.258
5040 IF V1>700 THEN S1=S2
5045 S1=S1/2
5050 S4= (I/G2)^.9   GOTO 5060
5055 S4=(I+50)/(G2+50)
5060 S3=S1*S4
5070 RETURN
5080 REM END OF SUB
5500 REM SUBROUTINE TO CALCULATE BURN AREA
5510 IF V1>475 THEN 5550
5520 IF T1<.042 THEN 5540
5530 B1=6262*T1^1.62  GOTO 5580
5540 B1=-2830*T1+165.3  GOTO 5580
5550 IF T1<.032 THEN 5570
5560 B1=8720*T1^1.62  GOTO 5580
5570 B1=-3833*T1+146.7
5580 B1=(2.1/L1)*B1 J1=0
5590 FOR M=1 TO G2
5591 IF A+D7(M)<G1 THEN 5594
5592 D7=G1-A  GOTO 5600
5593
5594 IF A-D7(M)>0  THEN 5596
5595 D7=A  GOTO 5600
5596 D7=D7(M)
5600 J2=J2+INT(D7(M)+D7+.5)
5610 NEXT M
5620 IF D5> G2 THEN 5680
5630 A2=D5+J2
5640 GOTO 5690
5680 A2=G2+J2
5690 B2=A2*100/(G1*G2)
5700 J2=0
5710 IF .5*B1*W1*L1 > (D2     )*W1 THEN 5730
5720 B1=.5*B1 + (D2     )*W1/(L1*W1)
5730 IF .5*B1*L1*W1 > (L1-(D2     ))*W1 THEN 5750
5740 B1= .5*B1 + ((L1-(D2     ))*W1)/(L1*W1)
5750 RETURN
5760 REM END OF SUB
6000 END
READY
```

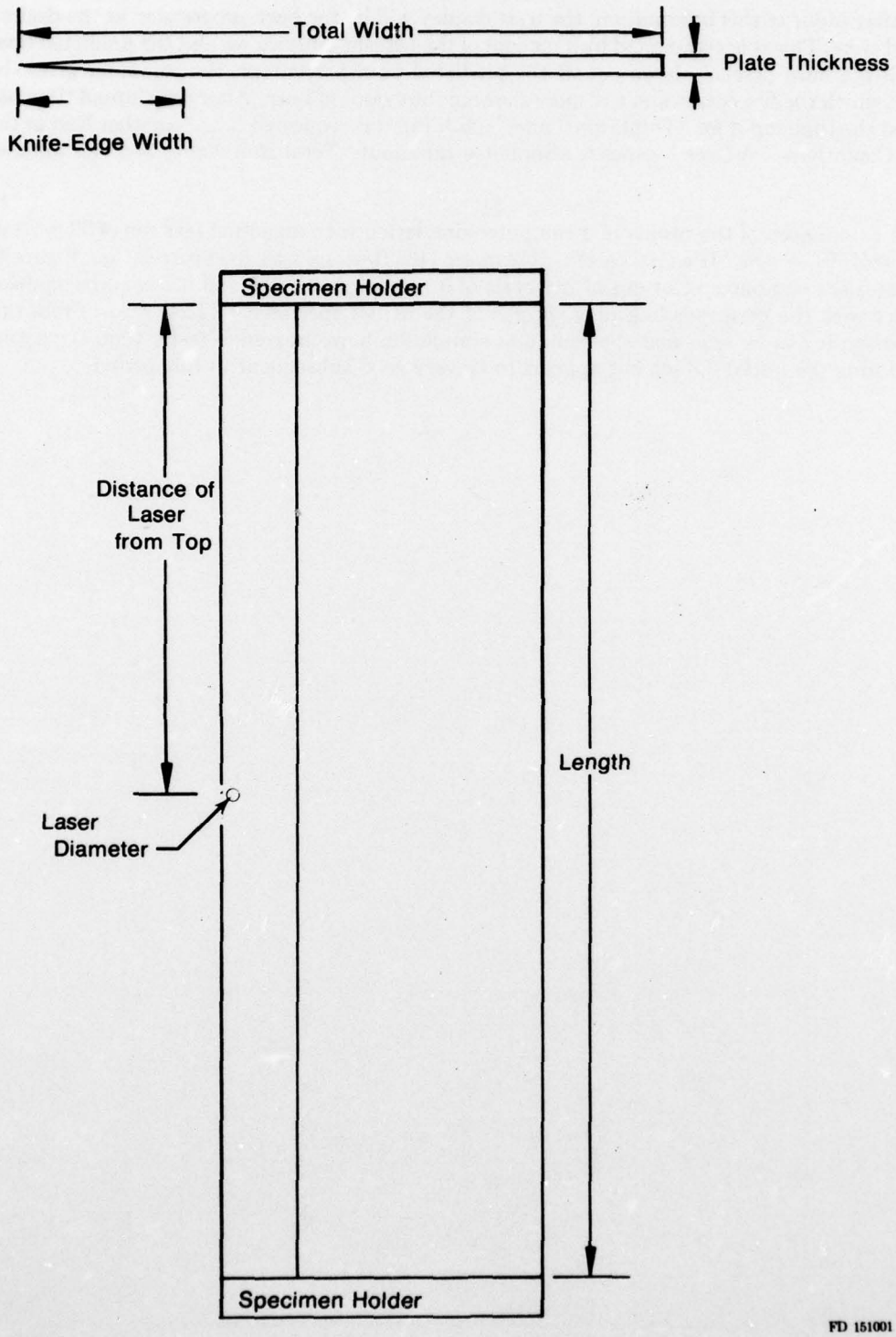

Figure 44. Specimen Configuration Related to Simulation

After input of this information, the next display will be the burn progression at the desired elapsed time. This is accompanied by a readout of the percent burn shown and the predicted final burn. If the burn percent shown equals the predicted burn percentage, the computer gives the time at which the fire ceases and a display showing the extent of burn. After the elapsed time has reached the time input for "Total Run Time," a last input is requested ___ "Another Run at the Same Conditions." A "yes" response stimulates the input "Total Run Time, Sec" for another run.

A comparison of the results of a computer simulation with an actual test run of Ti 8-1-1 at 458°C (857°F) — 0.69 MPa (100 psia) — 142 m/sec (465 ft/sec) shows good correlation. Figure 45 illustrates the computer print-out at intervals of 0.1, 0.2, 0.3, 0.4, 0.5 and 0.7 sec after ignition together with the corresponding photographs of the actual specimen (N2-24) burn. From this comparison it can be seen that the computer simulation burn progresses faster than the actual burn during the initial 0.3 sec but appears to be very good subsequent to this period.

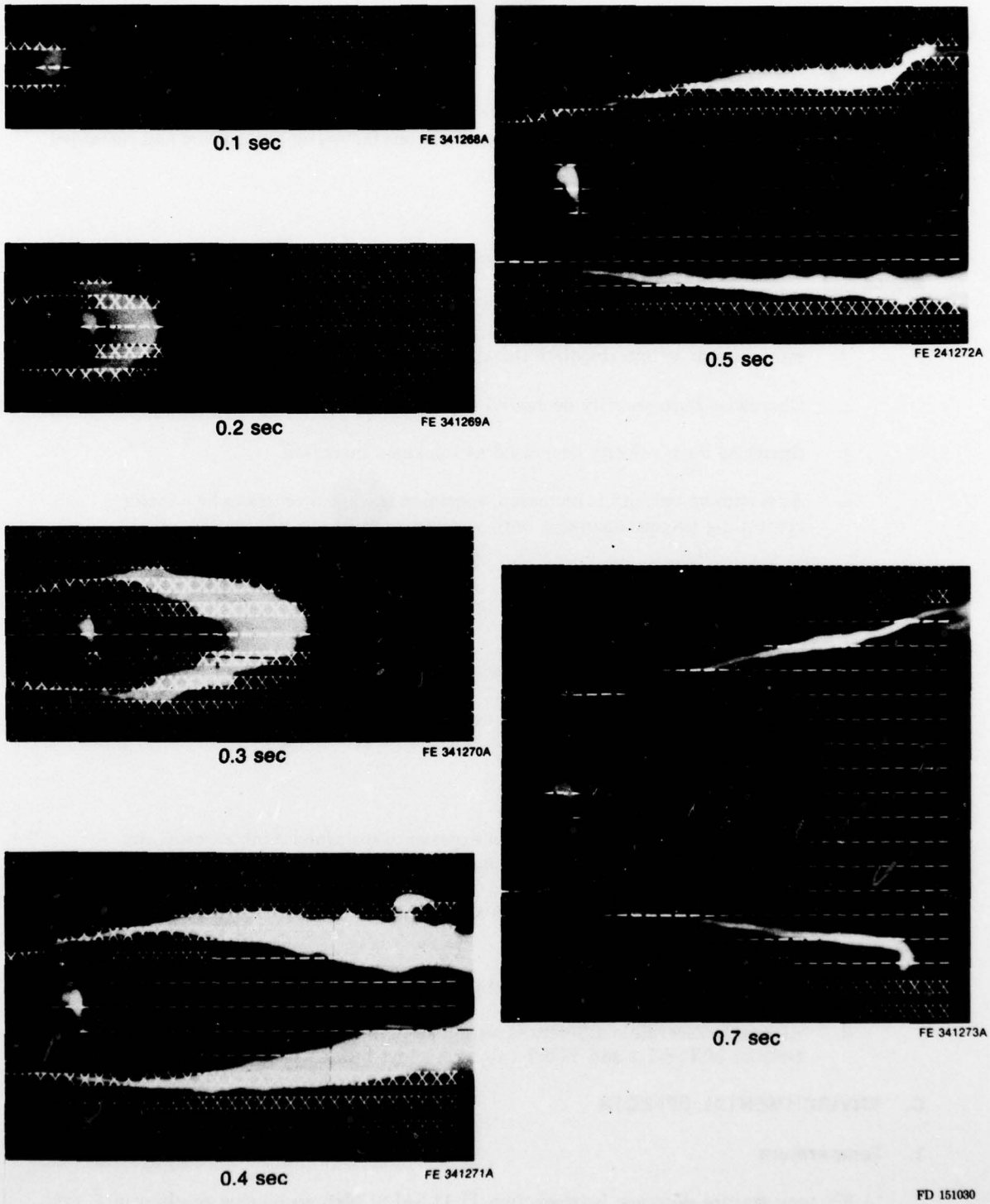

Figure 45. Comparison of Computer Simulation With Actual Specimen Burn

SECTION V

CONCLUSIONS

Based upon the experimental test results obtained during this program, the following conclusions were reached relative to the influence of various factors on the ignition and sustained combustion of the titanium alloys investigated.

A. THICKNESS EFFECT

For the alloy Ti 8-1-1, specimen thickness was found to have the following well-defined effects:

1. Burn severity was greatest for the thinnest and thickest specimens and was minimum at an intermediate thickness.

2. Chordwise burn velocity decreased as thickness increased.

3. Spanwise burn velocity decreased as thickness increased.

4. As airstream velocity is increased, specimen thickness ceases to be a factor controlling average spanwise burn velocity.

B. ALLOY EFFECT

1. Ignition Time

a. Alloys which did not burn (only notched) had definite lower ignition times.

b. Alloy Ti 13.5Al-21.5Nb had ignition times consistantly higher than the other alloys tested.

2. Combustion

a. Alloys Ti 20Ni and Ti 13Cu did not experience sustained combustion at any of the test environmental conditions.

b. Alloys Ti 13V-11Cr-3Al, Ti 13.5Al-21.5Nb and Beta III burned at low to moderate severity.

c. Ti 5Ni and Ti 10Ni burned moderately to severely.

d. Although discernible differences were measured in the combustion characteristics of Ti 8-1-1 and Ti 6-2-4-6, both alloys burned severely in all tests.

C. ENVIRONMENTAL EFFECTS

1. Temperature

A 6% temperature decrease between two Ti 13.5Al-21.5Nb specimens resulted in a 17% decrease in average chordwise burn velocity and a 23% decrease in burn severity.

2. Pressure

Tests of alloys Ti 13.5Al-21.5Nb and Beta III established that pressure has a greater influence than temperature on average chordwise burn velocity and an equal but opposite influence on burn severity.

3. Airstream Velocity

a. The burn severity of alloy Ti 13.5Al-21.5Nb was very close to being unaffected by changes in airstream velocity.

b. The burn severity of alloys Ti 5Ni and Ti 10Ni decreased significantly when airstream velocity was increased from 137 m/sec (450 ft/sec) to 244 m/sec (800 ft/sec).

c. The average chordwise and spanwise burn velocities, for all alloys tested, increased with increase in airstream velocity.

SECTION VI

RECOMMENDATIONS

As a result of the experimental work preformed under this program, the following recommendations are submitted to guide future work in the area of titanium alloy ignition and combustion:

1. An alloy screening effort should be conducted in which alloying elements (known to retard combustion) are added to titanium in varying amounts. This program would include mechanical property characterization in addition to ignition and combustion tests.

2. Because of the tendency toward higher pressures in advanced gas turbine engines, a program should be conducted to extend the data base of pressure variation as it affects the ignition and combustion of burn-resistant alloys.

3. Physical properties such as melting point, oxide solubility, heat of combustion, thermal conductivity and diffusivity, viscosity of the melt and surface tension (wettability) of melt on solid significantly influence the ignition and sustained combustion properties of titanium alloys. Data on these physical properties, however, is generally not available. A comprehensive effort is required to determine these properties, particularily for nonburning alloys, to serve as a guide to the formulation of new nonburning alloys having acceptable mechanical properties.

DISTRIBUTION LIST

Naval Weapons Center
China Lake, Calif. 93555
Attn: D. H. Bergevin (1)
J. Fontenot (1)
Code 3183

National Bureau of Standards
325 Broadway
Boulder, Colorado
Attn: A. F. Clark (1)
J. C. Moulder (1)
D. Strobridge (1)

Northwestern University
Evanston, Illinois
Attn: R. Burton

Department of the Air Force
Aeropropulsion Laboratory
WPAFB, Ohio 45433
Attn: C. Elrod (1)
L. O. Bery (1)

Pratt & Whitney Aircraft
East Hartford, Ct. 06108
Attn: W. F. Laverty (1)
M. Freling (1)

Department of the Air Force
Air Force Materials Laboratory
WPAFB, Ohio 45433
Attn: S. R. Lyon (1)
B. Cohen (1)
S. G. Lee (1)
W. O'Hara (1)

Department of Navy
Naval Air Systems Command
Washington, D. C. 20361
Attn: J. Hoffner

Department of Mechanical Engineering Code 69-BL
Naval Postgraduate School
Monterey, Ca. 93940
Attn: D. H. Boone

NASA Lewis Research Center
21000 Brookpark Road
Cleveland, Ohio 44135
Attn: L. P. Ludwig (1)
S. Young (1)
J. Merutka (1)

U. S. Army Materials and Mechanics
Research Center
Watertown Arsenal
Watertown, Ma. 02172

Metals and Ceramics Information Ctr.
Battelle Memorial Institute
505 King Avenue
Columbus, Ohio 43201

National Aeronautics and Space Admin.
600 Independence Avenue
Washington, D. C. 20546

United Technology Research Lab
East Hartford, Ct. 06108

Clemson University
College of Engineering
Clemson, S. C. 29631
Attn: J. S. Wolf

Garret Corporation
Air Research Division
Phoenix, Arizona 85001
Attn: Mr. Don R. Schuyler

L.T.V. Aerospace Corporation
Vought Aeronautics Division
P. O. Box 5907
Dallas, Texas 75222
Attn: Mr. A. Hohman (1)
B. A. Forcht (1)

Energy Research and Development Agency
Document Library
Germantown, Md. 21403

Grumman Aerospace Corp.
Bethpage, N. Y. 11714
Attn: P. N. Adler

National Science Foundation
Division of Materials Research
Washington, D. C. 20550

General Motors Corporation
Detroit Diesel Allison Div.
Materials Laboratories
Indianapolis, Ind. 46202
Attn: M. Herman

McDonnell Aircraft Co.
St. Louis, Mo. 64166
Attn: E. R. Fannin

Lockheed-Georgia Co.
Marietta, Georgia 30060
Attn: W. C. Herron

Rockwell International
Rocketdyne Division
Canoga Park, Ca. 91305

Southern Research Institute
2000 9th Avenue South
Birmingham, Alabama 35205
Attn: Charles Bates

Naval Air Propulsion Center
Box 7176
Trenton, N. J. 08628
Attn: Mr. J. Glatz (1)
V. Labosky (1)
R. Vizzini (1)

United Technologies Corporation
Pratt & Whitney Aircraft Group
Government Products Division
P. O. Box 2691
West Palm Beach, Fla. 33402
Attn: M. Glickstein (1)
V. Anderson (5)
B. Manty (1)
S. Bonifazi (1)
C. Stevens (1)
R. Athey (1)
M. Allen (1)
R. Hecht (1)
A. Hodges (1)
P. Davisson (1)
J. B. Moore (1)
J. Morris (1)
W. Stott (1)
A. Zabelny (1)
D. Enos (1)
H. Gibson (1)